IDA PAPER P-2335

IDA GAMMA-RAY LASER ANNUAL SUMMARY REPORT (1989)

Investigation of the Feasibility of Developing a Laser Using Nuclear Transitions

Bohdan Balko
Irvin W. Kay
John Neuberger
Gary Herling

April 1992

Prepared for
Strategic Defense Initiative Organization
InnovativeScience and Technology Office

Dwight Duston, *Director*

INSTITUTE FOR DEFENSE ANALYSES
1801 N. Beauregard Street, Alexandria, Virginia 22311-1772

IDA Log No. HQ 90-35218

DEFINITIONS

IDA publishes the following documents to report the results of its work.

Reports

Reports are the most authoritative and most carefully considered products IDA publishes. They normally embody results of major projects which (a) have a direct bearing on decisions affecting major programs, (b) address issues of significant concern to the Executive Branch, the Congress and/or the public, or (c) address issues that have significant economic implications. IDA Reports are reviewed by outside panels of experts to ensure their high quality and relevance to the problems studied, and they are released by the President of IDA.

Group Reports

Group Reports record the findings and results of IDA established working groups and panels composed of senior individuals addressing major issues which otherwise would be the subject of an IDA Report. IDA Group Reports are reviewed by the senior individuals responsible for the project and others as selected by IDA to ensure their high quality and relevance to the problems studied, and are released by the President of IDA.

Papers

Papers, also authoritative and carefully considered products of IDA, address studies that are narrower in scope than those covered in Reports. IDA Papers are reviewed to ensure that they meet the high standards expected of refereed papers in professional journals or formal Agency reports.

Documents

IDA Documents are used for the convenience of the sponsors or the analysts (a) to record substantive work done in quick reaction studies, (b) to record the proceedings of conferences and meetings, (c) to make available preliminary and tentative results of analyses, (d) to record data developed in the course of an investigation, or (e) to forward information that is essentially unanalyzed and unevaluated. The review of IDA Documents is suited to their content and intended use.

The work reported in this document was conducted under contract MDA 903 84 C 0031 for the Department of Defense. The publication of this IDA document does not indicate endorsement by the Department of Defense, nor should the contents be construed as reflecting the official position of that Agency.

IDA PAPER P-2335

IDA GAMMA-RAY LASER ANNUAL SUMMARY REPORT (1989)

Investigation of the Feasibility of Developing a Laser Using Nuclear Transitions

Bohdan Balko
Irvin W. Kay
John Neuberger
Gary Herling

April 1992

INSTITUTE FOR DEFENSE ANALYSES
Contract MDA 903 89 C 0003
Task T-R2-597.03

REPORT DOCUMENTATION PAGE

Form Approved
OMB No. 0704-0188

1. AGENCY USE ONLY *(Leave blank)*	2. REPORT DATE	3. REPORT TYPE AND DATES COVERED
	April 1992	Final--January 1990-March 1992

4. TITLE AND SUBTITLE
IDA Gamma-Ray Laser Annual Summary Report (1989): Investigation of the Feasibility of Developing a Laser Using Nuclear Transitions

5. FUNDING NUMBERS
C - MDA 903 89 C 0003

T- T-R2-597.03

6. AUTHOR(S)
Bohdan Balko, Irvin W. Kay, John Neuberger, Gary Herling

7. PERFORMING ORGANIZATION NAME(S) AND ADDRESS(ES)
Institute for Defense Analyses
1801 N. Beauregard St.
Alexandria, VA 22311-1772

8. PERFORMING ORGANIZATION REPORT NUMBER
IDA Paper P-2335

9. SPONSORING/MONITORING AGENCY NAME(S) AND ADDRESS(ES)
Strategic Defense Initiative Organization
Innovative Science and Technology Office
The Pentagon, Room 1E167
Washington, DC 20301-7100

10. SPONSORING/MONITORING AGENCY REPORT NUMBER

11. SUPPLEMENTARY NOTES

12a. DISTRIBUTION/AVAILABILITY STATEMENT
Approved for public release; distribution unlimited.

12b. DISTRIBUTION CODE

13. ABSTRACT *(Maximum 200 words)*

This paper generalizes the Haake-Reibold model of superfluorescence to take into account certain effects that, while negligible for atomic emission, are important for the nuclear case. Comparisons are made of three different approaches to numerical computation based on the model, and a number of explicit calculations are made to illustrate the behavior of the emitted pulse under various conditions. In addition, the paper presents detailed analyses of the effects of homogeneous and inhomogeneous broadening and relaxation on superfluorescent emission.

14. SUBJECT TERMS
gamma-ray laser, graser, nuclear superfluorescence (SF), Haake-Reibold model of SF, nuclear isomers, homgeneous and inhomogeneous broadening relaxation

15. NUMBER OF PAGES
136

16. PRICE CODE

17. SECURITY CLASSIFICATION OF REPORT	18. SECURITY CLASSIFICATION OF THIS PAGE	19. SECURITY CLASSIFICATION OF ABSTRACT	20. LIMITATION OF ABSTRACT
UNCLASSIFIED	UNCLASSIFIED	UNCLASSIFIED	SAR

NSN 7540-01-280-5500

Standard Form 298 (Rev. 2-89)
Prescribed by ANSI Std. Z39-18
298-102

PREFACE

In January 1985 the Director of the Science and Technology Directorate of the Strategic Defense Initiative Organization (SDIO) asked members of the IDA research staff to investigate the feasibility of developing a γ-ray laser. The staff determined what work had been done, who was currently working in the field, and what work should be encouraged or supported. A workshop was convened for researchers directly involved both in gamma-ray laser work and in ancillary fields such as nuclear structure, radiation propagation in crystals, Mössbauer Effect, and optical lasers. Next, an in-house study was undertaken to clarify critical issues concerning the various pumping schemes proposed at the workshop as well as systems questions about the γ-ray laser as a working device.

The proceedings of the workshop were published in the form of a report to the Innovative Science and Technology Office (IST) of the SDIO. The work completed in 1985 was presented in IDA Paper P-2021.

In 1986, the in-house work focused on extending the data base, the nature of superradiance in the γ-ray laser context, and a detailed investigation of the upconversion pumping scheme. A discussion of nuclear systematics, investigations of electron-nuclear-driven pumping, and lifetime measurements rounded out that study. The results of the FY 1986 effort were also presented in an IDA paper, P-2004.

In 1987, the IDA research staff looked at the state of the art and assessed the situation in γ-ray laser work with focus on two areas of research interest critical to concepts for developing a γ-ray laser. Heating effects associated with upconversion techniques were discussed. The sources of inhomogeneous broadening which destroy the Mössbauer Effect were investigated and techniques available for restoring the resonance by external or internal fields were considered (IDA Paper P-2083).

In 1988 the in-house work concentrated on (1) establishing a theoretical model of nuclear superfluorescence which took into account specific characteristics of nuclear radiation emission and transport that are important for superfluorescence on the nuclear scale, (2) examining in more detail and for more realistic parameters the heating effects

inherent in upconversion concepts, and (3) examining the speed of response of nuclei to applied external fields, as exhibited by their spectra (IDA Paper P-2175).

The 1989 effort described in the present document concentrated on developing a model of nuclear superfluorescence that included:

1. Multilevel systems,
2. Incoherent pumping at finite rates,
3. Spatial attenuation of the electromagnetic field in the active region,
4. Dephasing due to inhomogeneous broadening,
5. Population depletion due to competing processes like internal conversion and spontaneous transverse emission.

This was done by generalizing the Haake-Reibold model of superfluorescence based on Maxwell-Bloch equations. The effects of inhomogeneous broadening on superfluorescence were studied using a theory developed by J. Eberly. The enhancement of superfluorescence in inhomogeneously broadened systems by time-dependent hyperfine interactions was investigated using the theory developed by M. Blume. We also investigated coherent aspects of nuclear emission and absorption in the presence of homogeneous and inhomogeneous broadening of source and absorber.

The development of a γ-ray laser is viewed as a high-risk/high-payoff undertaking. IDA's involvement focuses on minimizing the risk and on striving to redirect the effort when proposed schemes are shown not to be feasible.

ABSTRACT

This paper generalizes the Haake-Reibold model of superfluorescence to take into account certain effects that, while negligible for atomic emission, are important for the nuclear case. Comparisons are made of three different approaches to numerical computation based on the model, and a number of explicit calculations are made to illustrate the behavior of the emitted pulse under various conditions. In addition, the paper presents detailed analyses of the effects of homogeneous and inhomogeneous broadening and relaxation on superfluorescent emission.

CONTENTS

FIGURES

TABLES

SUMMARY

This report describes the 1989 research effort by members of the IDA staff in the field of γ-ray lasers. The work is part of a continuing task in support of the Innovative Science and Technology Office (IST) of the Strategic Defense Initiative Organization (SDIO). The development of a γ-ray laser is a high-risk science and technology undertaking. IDA involvement has focused in large measure on minimizing the risk and attempting to redirect the program as quickly as possible when proposed schemes prove infeasible. The report is presented in three independent chapters.

Chapter I discusses a generalized version of the Haake-Reibold model of superfluorescence in a multilevel system of emitters, having up to five energy levels. The generalized version takes into account finite pumping rates, spatial attenuation of the electromagnetic field, dephasing, and population depletion due to processes such as internal conversion and spontaneous, but noncollective, emission. These phenomena, which have not been considered together in a single theory heretofore, are important for the investigation of the feasibility of nuclear superfluorescence.

Calculations performed with the Haake-Reibold model show that nuclear superfluorescence may be less demanding on the real nuclear and solid state properties than was previously predicted by other authors.

Chapter II discusses the effects of inhomogeneous broadening on reducing superfluorescent emission and the effects of time-dependent interactions on enhancing such emission. The effects are functions of time (after inversion) unlike similar effects in continuous wave (CW) or pulsed (amplified spontaneous emission) lasing.

Chapter III discusses the effect of inhomogeneous broadening on emission and absorption of γ-rays by nuclei. The phenomena is treated as incoherent and coherent processes to examine claims made by some investigators that homogeneous broadening can be used to overcome reductions of resonant absorption produced by inhomogeneous broadening. It turns out that in both cases the resonant absorption (Mössbauer Effect) is reduced by a factor γ/Γ, where γ is the radiative linewidth and Γ the total linewidth of the system and the predicted enhancement does not occur. The total linewidth includes the

radiative process, internal conversion, cooperative transitions, and time-dependent fields that tend to broaden the emission line.

I. INVESTIGATION OF NUCLEAR SUPERFLUORESCENCE WITH THE GENERALIZED HAAKE-REIBOLD STOCHASTIC SOURCE APPROACH

A. INTRODUCTION

1. Background

Superfluorescence (SF) and superradiance (SR) are both examples of the cooperative, spontaneous emission of coherent radiation by identical radiators such as atoms, molecules, or nuclei. Intense, directed pulses of duration much shorter than the spontaneous emission lifetime of an individual radiator (Ref. 1) characterize the radiation, which has been observed experimentally in molecular and atomic systems, e.g., CH_3F, HF, Na, Ca, Tl, $KCl:O_2$, Sr, and Li. Theoretical models that successfully explain the observations have been developed.

For nuclear lasing, which has special pumping problems (Ref. 2), it should be easier to invert a population to an isomeric level with a long lifetime than to one with a short lifetime. On the other hand, during the actual lasing process the emission lifetime should be as short as possible. Thus, because of its characteristically fast radiation, some (Refs. 2, 3) have recommended SF as a possible alternative to stimulated emission as a viable or preferred process.

A recent IDA paper (Ref. 3) discussed some aspects of nuclear SF and compared it to lasing and amplified spontaneous emission (ASE). Results indicate that electronic attenuation plays a more complicated role in generating SF than in those processes. It does not lead to the threshold required by the Schawlow-Townes condition for lasing and ASE, but rather forces a gradual reduction of emission intensity. The paper's calculations were based on a three-state model with some restrictive conditions that permitted an effectively closed form solution.

The present paper uses a five-state model and a Monte Carlo technique for numerical computations. The treatment is more general and takes into account interacting physical mechanisms that the earlier nuclear SF work ignored.

2. Comparison of Atomic and Nuclear SF Problems

Nuclear SF, which imposes special conditions on the nuclei and their environment, has not yet been observed. For SF certain parameters, comparative values of which appear in Table 1, are unimportant in the atomic domain but are critical in the nuclear. The parameters in Table 1 determine the gain coefficient K associated with an amplifying medium for typical atomic and nuclear systems. The gain coefficient is given roughly by[1]

$$K = \overbrace{\frac{\lambda^2 \beta_R}{2\pi(1+\alpha)}\left(\frac{\Gamma}{\Gamma+\Gamma_g}\right)\frac{fg_N}{(1+a)}}^{\sigma_R}\overbrace{\left(n_e - \frac{g_e}{g_g}n_g\right)}^{\Delta n^*} - M\mu \quad , \tag{1}$$

where σ_R is the effective nuclear resonance cross-section, and Δn^* is the population inversion achieved by the pumping process. The *M* depends on the laser operating mode as discussed by Trammell and Hannon (Ref. 4). For steady state operation M = 1.

In Eq. (1), σ_R is the maximum nuclear resonant absorption cross-section given by

$$\sigma_R = \frac{\lambda^2 \beta_R}{2\pi\,(1+\alpha)}\,\frac{fg_N}{(1+a)}\left(\frac{\Gamma}{\Gamma+\Gamma_g}\right) \quad ,$$

with λ the wavelength of the photon emitted in the resonant transition, α the internal conversion coefficient, and β_R the branching ratio. The quantity Γ is the total width of the nuclear excited level decaying with transition energy E_0, and Γ_g is the total width of the lower level. Generally, the experimental linewidth is often much larger than Γ because of homogeneous broadening due to competing transitions, the final nuclear state lifetime, and inhomogeneous line broadening.[2]

Equation (1) is the same as that given for the gain coefficient by Baldwin and Feld (Ref. 5), except for two additions. One, which takes into account spatial attenuation of the electromagnetic field, is the second term on the righthand side. The other is the factor 1/(1 + a), which takes into account inhomogeneous broadening.

---

1 A more detailed treatment (Ref. 3) of SF shows that the relationship between the attenuation μ and the stimulated gain $\sigma_R \Delta n^*$ is more complicated than that depicted in Eq. (1).

2 The major contributions to inhomogeneous broadening come from hyperfine interactions such as the electric monopole (isomer shift), magnetic dipole (Zeeman), and electric quadrupole (electric field gradient).

Table 1. Comparison of Characteristic Atomic (Optical) and Nuclear Mössbauer Parameters

	Parameter	Typical Optical Atomic	Typical Nuclear	Possible Modification Factor	Modification Technique
Energy	E_0 (eV)	eV	10^4 eV		
Wavelength	λ(Å)	10^4 Å	1 Å		
Recoilless Fraction	f	1	≈ 0	(0.95)	Mössbauer Effect
Inhomogeneous Broadening	a	small	10^2-10^6	x 10^{-4}	Dynamic Fields Relaxation
Competing Transitions (Internal conversion for nuclei)	α	small	10-100		
Attenuation	μ_a (cm^{-1})	0.01	1-1000	x 10^{-3}	Bormann Effect
Density	n (cm^{-3})	10^{10}-10^{15} *	10^{22}		

* SF observed in this density range in molecular and atomic systems (Ref.6).

The inhomogeneous broadening parameter a can be 10^6 or higher for isomeric nuclei of interest to the γ-ray laser concept under consideration. The parameter g_N is the coupling factor for the nuclei to the electromagnetic field, which for amorphous samples is equal to 1, and the parameter μ is the linear extinction coefficient for nonresonant absorption or inelastic scattering of photons primarily by the photoelectric effect.

First, it is clear from Eq. (1) that the nuclei participating in lasing have to belong to a Mössbauer isotope ($f > 0$), as even simple nuclear resonant scattering is not possible without this condition being fulfilled. Preferably, the Mössbauer isotope should be in a medium such that one has a high recoilless fraction ($f \approx 1.0$). Thus, the pumping

mechanism must be capable of achieving the required nuclear inversion (Δn^*) without destroying the Mössbauer Effect in the crystal. For direct pumping, the pumping power requirement for inverting the nuclear population of a given isotope is inversely proportional to the lifetime τ of the nuclear state. Thus in Table 1 we see the recoil ($f \approx 0$) inhomogeneous broadening ($a > 10^2$), internal conversion [high ($\alpha > 10$) for low energy γ-emission] and high attenuation ($\mu > 10$) combine to reduce the gain coefficient and the feasibility of lasing and SF for nuclear systems, whereas the possibility of high densities ($n \approx 10^{22}$) enhances the gain and feasibility of lasing and SF for nuclear systems.

3. SF Pulse Characteristics

Generally speaking, the emission of an SF pulse requires the preparation of an inverted population of identical radiators. Experimentally, the emitted pulses are characterized by a pulse width τ_{SR} and a delay time τ_D, following the inversion of the population. From simple theory, the relationship between τ_{SR} and τ_D and the density of cooperating radiators ρ, the natural radiative lifetime τ_0, the wavelength of the emitted light, λ, and the cavity length l can be obtained. In terms of these parameters

$$\tau_R = \frac{8\pi \tau_o}{\rho \lambda^2 l},$$

$$\tau_D = \frac{1}{2} \tau_R \ln N,$$

and the pulse intensity Is(t) is given by the "inverted pendulum expression"

$$Is(t) = \frac{1}{2} N/\tau_R \operatorname{sech}^2\left[\frac{1}{\tau_R}(t - \tau_D)\right]$$

(Ref. 7), where t is measured from the time of the (instantaneous) inversion.

Clearly, to describe experimental conditions more realistically it is necessary to invoke more detailed theories, which involve the parameters in Table 1 and Eq. (1).

4. Historical Approaches to Nuclear SF and Objectives of this Paper

This paper discusses an SF model that takes into account: (1) competing transitions, such as internal conversion; (2) transport phenomena causing electromagnetic spatial attenuation; (3) finite pumping times for the preparation of inversion by incoherent sources; (4) effects of inhomogeneous broadening on pulse emission. These phenomena lead to conditions for SF emission. Although characterized by distinct parameters, they

must be treated together in the same theory since the interplay between the different effects that they produce is too intricate to permit them to be treated separately.

Some effects have been considered separately by other authors, however. Trammell and Hannon (Ref. 4) addressed the feasibility of nuclear SF and compared SF to nuclear "pulsed" lasing or amplified spontaneous emission (ASE). They considered the effects on SF of inhomogeneous broadening and attenuation separately and introduced these parameters in an *ad hoc* fashion in the discussion. Their conclusions differ substantially from ours, in two important features. In our results, the effect of the attenuation is more gradual, and does not lead to a threshold effect as required by the Schawlow-Townes condition (see Ref. 3) for lasing. Also in our results the inhomogeneous broadening leading to a dephasing effect is time dependent. The effect is small at early times after inversion and increases with time.[3] Both of these effects when treated together in our theory produce a less restrictive condition on the feasibility of nuclear SF. Baldwin and Feld in a more recent paper (Ref. 5) using semiclassical theory, discuss SF emission, and derive minimum requirements for an experimental demonstration of phenomena. They do not consider inhomogeneous broadening, and grossly overestimate the effect of attenuation.

We plan to use the more complete theory developed in this paper to reevaluate the feasibility of demonstrating experimentally, with known isomers and available pumping sources, the occurrence of nuclear SF. The model described here assumes that a single, endfire mode exists in an active, acicular-shaped medium (i.e., a medium shaped like a long cylinder). Geometrical considerations leading to the treatment of more general shapes (other than acicular) will be left for future discussions.

5. SF Theory for Atomic Systems

In the introduction to Ref. 7 the authors, Bonifacio and Lugiato, distinguish between SR and SF. Both terms refer to the phenomenon of cooperative radiation by a system of identical emitters, which in their case are two-level atoms.

However, SR occurs when a coherent pulse excites the system into a collective state with a macroscopic electric dipole; the superradiant pulse is then attributed to emission by this dipole. On the other hand, SF occurs when, after some normal fluorescent emission to

---

[3] The rate is the same T_2^* but there is an exponential decrease in effect.

start the process, with no macroscopic dipole present initially, uncorrelated excited emitters spontaneously become correlated and then radiate cooperatively. At no time is there a macroscopic dipole present.

For the Bonifacio and Lugiato theoretical model of SF, the active volume containing the emitters is limited to an acicular shape: many wavelengths long and with a cross-section narrow enough to make the Fresnel number associated with diffraction of the radiation at one end nearly equal to 1. This condition limits the electromagnetic field within the volume to a pair of modes, characterized to a good approximation by left and right moving plane waves. The authors assume that these modes are completely independent and noninteracting, thereby reducing the analysis problem to one for a single mode.

In their analysis Bonifacio and Lugiato consider both Markovian and non-Markovian cases of the interaction between the local electromagnetic field and the atoms. For the non-Markovian case, in which a certain number of the emitted photons remain within the active volume long enough to reexcite some depleted atoms, the model predicts an experimentally observed ringing in the emitted pulse. For the Markovian case the model predicts that ringing will not occur because all emitted photons leave the volume before they can interact with any of the atoms.

The Bonifacio and Lugiato model is based entirely on the use of a density matrix that is a function of time but has no spatial dependence. Therefore, it does not take propagation into account directly. Nevertheless, it is able to predict ringing, which to some extent is due to propagation.

In this context it has been referred to as an average field model. Some (cf. Refs. 8, 9) contend that an average field model is incapable of predicting such phenomena as ringing correctly, arguing that it is not only necessary to treat propagation explicitly but also to include certain three-dimensional effects as well (e.g., field variations in the lateral directions).

Theoretical models that do treat propagation three dimensionally are either inappropriate, if the medium is crystalline, because they assume that the emitters are distributed randomly over some region (cf. Ref. 10); or else they are semiclassical (cf. Ref. 1) and therefore do not deal completely with the initial stage of superfluorescence. On the other hand, the medium considered specifically by Bonifacio and Lugiato is, in fact, a crystal, and the Bonifacio and Lugiato model is strictly quantum mechanical in nature.

If the emitters are nuclear rather than atomic, which is the case of interest here, the multilevel, one-dimensional SF model of Haake and Reibold (Ref. 11) may be more suitable than any of these. The effect of a crystalline medium should be particularly important when the emitters are nuclei because the spacing between them will generally be larger than a resonant wavelength, whereas when they are atoms the opposite is true. The Haake and Reibold model covers at least one-dimensional propagation completely, and, since quantum electro-dynamics plays a major role in its derivation, it should also cover the initial stage of SF adequately. The generalized version of the model defined here takes into account certain effects, such as losses due to internal conversion, that are negligible in the atomic case but are important in the nuclear case.

B. HAAKE-REIBOLD STOCHASTIC SOURCE APPROACH

The Haake-Reibold theoretical model of SF described in this section is a generalization of the one introduced by those authors in Ref. 11. For its derivation Ref. 11, which treats multilevel systems, refers to earlier papers (e.g., Ref. 12[4]) that deal with two-state systems using the same approach. These references give more or less detailed derivations of the two-state version only; however, as Haake and Reibold remark, they lay out all concepts needed for generalizing to the multilevel case.

Both versions use the Heisenberg picture and both approximate the discrete set of emitters as a continuous distribution in space. In effect, the polarization and occupation number (inversion) operators associated with the different energy levels become fields represented by continuous functions of distance and time. The Heisenberg equations of motion are formally similar to the Maxwell-Bloch equations of semiclassical models such as that presented in Ref. 1.

However, in deriving the semiclassical equations (using a classical electromagnetic field and, to take the emitters into account quantum mechanically, a nonrelativistic,

---

[4] Reference 12 proves that a classically stochastic noise source can replace the initial quantum electrodynamic vacuum fluctuations that are actually responsible for starting the superfluorescence process. This makes it possible to formulate an equivalent semiclassical initial value problem, the solution of which provides the temporal history of the radiated electromagnetic pulse. The proof goes even further, demonstrating that the noise source is Gaussian distributed and white.

Reference 12 also derives a one-dimensional SF model characterized by Maxwell-Bloch equations in which the polarization and inversion operators are continuous functions of space as well as time. The derivation predicts homogeneous broadening, giving an explicit value for the natural lifetime of the system of emitters. That is, the corresponding natural decay rate is not an *ad hoc* assumption in this model.

Schroedinger wave equation), Ref. 1 at first obtains the equations in terms of expectation values of the quantum mechanical observables: the induced polarization and the inversion. These quantities are continuous functions of time at each emitter and are coupled between the different emitter locations only through the electric field. Reference 1 replaces them with polarization and inversion densities, which, in effect, are classical fields also coupled to the electric field but depending continuously on both space and time.

After an inversion of a sufficiently large number of emitters to an unstable energy level, quantum fluctuations of the initial vacuum state electromagnetic field are generally regarded as responsible for triggering SF. In order to avoid the complications of a quantum field theoretical analysis, Ref. 1 introduces an *ad hoc* polarization noise source to start the process. Reference 12 proves that a classically stochastic polarization source, properly chosen, can in fact substitute for the quantum fluctuations, thereby justifying in part the less rigorous approach of Ref. 1.

The stochastic elements of the source assumed in Ref. 1 are terms with random phases that when summed have little effect on the early electric field intensity, which can be estimated by neglecting nonlinear interactions. The nonlinear interactions are small because they are quadratic in quantities that vanish in the limit as time approaches zero.

Reference 1 uses the results of such a calculation for a time near zero, but after the noise source becomes negligible, to obtain a value of the electric field. The quantity thus acquired is then available as an initial value for an initial value problem associated with the Maxwell-Bloch equations, the solution of which will determine the field at later times when the nonlinear interactions are no longer negligible.

The Haake and Reibold models also introduce a classically stochastic, Gaussian white noise source to replace the quantum field fluctuations as a means of starting the collective spontaneous emisssion that characterizes superfluorescence, but use the Ref. 12 result for this purpose. In addition, the introduction of other source terms of the same type provides the multilevel model with incoherent depletion effects at lower energy levels.

Reference 11 determines the second order statistics of the electric field and polarization at early times when the Maxwell-Bloch equations are effectively linear. Then, treating the Maxwell-Bloch equations as classical, it uses the results to generate a statistical distribution of initial values for calculating a corresponding distribution of solutions that are valid in the nonlinear regime. Essentially, this is a Monte Carlo approach to estimating various features of the emitted radiation, such as the delay time of the radiated pulse.

Although restricted to one spatial dimension, the Haake and Reibold models account explicitly for propagation of the emitted electromagnetic field as long as the geometrical configuration of the emitters limits the radiation to an endfire mode. For this purpose the assumed shape of the active region is acicular with an associated Fresnel number of the order of one.

The effect is to restrict the field to plane waves propagating to the left or to the right in the longitudinal direction. The models assume that these waves do not interact, i.e., that it is only necessary to consider one of them in calculating the radiation at a single end of the active region.

The most general multistate system of interest for analyzing the nuclear SF is one with five states for which the energy diagram is depicted in Fig. 1. Pumping is modeled by the transition from the storage level 4 to this upper lasing level 3. We allow for two lasing transitions (3 to 1 and 3 to 2) and the possibility of interference between them. Level 2 can depopulate to level 1 and level 1 to level 0.

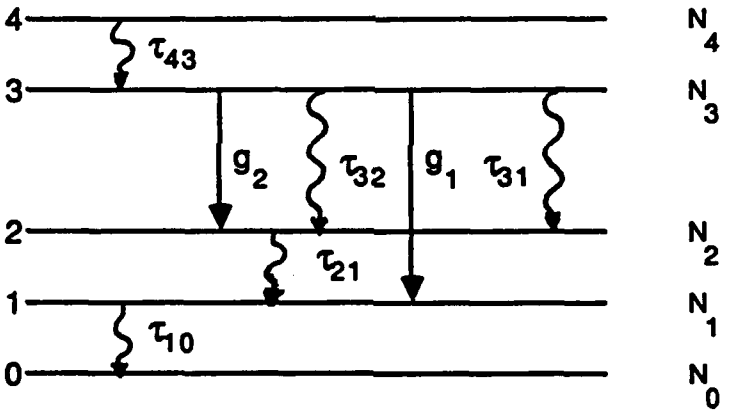

Figure 1. Energy Level Structure Assumed in the Calculations Described in the Paper. The two competing SF transitions are between upper state 3 and lower states 1 and 2 and are indicated by g_1 and g_2, respectively. Level 4 populates level 3, providing the inversion. The decay rates γ, Γ_3, Γ_2, and Γ_1 are given by τ_{43}^{-1}, $\left(\tau_{31}^{-1} + \tau_{32}^{-1}\right)$, τ_{21}^{-1} and τ_{10}^{-1}, respectively. Other depopulation transitions are generally allowed, but we indicate only those of interest at present.

The corresponding Haake and Reibold Maxwell-Bloch equations are

$$\frac{\partial}{\partial t} N_4 = -\gamma N_4 + \xi_4 \qquad (2\text{-a})$$

$$\frac{\partial}{\partial t} N_3 = -\left(E_{31}^{+} R_{31}^{+} + E_{32}^{+} R_{32}^{+} + E_{31}^{-} R_{31}^{-} + E_{32}^{-} R_{32}^{-}\right) - \Gamma_3 N_3 + \gamma N_4 - \xi_4 \qquad (2\text{-b})$$

$$\frac{\partial}{\partial t} N_2 = + \left(E_{32}^{+} R_{32}^{+} + E_{32}^{-} R_{32}^{-} \right) - \Gamma_2 N_2 + \beta \Gamma_3 N_3 + \xi_2 \qquad (2\text{-c})$$

$$\frac{\partial}{\partial t} N_1 = + \left(E_{31}^{+} R_{31}^{+} + E_{31}^{-} R_{31}^{-} \right) + \Gamma_2 N_2 - \Gamma_1 N_1 + (1-\beta) \Gamma_3 N_3 + \xi_1 \qquad (2\text{-d})$$

$$\frac{\partial}{\partial t} N_0 = \Gamma_1 N_1 \qquad (2\text{-e})$$

$$\frac{\partial}{\partial t} R_{32}^{\pm} = \left(N_3 - N_2 \right) E_{32}^{\mp} - E_{31}^{\mp} R_{21}^{\mp} - \frac{1}{2} \left[\Gamma_3 + \Gamma_2 + \Gamma_{\phi 2} \right] R_{32}^{\pm} + \xi_{32}^{\pm} \qquad (2\text{-f})$$

$$\frac{\partial}{\partial t} R_{31}^{\pm} = \left(N_3 - N_1 \right) E_{31}^{\mp} - E_{32}^{\mp} R_{21}^{\mp} - \frac{1}{2} \left[\Gamma_3 + \Gamma_1 + \Gamma_{\phi 1} \right] R_{31}^{\pm} + \xi_{31}^{\pm} \qquad (2\text{-g})$$

$$\frac{\partial}{\partial t} R_{21}^{\pm} = E_{31}^{\mp} R_{32}^{\mp} + E_{32}^{\pm} R_{21}^{\pm} - \frac{1}{2} \left[\Gamma_1 + \Gamma_2 + \Gamma_{\phi} \right] R_{21}^{\pm} + \xi_{21}^{\pm} \qquad (2\text{-h})$$

$$\frac{\partial}{\partial x} E_{3i}^{\pm} = g_i(t) R_{3i}^{\pm} - \frac{1}{2} \mu E_{3i}^{\pm} \ (i=1, 2) \quad , \qquad (2\text{-i})$$

which are a generalized version of the analogous equations introduced in Ref. 11 in which the population number operators are N_i, the photon field operators are $E_{ij}^{\pm}$, the nuclear polarization operators are $R^{\pm}_{ij}$ and the natural decay rates are Γ_i. Note that Γ_i, associated with a transition from the i^{th} energy level, is a decay rate that is not due to the collective emission process; rather, Γ_i takes into account decay due to other spontaneous, but noncollective, processes, such as internal conversion. Appearing in Eqs. (2-c) through (2-i) are four additional parameters: μ, which is a spatial attenuation coefficient, and $\Gamma_{\phi i}$ (i=1, 2) which are homogeneous line-broadening decay constants and act as dephasing parameters, and β which is a branching ratio for emissions from state 3 to states 1 and 2. In addition, the time dependence of the coupling parameter g, which in the Haake-Reibold theory is constant, introduces the inhomogeneous broadening effect on the SF; it is assumed to be exponential: $g_i'(t) = g_i \exp[-1/2\ \Gamma_{\theta i} t]$, where $\Gamma_{\theta i}$, which is the inhomogeneous broadening decay constant, is also the decay rate for the coupling parameter. Both $\Gamma_{\phi i}$ and $\Gamma_{\theta i}$ can be written as proportional to the natural line widths broadening parameters b and a (assumed for simplicity to be the same for both transitions $3 \rightarrow 2$ and $3 \rightarrow 1$), so that $\Gamma_{\phi i} = b\Gamma_i'$ and $\Gamma_{\theta i} = a\Gamma_i'$ where $\Gamma_i' = \Gamma_i + \Gamma_3$. The effect on SF of the inhomogeneous broadening through the time dependence of the coupling parameter g has been studied by several investigators (Refs. 7, 13). Chapter II of this report shows how the effect of inhomogeneous broadening can be reduced through relaxation or time-dependent hyperfine interactions.

The inhomogeneous terms of the form ξ_i in Eqs. (2) are noise sources that cause incoherent depletion at the various energy levels. The source ξ_4 provides for incoherent

pumping of energy level 4, from which energy decays at the same rate to level 3, causing the population inversion that eventually results in SF. The inhomogeneous terms of the form ξ_{ij} represent the noise sources that the model substitutes for the initially important quantum field fluctuations pumping and spontaneous decay effects on the SF triggering process.[5]

Reference 11 assumes that the fields ξ_4 and ξ_{32}, although quantum mechanical operators, are stochastic in the classical sense with the following statistical properties. They are statistically independent, white, and Gaussian with zero means and the second moments

$$< \xi_{32}^{+} \xi_{32}^{+} > = < \xi_{32}^{-} \xi_{32}^{-} > = < \xi_{32}^{-} \xi_{32}^{+} > = 0, \tag{3}$$

$$\begin{aligned} < \xi_4 (x, t) \xi_4 (x', t') > &= < \xi_{32}^{+} (x, t) \xi_{32}^{-} (x', t') > \\ &= (1/N) < N_4 (t) > \gamma \delta (x - x') \delta (t - t') \\ &= (1/N) e^{-\gamma t} \gamma \delta (x - x') \delta (t - t') \quad . \end{aligned} \tag{4}$$

A comparison of Eq. (3) with Eq. (4) verifies that the quantities ξ_{32}^{+} and ξ_{32}^{-} are, in fact, operators rather than c-numbers, since they do not commute. The term γ in Eq. (4) is dimensionless and is defined by the ratio of the superfluorescence time to the natural decay time from level 4 to level 3:

$$\gamma = \tau_{SF}/\tau_{43} \quad . \tag{5}$$

The quantity N is the number of radiators.

Although the polarization sources ξ_{32} and the population source ξ_4 are statistically independent, as indicated in Eqs. (3) and (4), Ref. 11 assumes that the parameters defining

---

5 The stochastic noise operators are defined by their statistics. Polder, Shuurmans, and Vrehens (Ref. 12) derived the classical noise equivalent sources from a quantum mechanical model. They identified three distinct components of the EM field, namely, (1) vacuum fluctuations, E_{vac}, (2) E_{dd} or dipole-dipole interaction between different atoms and (3) the self force or radiative reaction, E_{rr}. Initially, the only nonzero component is E_{vac}. This sets up correlations in the polarizations of atoms which produces a nonzero E_{dd}. The E_{vac} wave vectors corresponding to the appropriate geometry of the active region (cavity) set up the polarization appropriate for cooperative emission with those wave vectors. This results in the observed SF emission. The E_{rr} field gives rise to the natural width of the emission line only. [This interpretation arises naturally from the anti-normal ordering chosen by Polder et al. For a discussion of the influence of ordering of operators on interpretive questions, see P.W. Milonni and W.A. Smith, *Phys. Rev. A.* (1975).] Haake and Reibold (Ref. 11) use this theory to model noise sources which trigger SF. Their noise source is due to the incoherent pumping mechanism with time constant γ or the natural spontaneous decay from the excited state with time constant Γ_3. In the present development we use the noise source from the incoherent pumping mechanism, as described in Eqs. (4), for the SF triggering.

their probability distributions (i.e., the first and second moments) are identical. This is presumably justified by the fact that the same radiation field reservoir, consisting initially of the vacuum state electric field, generates both. The form of the source terms on the right-hand side of Eq. (2) is consistent with the stochastic source derived in Ref. 12.

C. COMPUTER CALCULATIONS, PART A

The computer calculations to be described here were done for only one SF transition ($3 \rightarrow 1$), the other transition was supressed. The calculations served two purposes: to check the codes, and to learn about the physics of nuclear SF predicted by the theory of Chapter II. We first wanted to check our codes by comparing our results with those obtained by other investigators and also to relate the calculated pulse shapes to physically meaningful parameters. We (1) investigated the dependence of the pulse shapes on the statistics and time dependence of the source terms ξi; (2) compared the full Monte Carlo calculations with the approximate result from the closed form solution obtained with the "triple integral" approach already introduced and described in an earlier report (Ref. 3); (3) compared their results with the average peak calculation described by Haake and Reibold (Ref. 11). We also studied the variation of the individual pulses obtained with different seeds for the random number generator used to provide the noise source characteristics that simulate the quantum fluctuations. All of these results are described in this section.

In Section IV we describe the results obtained with the Monte Carlo calculations designed to investigate and predict the SF pulse dependence on experimentally achievable parameters that could be used to select isomer candidates for nuclear SF experiments. The parameters studied were (1) the linear attenuation coefficient, $\mu(cm^{-1})$, (2) the lasing level spontaneous lifetime Γ (s^{-1}), including both radiative emission and internal conversion, (3) the inhomogeneous broadening parameter β giving the effective increase in linewidth of the total system in units of the natural linewidth and the effective number of cooperating nuclei N.

All of the calculated results are presented in normalized units consistent with the usage in Eqs. (2-a) through (2-i). In these units, time is given in units of the SF time τ_{SF} defined as

$$\tau_{SF} = \frac{8\pi \tau_0}{3\rho\lambda^2 l} \ ,$$

where τ_0 is the natural lifetime of a solitary nucleus, ρ is the density in the active volume, λ is the wavelength of the emitted radiation, and the length is normalized to l, the length of the cylindrical active region. In Fig. 2 we show a typical SF pulse and define some parameters. The phenomenon giving rise to multiple pulses (ringing) has been discussed in the literature (Refs. 3, 7). We will be mostly concerned with single pulses. In Fig. 3 we compare the results obtained with:

(1) the Monte Carlo solution of Eqs. (2-a) through (2-i),

(2) the "triple integral" solution described in Ref. 12,

(3) the average peak result obtained by Haake and Reibold (Ref. 11) and described in Appendix B.

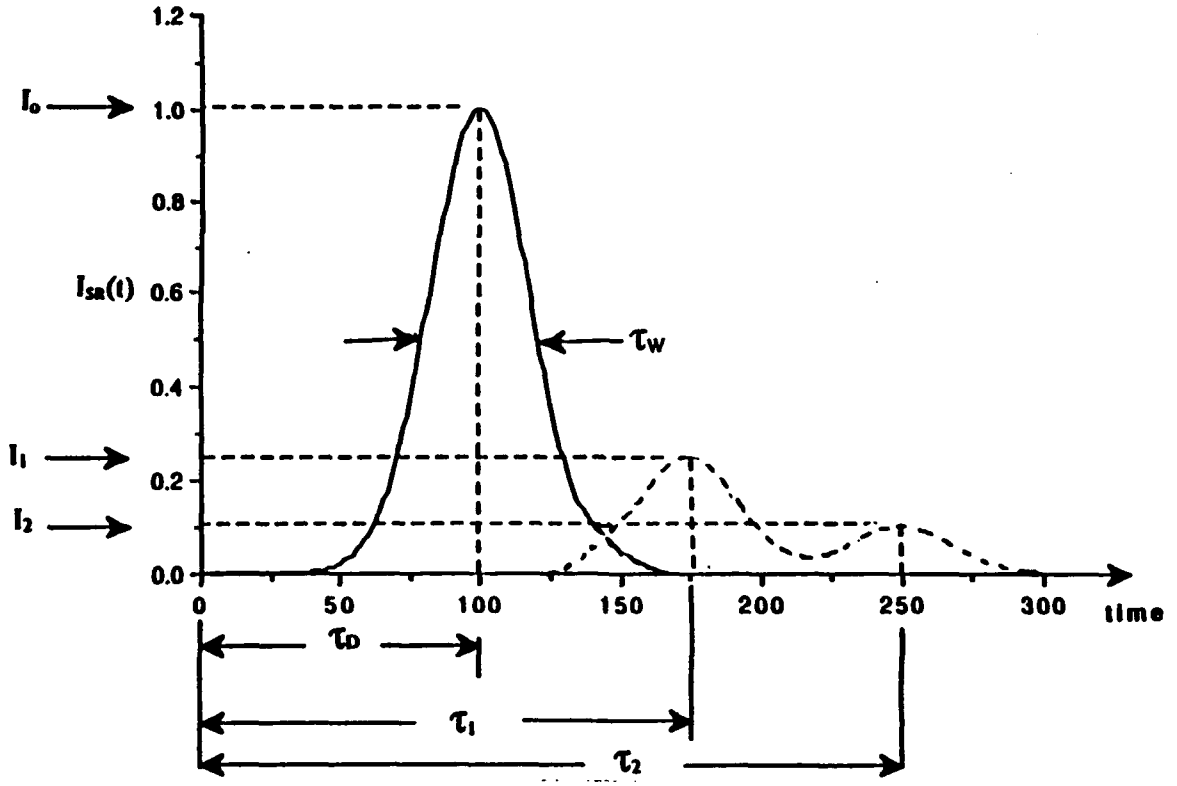

Figure 2. Characteristics of SF Pulses. Generally, one observes one or more pulses. For a single pulse (or the first pulse) indicated by the heavy continuous line, we define a delay time τ_D, and a width τ_W in units of τ_{SF} and an intensity I_o. In the inverted pendulum model (Ref. 7), $\tau_W = \tau_{SF}$. It is observed experimentally in general that $\tau_W > \tau_{SF}$ and this is also obtained from the more sophisticated models. The other pulses, indicated by the dashed line, if present, have their own characteristics.

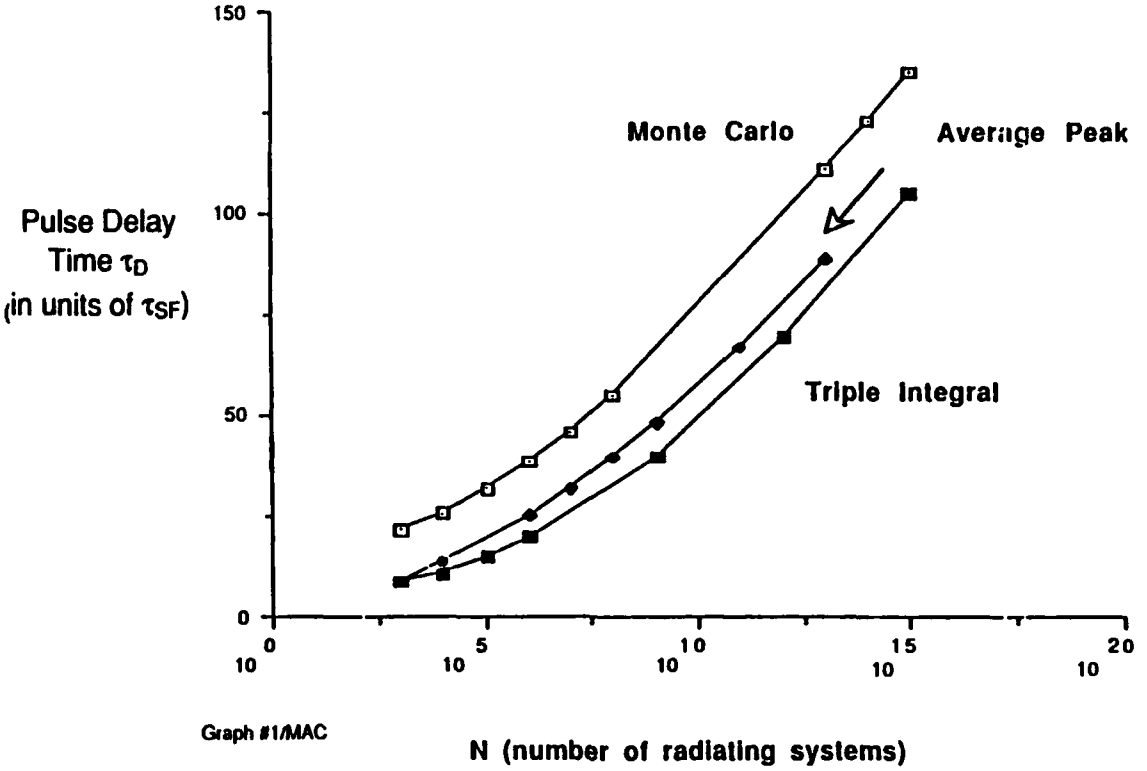

Figure 3. SF Delay Time τ_D versus Number of Cooperating Systems N.

The triple integral solution thus obtained is based on an averaging procedure and average field approximation. Its main benefit is that the key parameters such as N, Γ, and μ are explicitly exhibited in the final analytical result and thus their effect on the evolution of the pulse shape can be easily followed and understood in physically meaningful terms. Averaging over the noise sources, using the assumed statistics and definitions of the correlations as they appear in the analyses, also obviates the need for Monte Carlo numerical techniques. The disadvantage is the loss of generality. The average peak delay time was calculated from an expression (procedure) derived in Ref. 11.

The three curves giving the delay time τ_D as a function of the number of cooperating nuclei, N, for the three different calculations differ by about 40 percent at the low values of N and less than 25 percent at the high values of N in Fig. 3. This is satisfactory agreement considering the different assumptions made in arriving at the results. The Monte Carlo

result was obtained by assuming a standard deviation varying with time as $\sqrt{\frac{\gamma}{N}}\, e^{-\frac{1}{2}\gamma t}$ in the Gaussian noise distribution consistent with Ref. 10. This condition was imposed on the random number generator statistics as described in Appendix A.

In the triple integral (TI) result the noise terms were replaced by their correlations after averaging over space. One would expect a shorter delay because of the loss of spatial variability and reduction of the effect of the lower fields at the left end of the active region. This can be seen more clearly when we look at the spatial distribution of fields in the active volume. The difference in results obtained with the TI calculation and the average peak calculation is, not surprisingly, small, about 5 percent at the high values of N and negligible at the low values.

In Fig. 4 we show the variation of the Monte Carlo results for different values of the variance assumed in the noise distribution. Higher variance means more of the larger noise components in the fluctuations, consequently shorter delay times. The average peak and TI results of Fig. 3 fall somewhere around the value of variance in the noise of 10. The noise source in all of the Monte Carlo calculations varied exponentially with time with the exception of the results shown in Fig. 5. For these calculations in addition to the exponential variation, a square pulse and a step function pulse were used as shown in the insert. All of the pulses had the strength of the exponential at $t = 0$ with the square pulse nonzero between $t = 0$ and t_2, the second time step in the calculation. The step pulse gives the same results as the exponental for low values of the pumping rate γ, whereas the square pulse gives a longer delay at these pumping rates. Note that the SF pulse delay τ_D, indicating the appearance of the SF pulse, is on the order of the pumping time (γ^{-1}). Thus the noise source has a longer time to act on and affect the radiators. For larger pumping rates the exponential and square noise pulses give identical results and the τ_D produced by the step pulse also approaches the same result.

Finally, in this basic computer study we looked at the variation in the individual pulses as the seed of the random number generator was varied. Figure 6a shows the individual pulses and Fig. 6b some average results. For our work, averaging 25-100 pulses seemed sufficient. The statistics of the variation in the pulses as represented by τ_D, τ_W, and I_o, are discussed by Haake and Reibold (Ref. 11).

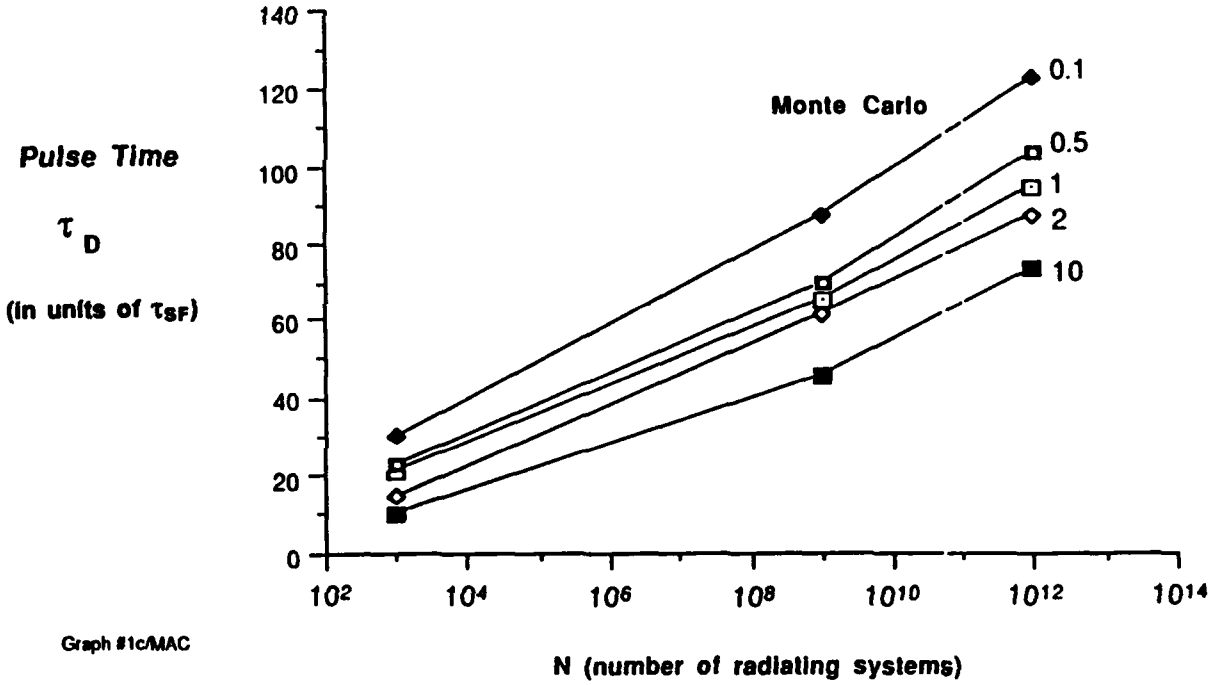

Figure 4. Delay Time τ_D versus Number of Cooperating Systems N. The numbers on the curves represent different values of the noise variance.

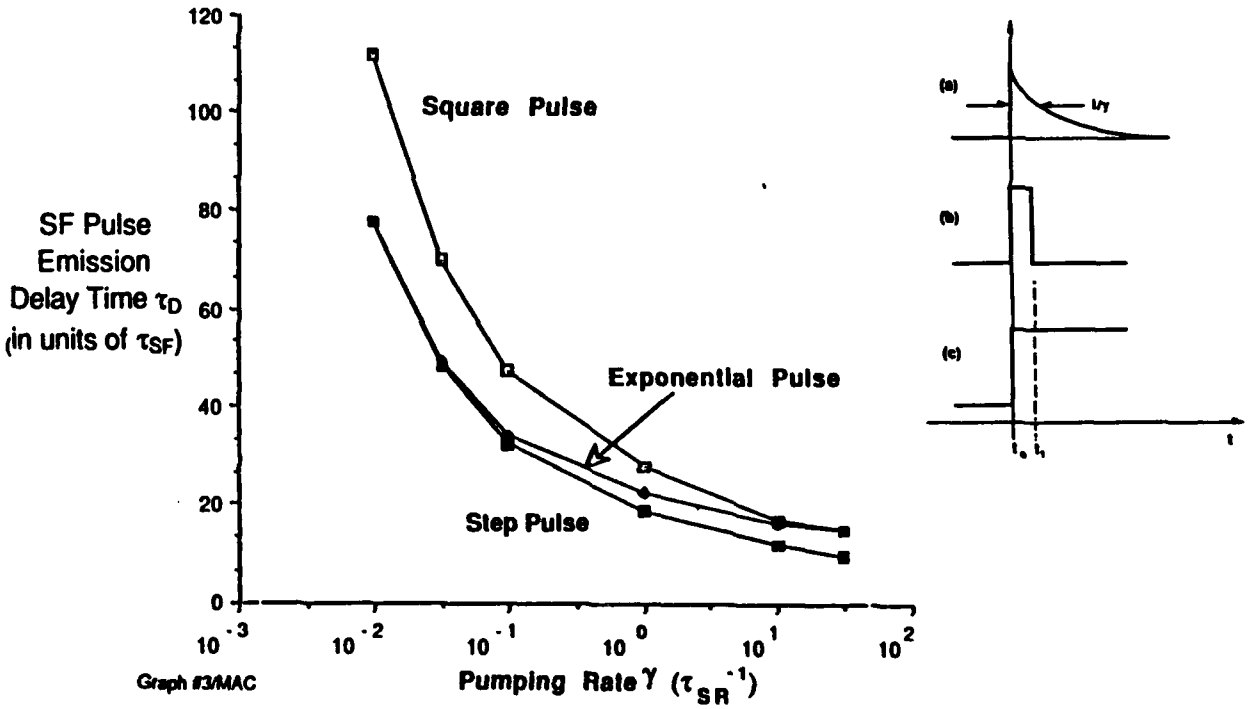

Figure 5. SF Pulse Emission as a Function of the Time Variations in the Strength of the Noise. Square pulse, exponential pulse, and step pulse time variations in the noise strength were used as shown in the inset.

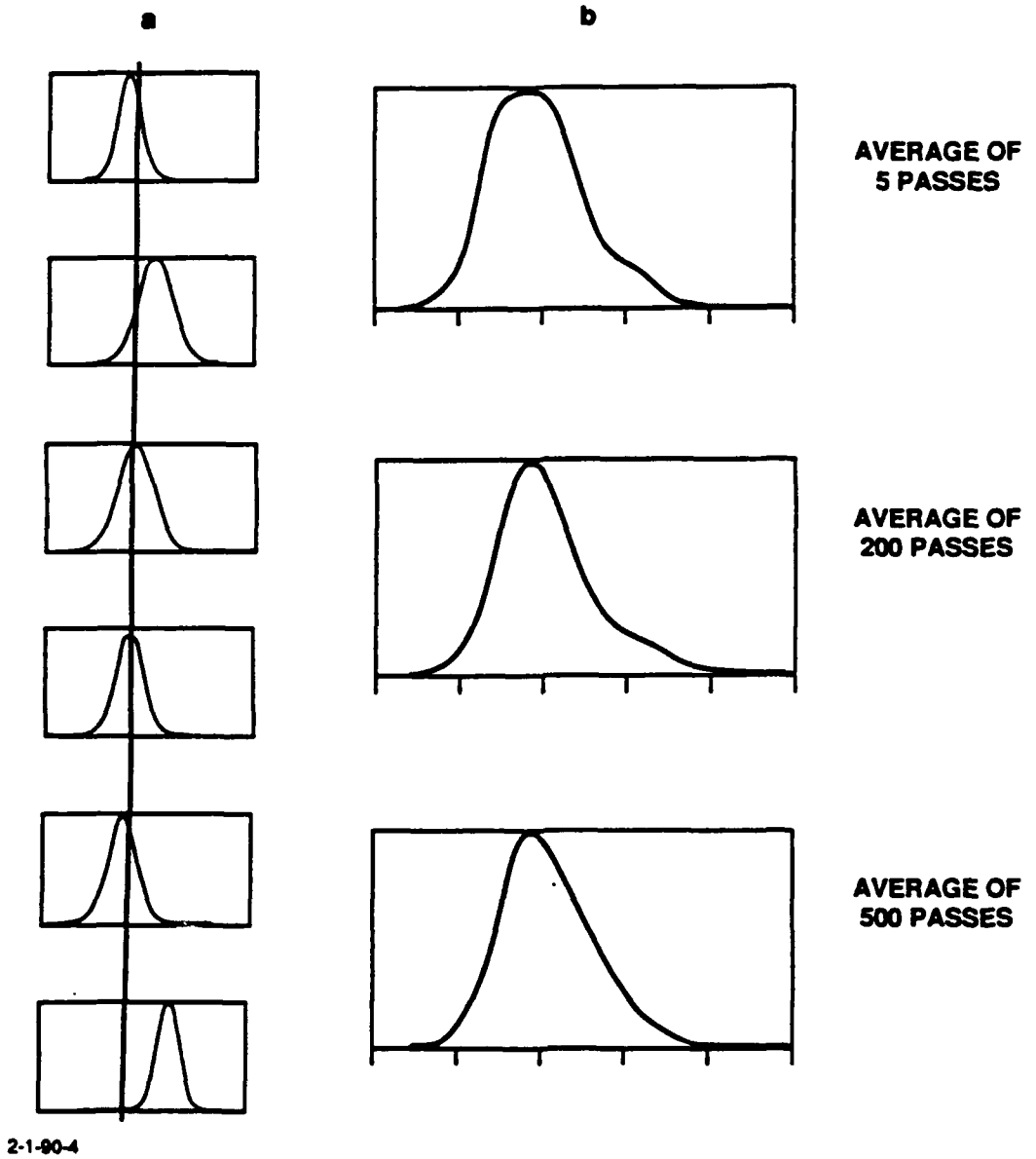

Figure 6. Variations in the Pulses for Different Seed Values of the Random Number Generator. The pulses shown on the left are from single runs with different seeds. The pulses on the right represent averages with different numbers of pulses (5, 200, 500) as shown above.

D. COMPUTER CALCULATIONS, PART B

In this chapter we first discuss the pulse characteristics as a function of the pumping rate γ, the linear attenuation coefficient μ, and the inhomogeneous and homogeneous broadening parameters a and b for different numbers of cooperating nuclei. We then present some results which show both the spatial distribution of fields in the active region and the temporal pulse evolution under different conditions. The spatial distributions can be displayed on the terminal screen of a computer as a series of time-delayed curves simulating a movie of the phenomena occurring in the active region.

In Fig. 7 we show the pulse emission delay time as a function of the pumping rate for three values of the cooperation number ($N = 10^3, 10^8, 10^{12}$). In units of τ_{SF} for larger N the delay time increases, but in physical units (seconds) the delay time actually decreases because τ_{SF} goes like $\frac{1}{N}$. If the pumping time is essentially over before the pulse starts, the pumping rate has no effect on the pulse shape.

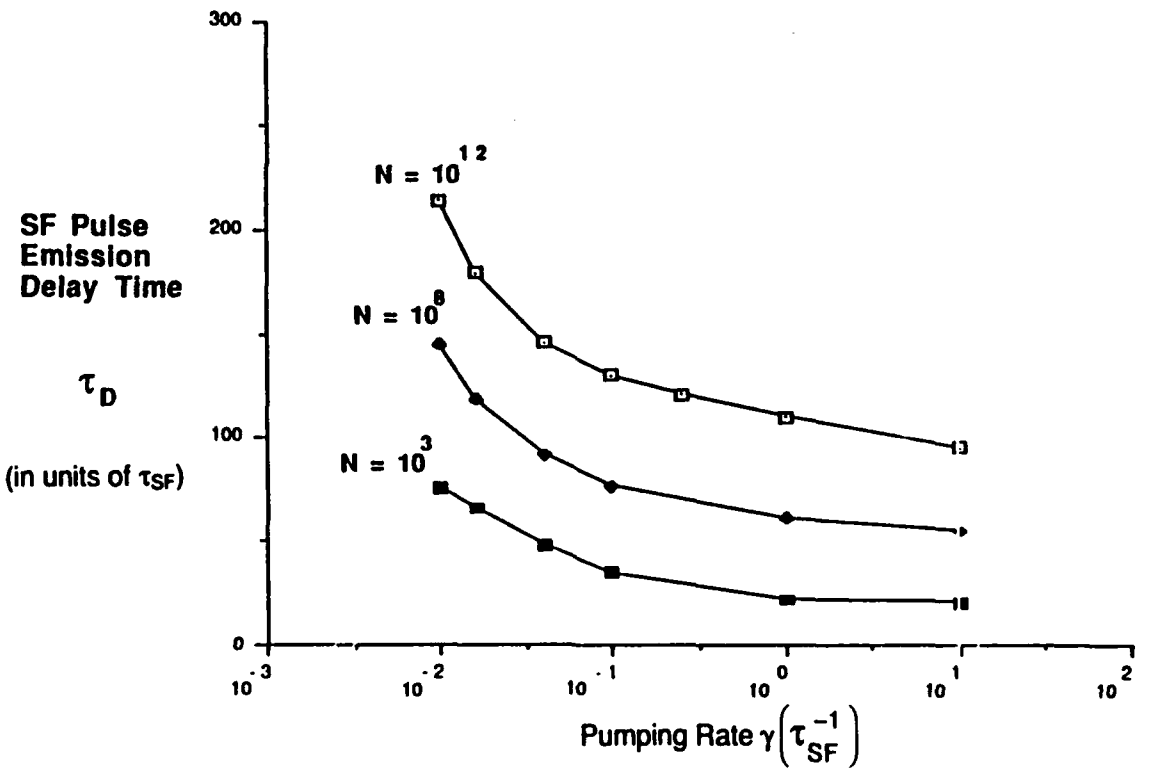

Figure 7. SF Pulse Emission Delay Time τ_D as a Function of the Pumping Rate γ for Different Values of the Cooperation Number N. Note that although the delay time is greater for larger N when expressed in units of τ_{SF} it is actually smaller when expressed in seconds because τ_{SF} goes like $\frac{1}{N}$.

We have already discussed the nonthreshold-like effect of the attenuation coefficient μ on the SF phenomena (Ref. 3). The attenuation shifts the peak to longer times. If there are no dephasing mechanisms reducing the dipole being built up by the quantum fluctuations (noise term ξ) the SF peak will decrease but not completely disappear. This will happen unless the inversion is destroyed by some depopulation process, like internal conversion or some other competing transition. This gradual decrease in the peak due to μ is characteristic of SF. A stimulated emission process, on the other hand, shows a threshold beyond which no gain occurs.

Figures 8 and 9 exhibit these trends, with Fig. 8 showing the increase in the delay time as μ increases, and Fig. 9 showing the decrease of the peak intensity, which will eventually reach the value of uncooperative spontaneous emission as μ is increased.

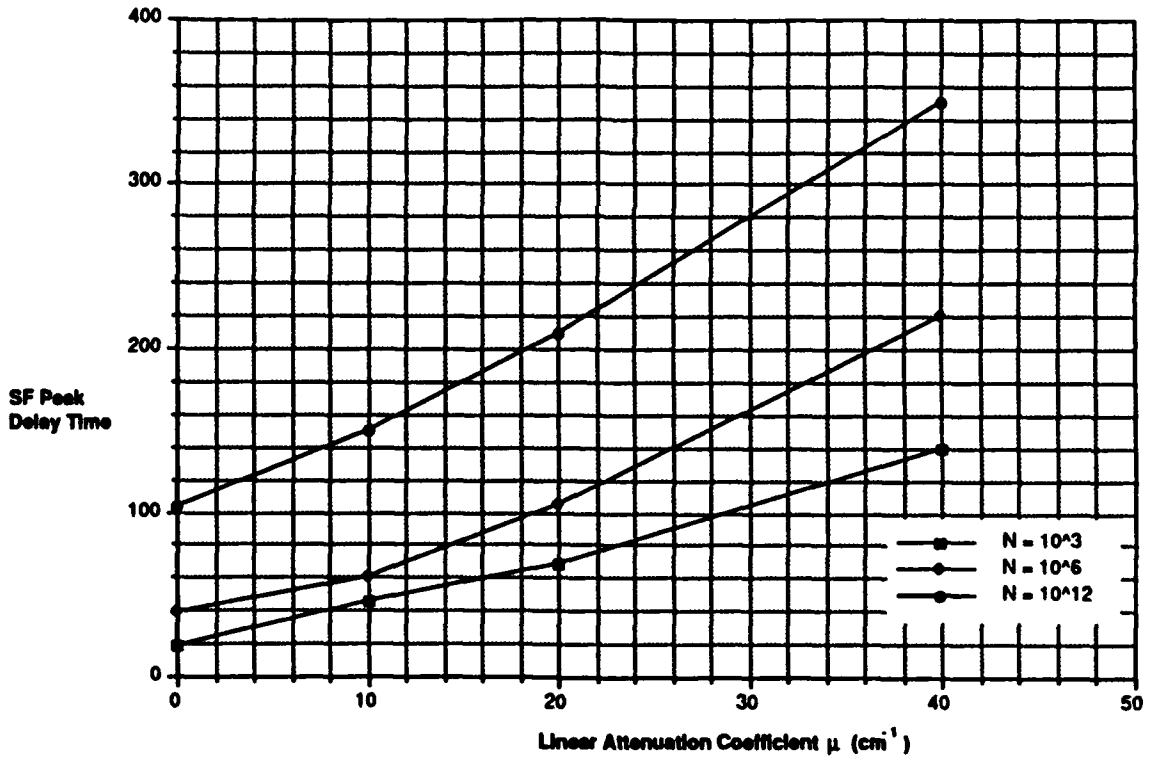

Figure 8. SF Pulse Emission Delay Time τ_D as a Function of the Linear Attenuation Coefficient μ for Different Values of the Cooperation Number N.

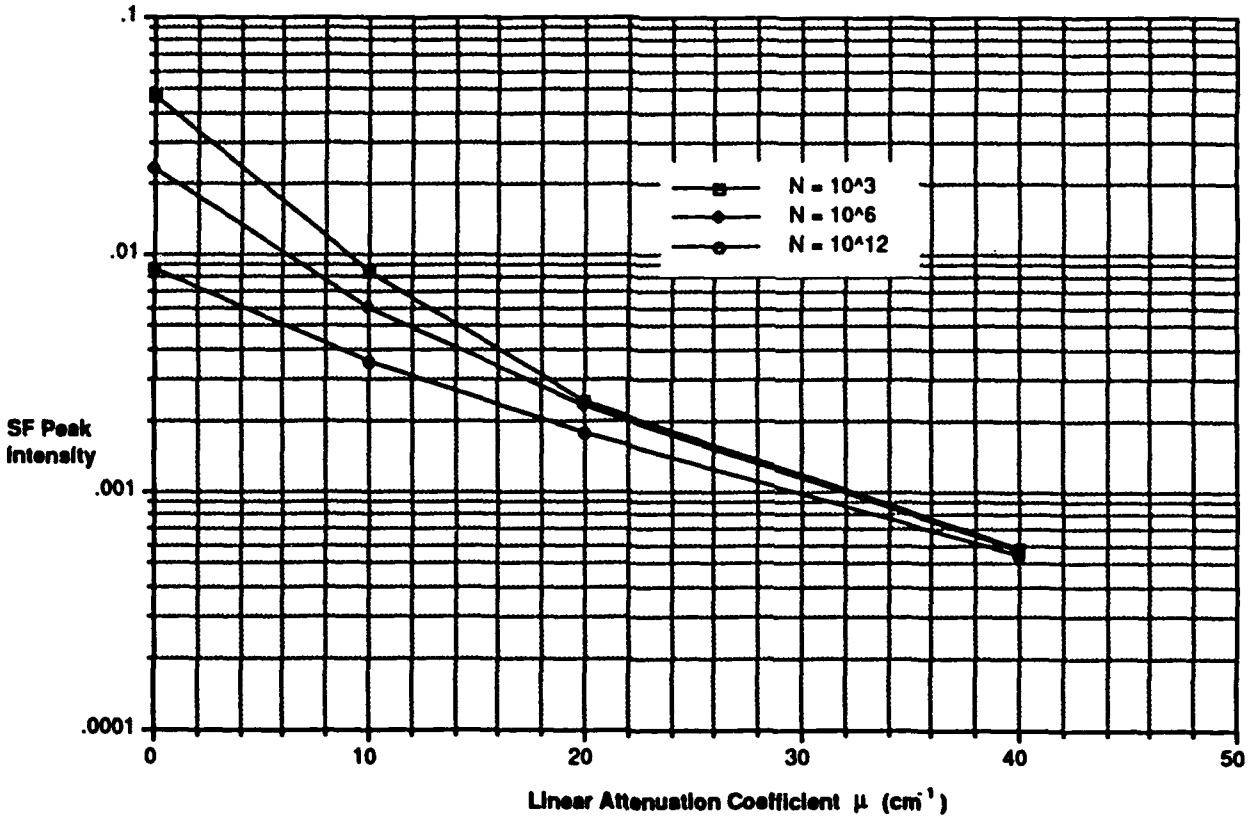

Figure 9. SF Pulse Emission Intensity I_o as a Function of the Linear Attenuation Coefficient μ for Different Values of the Cooperation Number N.

We now turn to the line-broadening mechanisms. Homogeneous broadening appears in the Maxwell-Bloch equations only through the dephasing rate $\Gamma_\phi = b\Gamma_3$, where b is the homogeneous broadening parameter and Γ_3 the natural decay rate of level 3. Inhomogeneous broadening is taken account of in the Maxwell equation (2-h) through the time dependence of the coupling parameter $g_i(t)$, consistent with the results of Ref. 7 and Ref. 13. We assume this dependence to be exponential in time with a decay rate or dephasing rate of $\Gamma_\theta = a\Gamma_3$.

The relation of the dephasing factor to the individual, slightly different, resonance energies at different nuclei (inhomogeneous broadening) is discussed in Chapter II of this report. In that chaper we also show how relaxation can reduce the broadening effect and thereby recover the SF pulse. In the present paper we study the production of the SF pulse as a function of b or a, described by Eqs. (2-a)-(2-i).

The results are shown in Figs. 10a and 10b where the natural decay was assumed to be $\Gamma = 10^{-4}$. At low values of b or a (when $\Gamma_\phi, \Gamma_\theta << \tau_D^{-1}$) there is no noticeable effect on either the delay time or the intensity. At around b, $a = 10^2$ ($\Gamma_\phi, \Gamma_\theta = 10^{-2}$) the pulse delay increases, and reaches a maximum, while the intensity starts to decrease. For b, $a > 10^3$ the delay time decreases but the intensity drops to the spontaneous non-cooperative value. The increase in τ_D occurs during the time when the dephasing effect of Γ_ϕ or Γ_θ partially neutralizes the correlations built up by the electric field vacuum state fluctuations, and consequently more time is required to build up the SF pulse. The decrease of both τ_D and I_o indicates the complete breakup of SF past a certain time, and thus only the initial part of the SF peak appears, but becomes smaller as a or b increases. The only difference between the effects of a and b on the SF pulse is the stronger reduction in the peak intensity I_o and the more pronounced increase in the delay time τ_D due to the inhomogeneous broadening as compared to the homogeneous broadening, for the same amount of broadening a = b.

Some insight into the difference between homogeneous and inhomogeneous broadening in producing an effect on the SF emission can be obtained by considering equations (2-f) through (2-i). Restricting ourselves to one transition (3 to 1) only, after dropping the subscripts we have

$$\frac{\partial R^{\pm}}{\partial t} = f(x,t)E^{\pm} - \frac{1}{2}\left[\Gamma + \Gamma_\phi\right]R^{\pm} + \xi^{\pm} \qquad (2\text{-g})'$$

$$\frac{\partial E^{\pm}}{\partial x} = g_1(t)R^{\pm} - \frac{1}{2}\mu E^{\pm} \qquad (2\text{-i})'$$

where $f(x, t) = 2N_3(t) + N_4(t) - N_o$.

Equation (2-g)' and (2-i)' can be combined together, assuming an exponential form of g(t),

$$\frac{\partial^2 E^{\pm}}{\partial t \partial x} = \left[g(t)\, f(x,t) - \frac{1}{4}\left(\Gamma + \Gamma_\phi + \Gamma_\theta\right)\mu \right]E^{\pm}$$

$$- \frac{1}{2}\left(\Gamma + \Gamma_\phi + \Gamma_\theta\right)\frac{\partial E^{\pm}}{\partial x} - \frac{1}{2}\mu\frac{\partial E^{\pm}}{\partial t} + g(t)\xi^{\pm}$$

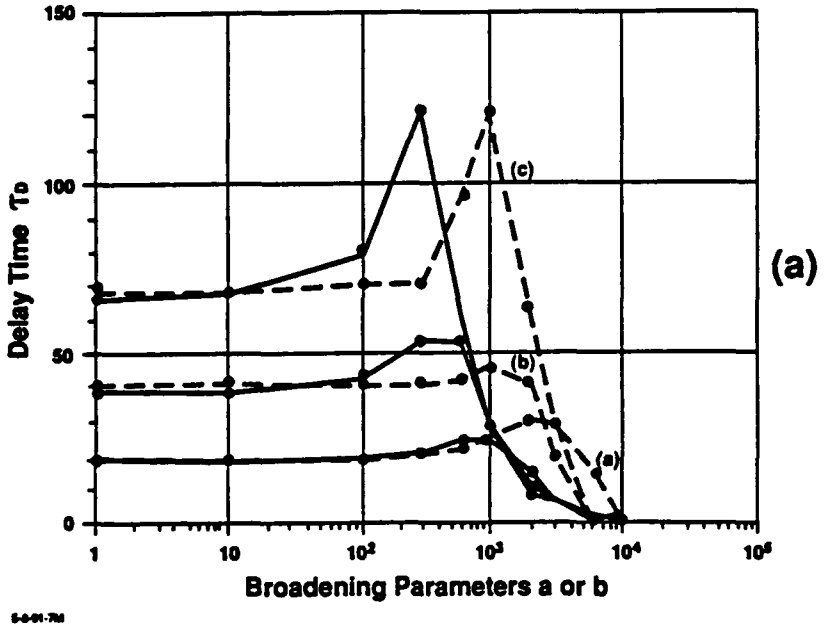

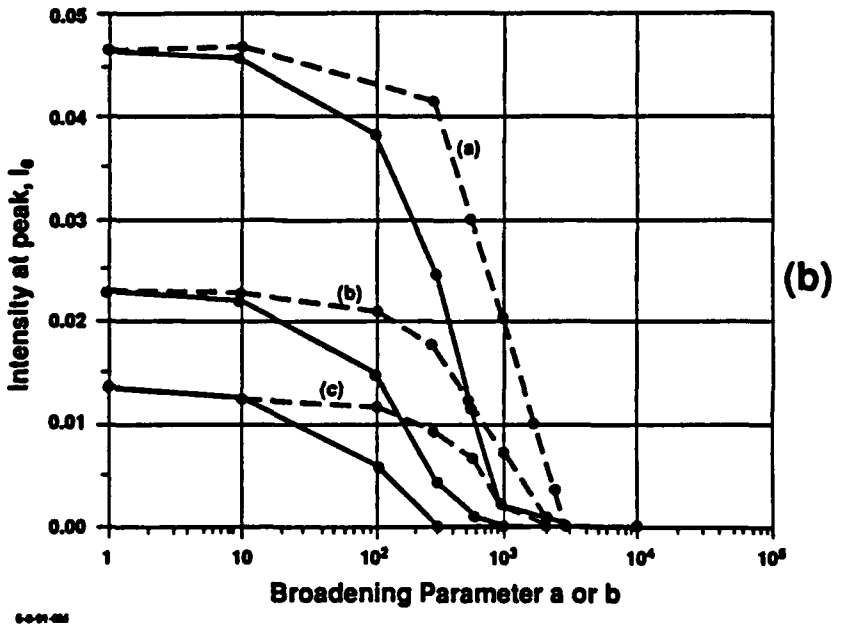

Figure 10(a). SF Pulse Emission Delay Time τ_D as a Function of the Homogeneous Broadening Parameter b (solid line) and the Inhomogeneous Broadening Parameter a (dashed line). Curves (a), (b) and (c) were obtained with N = 10^3, 10^6, 10^9, respectively. (b) SF Pulse Emission Intensity I_o as a Function of the Broadening Parameters a and b.

We see from the above that the inhomogeneous broadening not only contributes an additional term to the homogeneous effect but also through the time dependence on g(t) reduces the coupling. This enhanced destructive effect is reflected in our Monte Carlo results. Figure 8 exhibits the effect of the two broadening mechanisms on the full SF pulse shape when a and b take on the values 200, 500, and 1000. In Figs. 11(a), (b), and (c) a = 0 and in Figs. (d), (e) and (f) b = 0. In Fig. 11(a) the dashed line represents, for comparison, the pulse with no broadening a = b = 0, and the solid line, the pulse when a = 0, b = 200. As expected, from Figs. 10(a) and (b) the pulse intensity decreases more with inhomogeneous broadening and the pulse spreads out more than with the homogeneous broadening. The delay time is also affected differently at these values of the parameters.

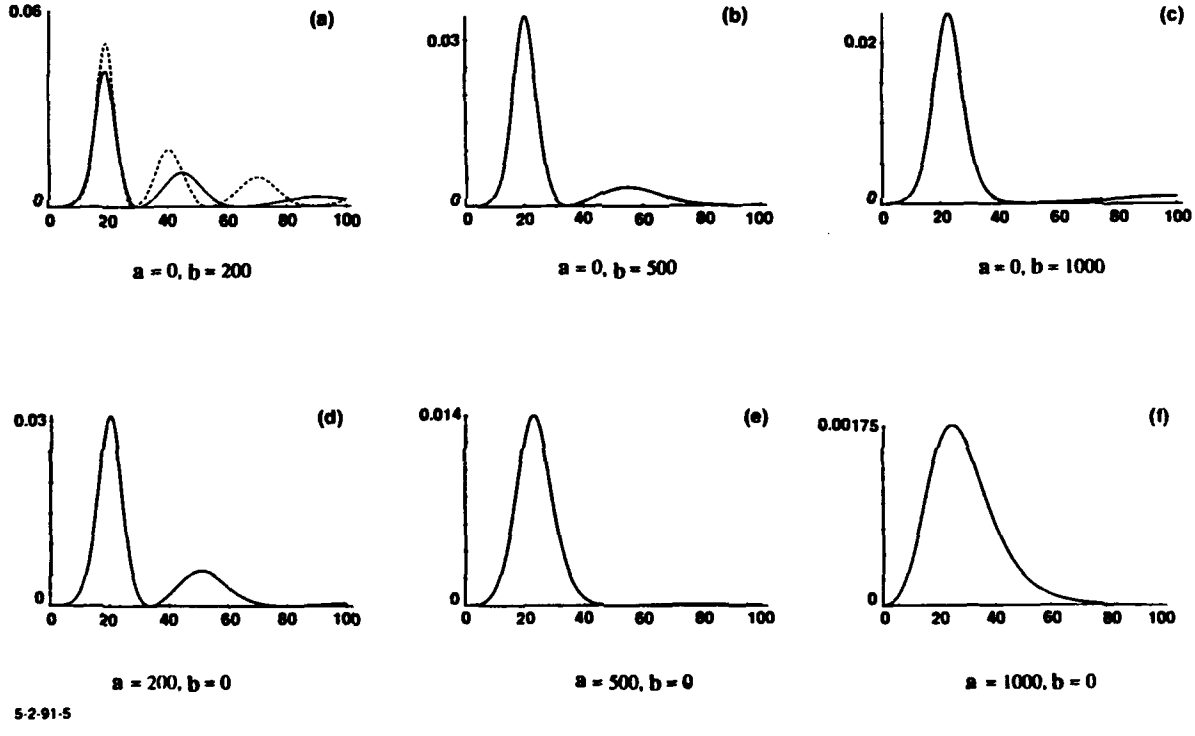

Figure 11. SF Pulse Emission Intensity I_o as a Function of the Homogeneous Broadening Parameter a and the Inhomogeneous Broadening Parameter b.

E. TEMPORAL VARIATION OF FIELDS INSIDE THE ACTIVE MEDIUM

The solution of Eqs. (2-a)-(2-h) is a function of space and time. We have so far discussed the emission of the SF pulse from the right face of the active medium as a function of the characteristics of the medium. This is what would be measured in an experiment. It is interesting to make use of the information about the activity in the medium as the pulse develops and propagates through the medium. We are considering the geometry shown in Fig. 12.

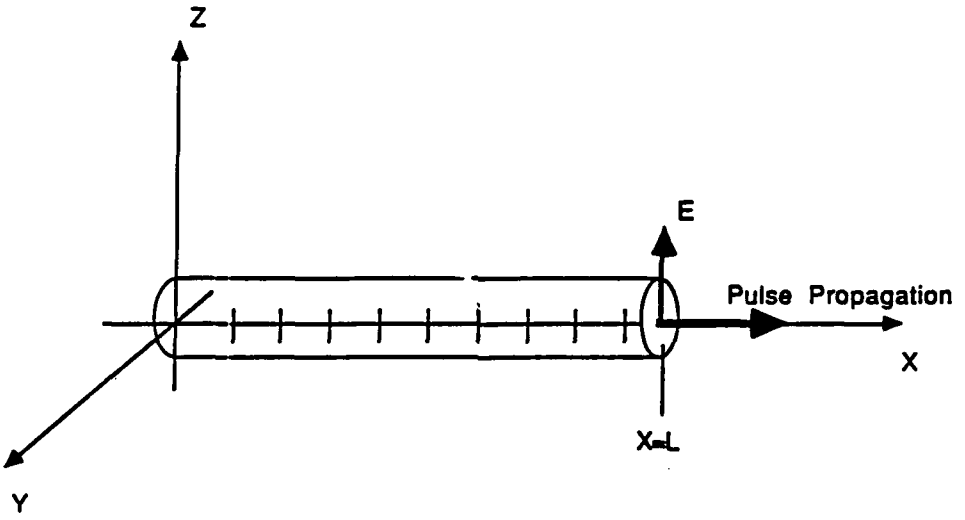

Figure 12. Schematic of the Geometry Used in the Calculations of the Internal Fields in the Active Region.

The fields inside the medium ($o < x < l$) are functions of x and t, polarized in the z direction. The fields at $x = l$ give the emitted pulse propagating in the positive x direction. The results of our study are summarized by eight runs for the parameters given in Table 2.

The result of the eight runs are shown in three types of figures. One set of figures (type 1) gives the temporal variation of the normalized level densities N_4, with initial values $N_4(0) = 1$, $N_3(t)$ and $N_1(t)$ with initial values zero, $E^+(t)$ and I(t). These parameters are plotted in Figs. 13-20 with N_4, N_3, N_1, E^+ and I plotted as graphs (a)-(f) of these figures, respectively. The second set of figures (type 2) gives the spatial variation of $E^+(x)$, $R^+(x)$ and I(x) at selected times. The electric field E^+ for the different runs is plotted in Figs. 20(a)-28(a), polarization $R^+(x)$ in Figs. 20(b)-28(b) and the intensity in Figs. 20(c)-28(c). The final set of figures (type 3) gives three dimensional plots of intensity I(x,t), as a function of position in the active medium and time. These plots are given in Figs. 28-36 for runs 1 through 8, respectively, with the parameters for these runs given in Table 2.

Table 2. Parameter Values Characterizing the SF Calculations of Runs 1-8

Parameter	Run No.							
	1	2	3	4	5	6	7	8
γ	10	10	1	0.1	10	10	1	10
Γ	10^{-4}	10^{-4}	10^{-4}	10^{-4}	10^{-4}	10^{-4}	10^{-2}	10^{-3}
μ	0	0	0	0	10	5	5	5
N	10^{3}	10^{6}	10^{3}	10^{3}	10^{3}	10^{3}	10^{3}	10^{3}

For runs with $\mu = 0$ (1, 2, 3, 4) the spatial variations of the fields, in particular the intensity, is monotonically increasing with an increasing slope, whereas for runs with $\mu \neq 0$ (runs 5, 6) the electric field changes sign; consequently, at some point in the region the intensity goes to zero. From Eq. (2-h), which gives the only gradient term, one can see that this happens when the build up in the polarization and the electric field are such that

$$E(x) = g_1 \int_0^x R(x) - \mu \int_0^x E(x) = 0 \quad .$$

This result clearly indicates that for maximum intensity out of the active region the length of the region has to be carefully selected with consideration of the attenuation μ in the medium and the coupling constant g_1 between the nuclei and the electromagnetic field. The actual position of the null in the intensity is not an obviously simple function of μ and cannot be obtained from analyses, such as the triple integral approach, which average over the spatial variable. In runs 7 and 8 there is a minimum but not a complete extinction of the field at some x value. Further analysis of the transport phenomena is required to understand the full significance of the effect of propagation in the active region and the generation of the SF pulses for arbitrary conditions.

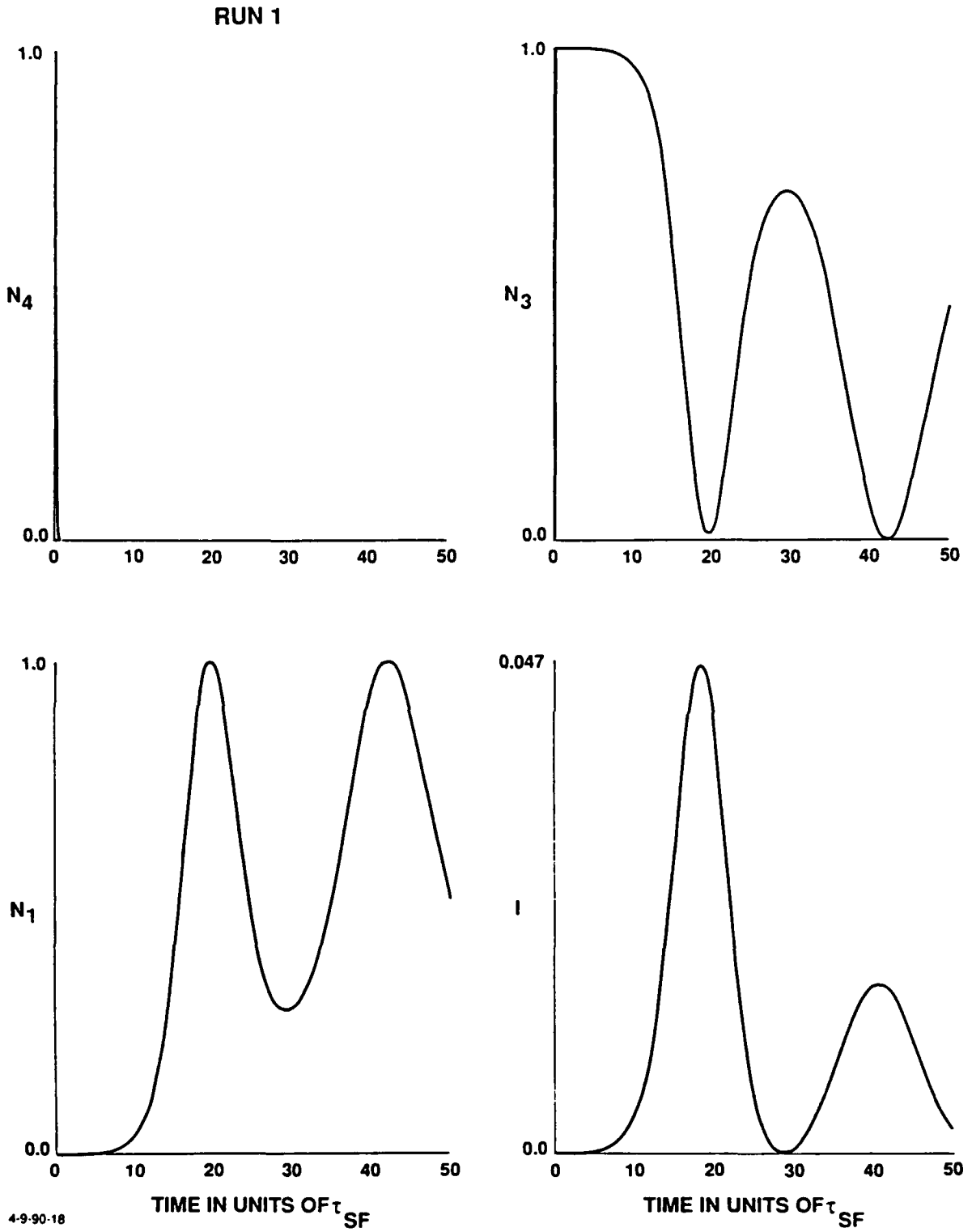

Figure 13. SF Pulse Characteristics for Input Parameters of Run 1 (see Table 2). The top two curves show the variation of level densities N_4 and N_3, calculated at x = *l*. The bottom two curves give the level density N_1 and the pulse intensity. ($\gamma = 10$, $\Gamma = 10^{-4}$, $\mu = 0$, $N = 10^3$)

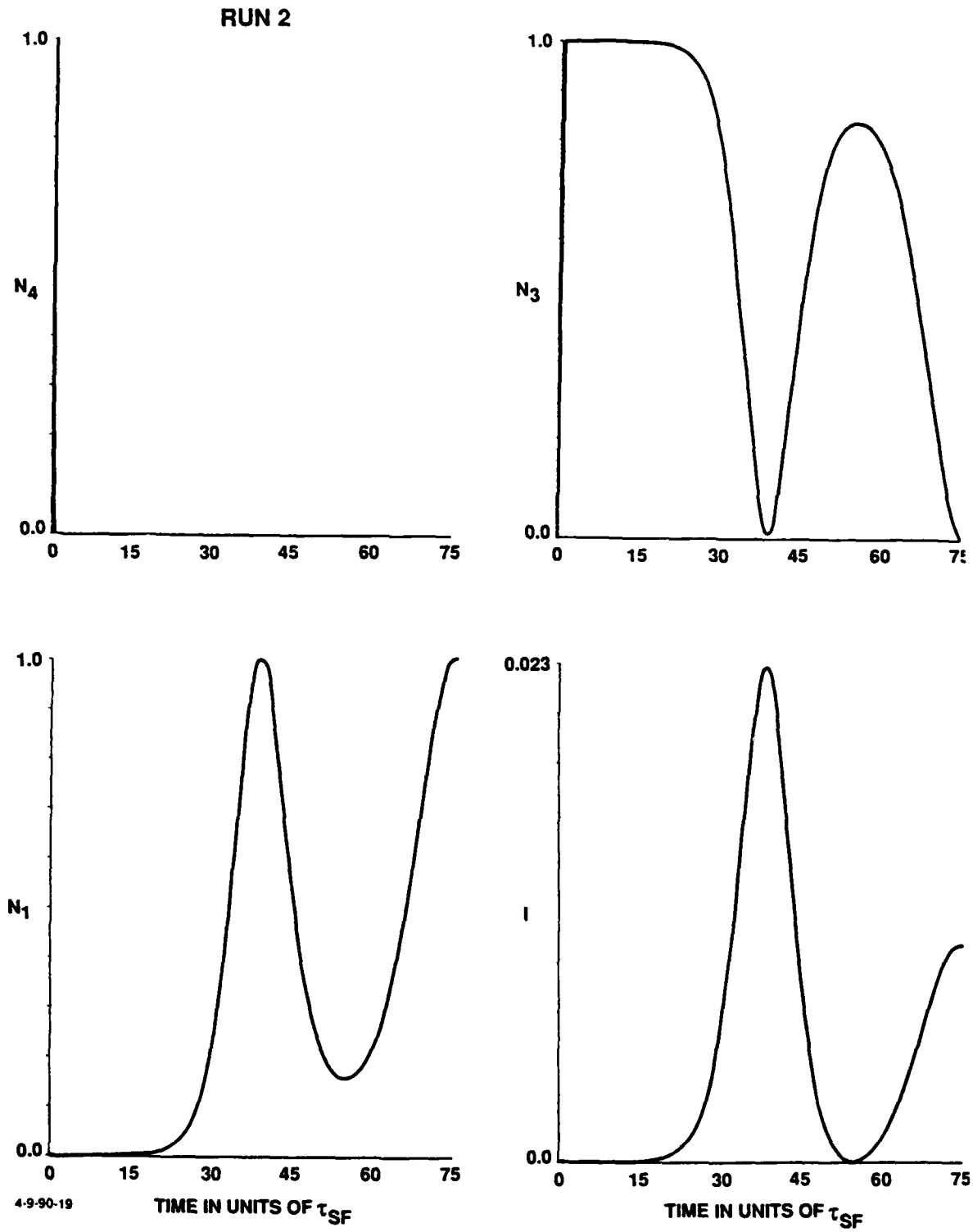

Figure 14. SF Pulse Characteristics for Input Parameters of Run 2 (see Table 2). The top two curves show the variation of level densities N_4 and N_3, calculated at x = *l*. The bottom two curves give the level density N_1 and the pulse intensity. ($\gamma = 10$, $\Gamma = 10^{-4}$, $\mu = 0$, $N = 10^6$)

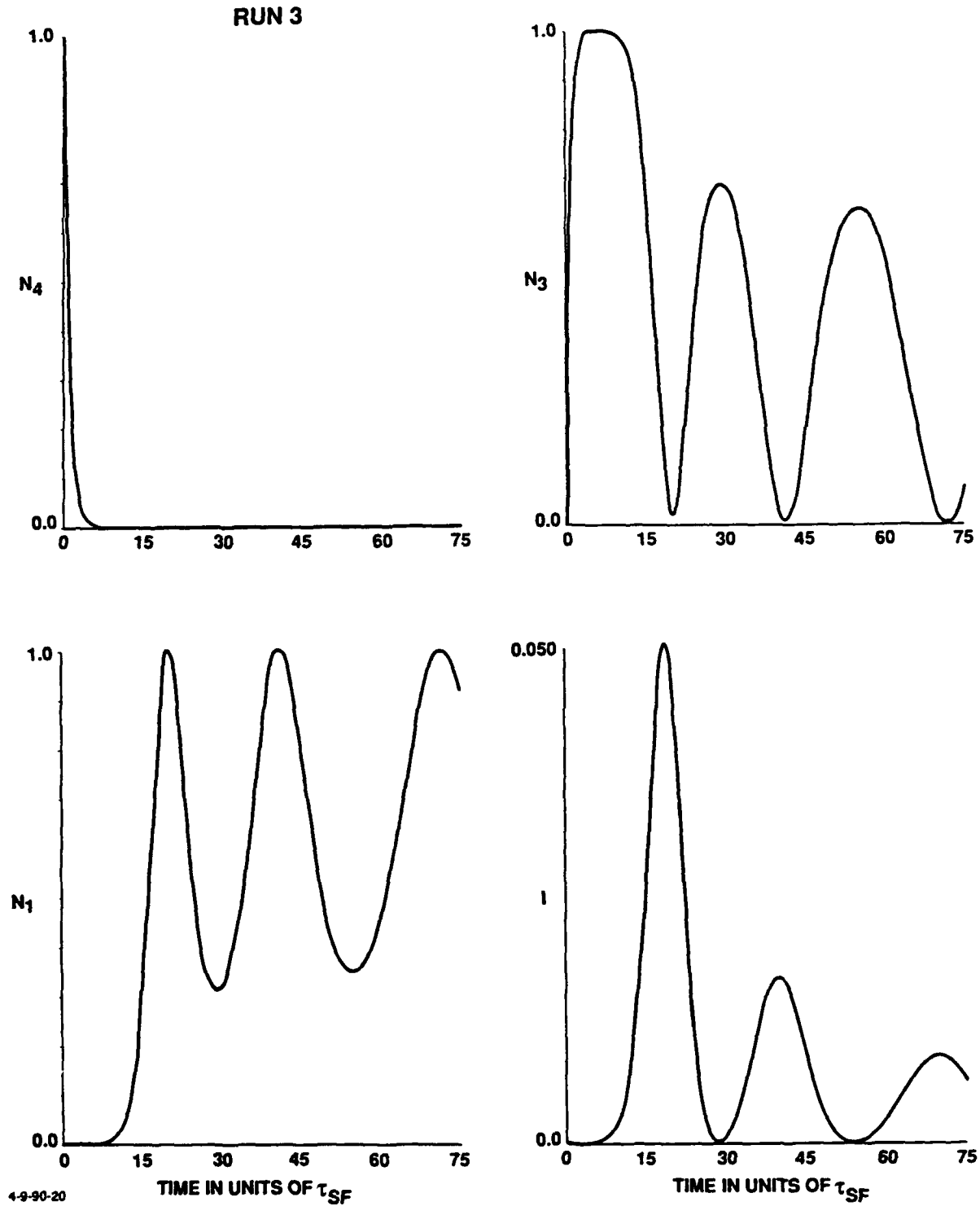

Figure 15. SF Pulse Characteristics for Input Parameters of Run 3 (see Table 2). The top two curves show the variation of level densities N_4 and N_3, calculated at $x = l$. The bottom two curves give the level density N_1 and the pulse intensity. ($\gamma = 1$, $\Gamma = 10^{-4}$, $\mu = 0$, $N = 10^3$)

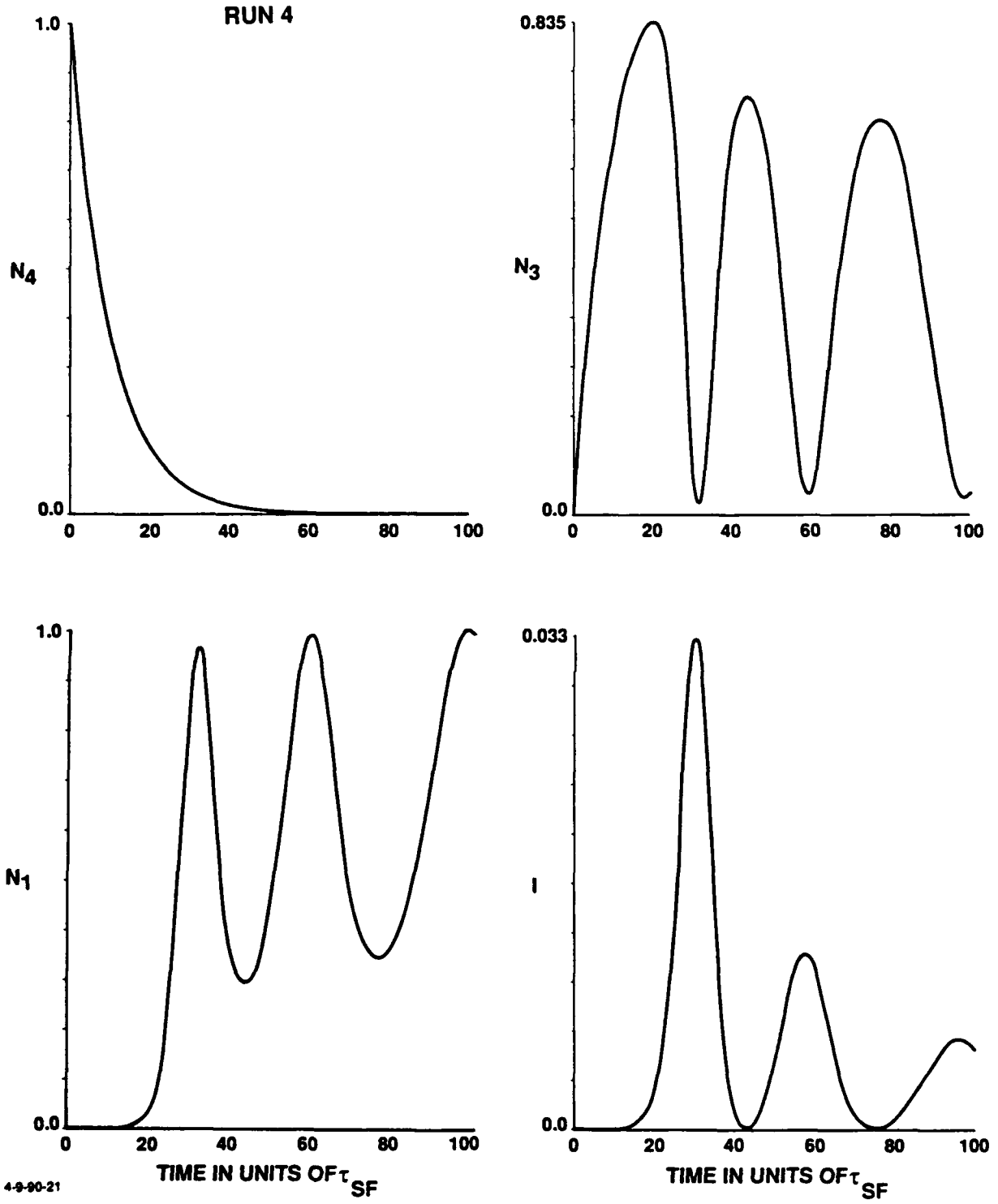

Figure 16. SF Pulse Characteristics for Input Parameters of Run 4 (see Table 2). The top two curves show the variation of level densities N_4 and N_3, calculated at x = *l*. The bottom two curves give the level density N_1 and the pulse intensity. ($\gamma = 0.1$, $\Gamma = 10^{-4}$, $\mu = 0$, $N = 10^3$)

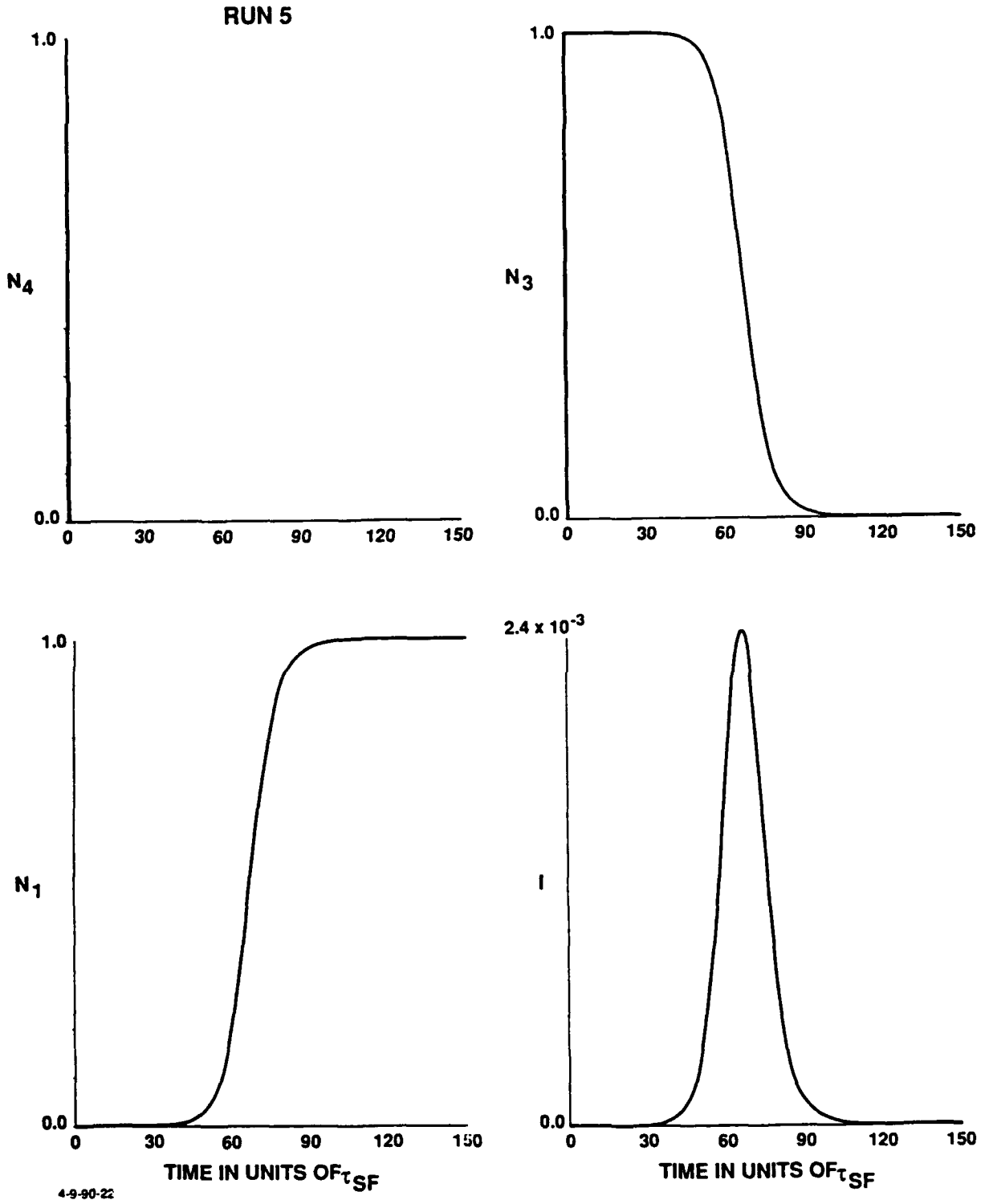

Figure 17. SF Pulse Characteristics for Input Parameters of Run 5 (see Table 2). The top two curves show the variation of level densities N_4 and N_3, calculated at x = *l*. The bottom two curves give the level density N_1 and the pulse intensity. ($\gamma = 10$, $\Gamma = 10^{-4}$, $\mu = 10$, $N = 10^3$)

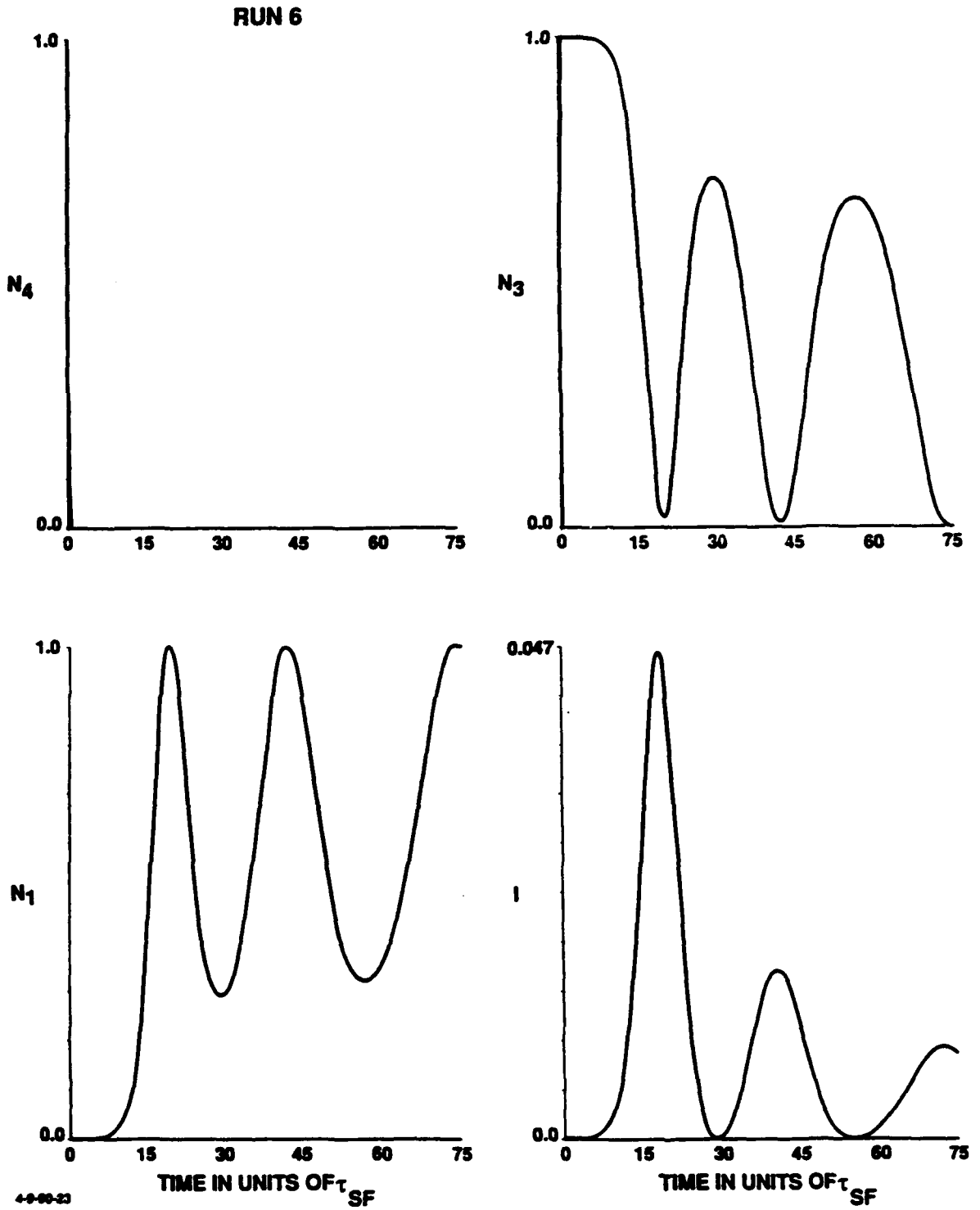

Figure 18. SF Pulse Characteristics for Input Parameters of Run 6 (see Table 2). The top two curves show the variation of level densities N_4 and N_3, calculated at $x = l$. The bottom two curves give the level density N_1 and the pulse intensity. ($\gamma = 10$, $\Gamma = 10^{-4}$, $\mu = 5$, $N = 10^3$)

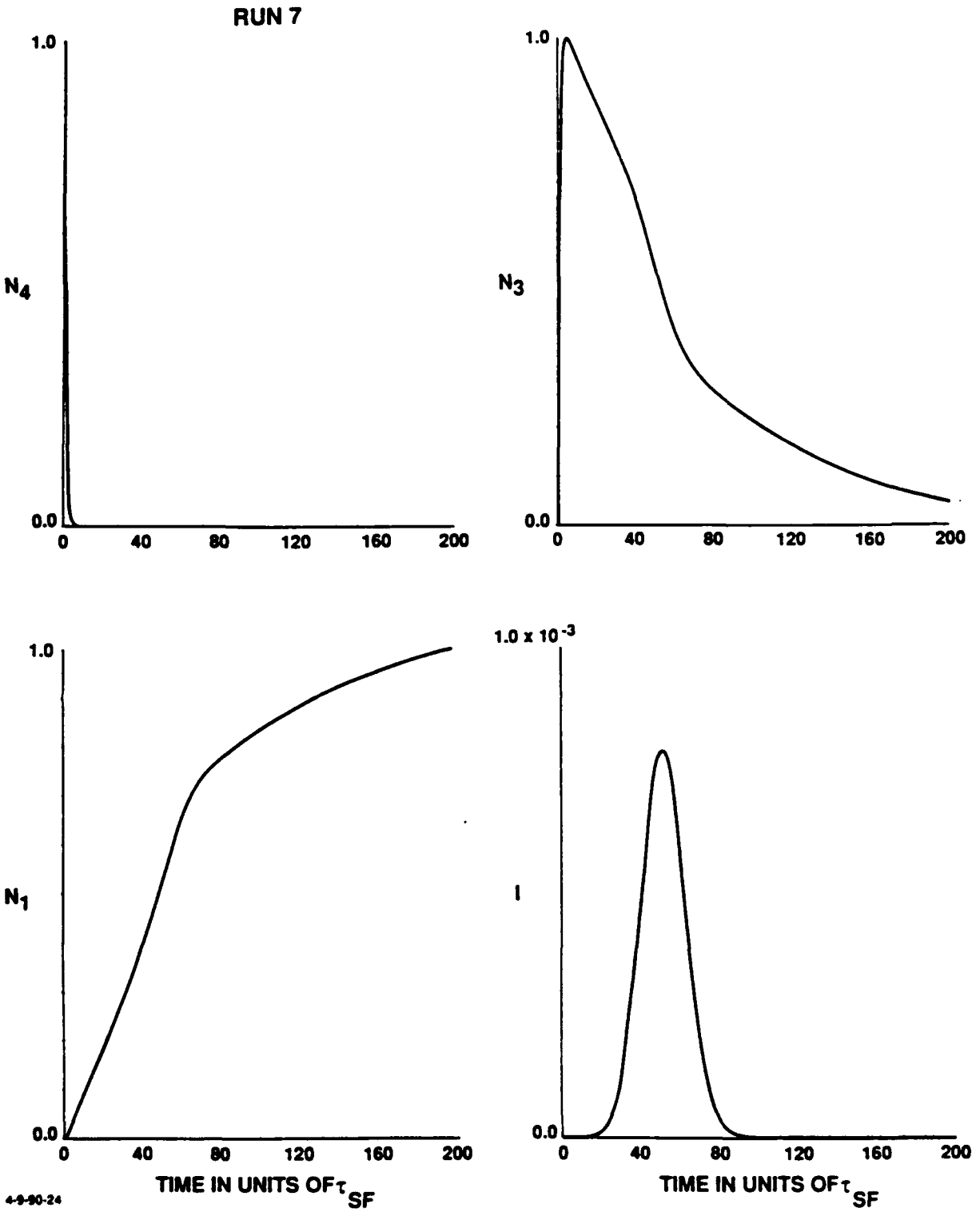

Figure 19. SF Pulse Characteristics for Input Parameters of Run 7 (see Table 2). The top two curves show the variation of level densities N_4 and N_3, calculated at $x = l$. The bottom two curves give the level density N_1 and the pulse intensity. ($\gamma = 1$, $\Gamma = 10^{-2}$, $\mu = 5$, $N = 10^3$)

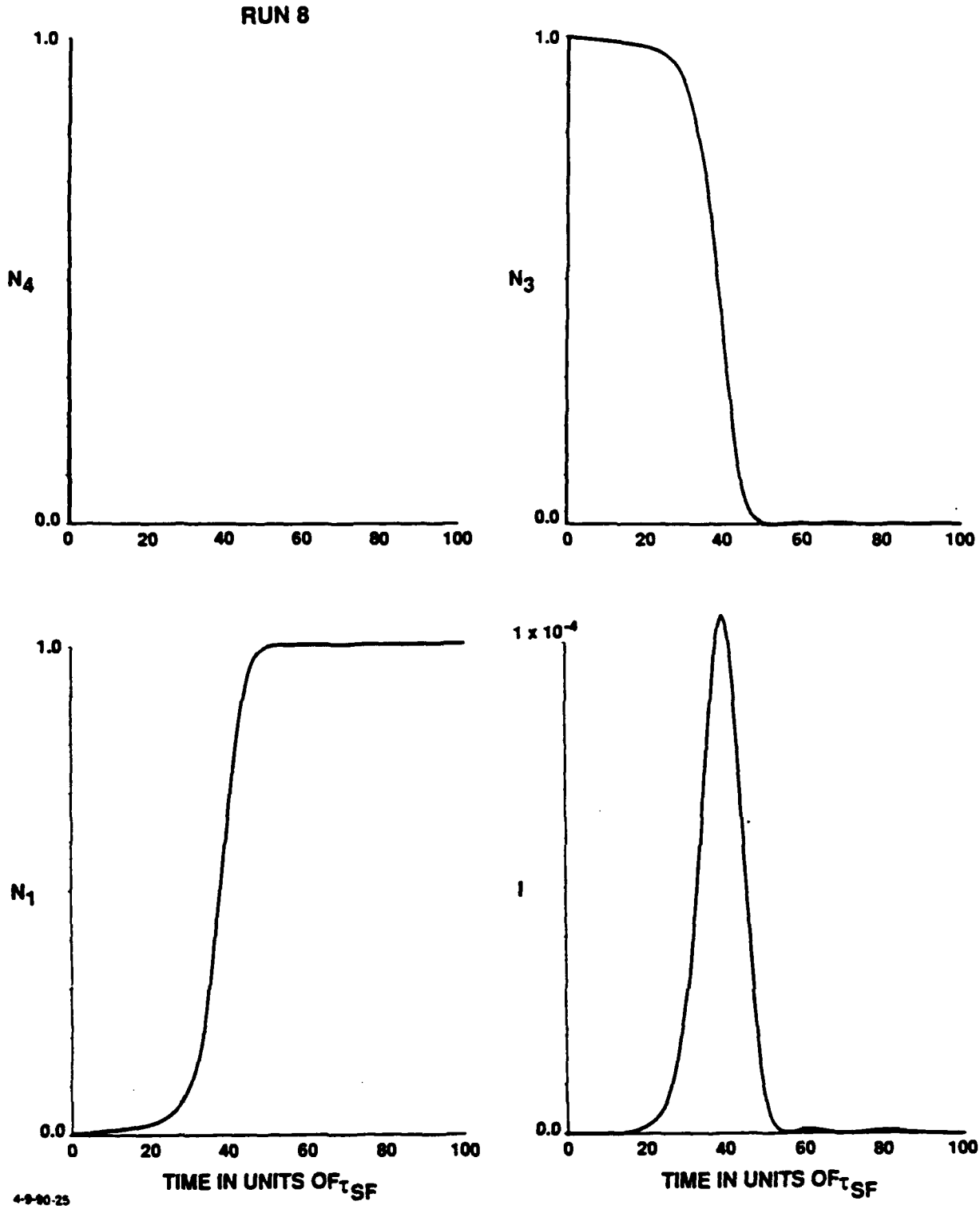

Figure 20. SF Pulse Characteristics for Input Parameters of Run 8 (see Table 2). The top two curves show the variation of level densities N_4 and N_3, calculated at $x = l$. The bottom two curves give the level density N_1 and the pulse intensity. ($\gamma = 10$, $\Gamma = 10^{-3}$, $\mu = 5$, $N = 10^3$)

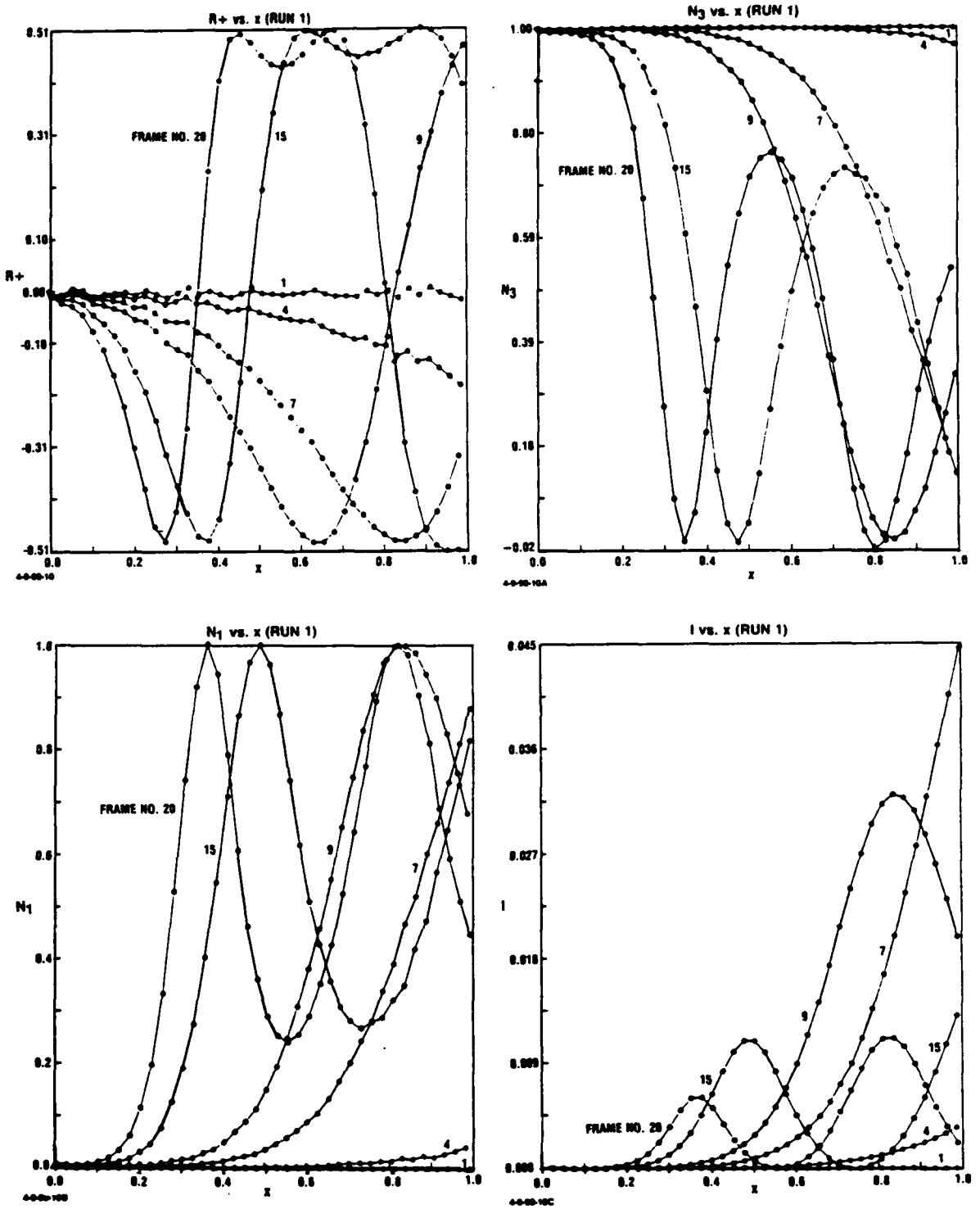

Figure 21. Plot of the Spatial Variation of the Polarization $R^+(x)$, Number Density $N_3(x)$, Field $N_1(x)$, and Intensity $I(x)$ at Different Times Indicated by Frame Numbers. The times corresponding to frame numbers are given by 2.5 τ_{SF} x (frame number) and the pulse corresponding to these data (Run 1) as shown in Fig. 13. ($\gamma = 10$, $\Gamma = 10^{-4}$, $\mu = 0$, $N = 10^3$)

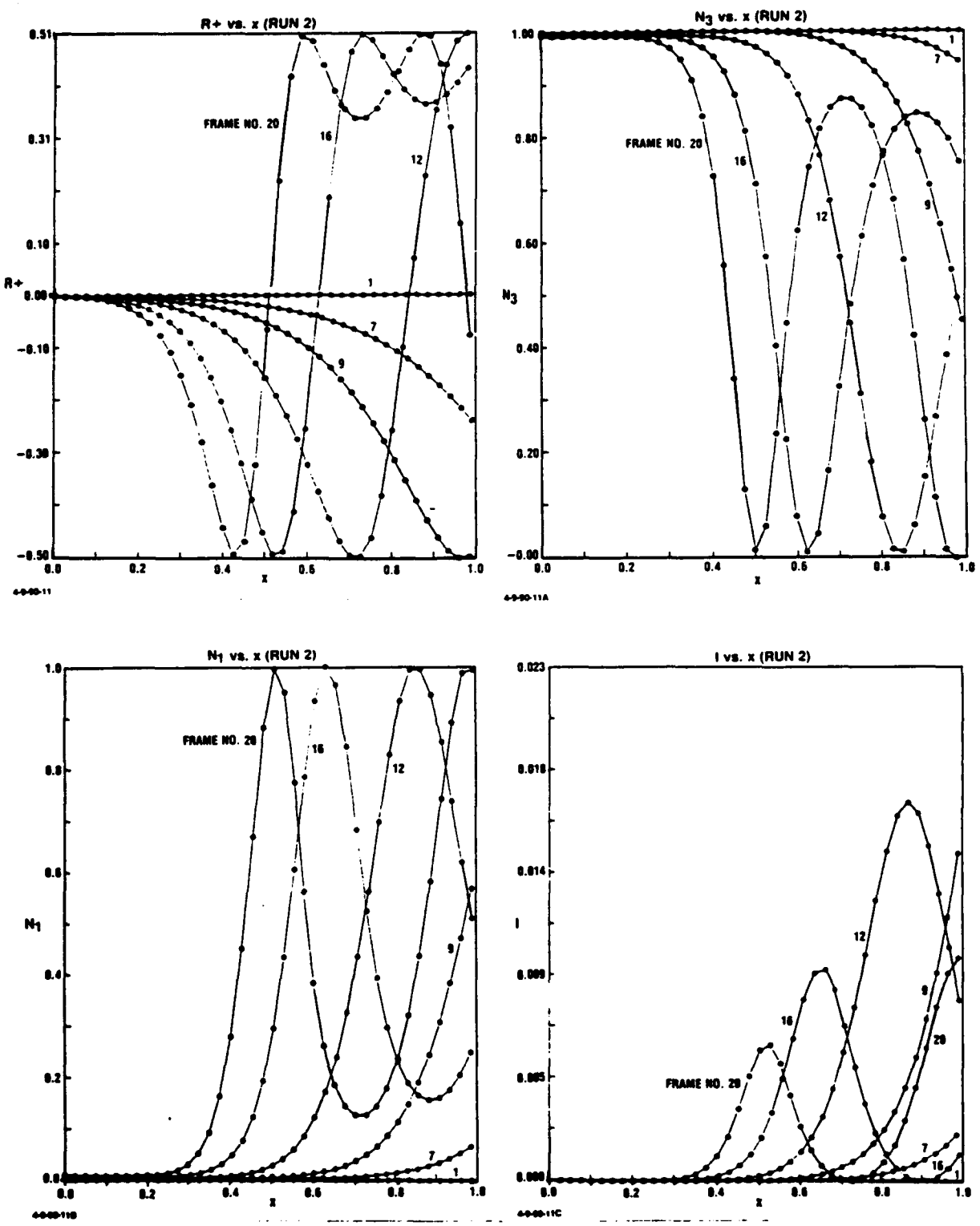

Figure 22. Plot of the Spatial Variation of the Polarization $R^+(x)$, Number Density $N_3(x)$, Field $N_1(x)$, and Intensity $I(x)$ at Different Times Indicated by Frame Numbers. The times corresponding to frame numbers are given by 3.75 τ_{SF} x (frame number) and the pulse corresponding to these data (Run 2) as shown in Fig. 14. ($\gamma = 10$, $\Gamma = 10^{-4}$, $\mu = 0$, $N = 10^6$)

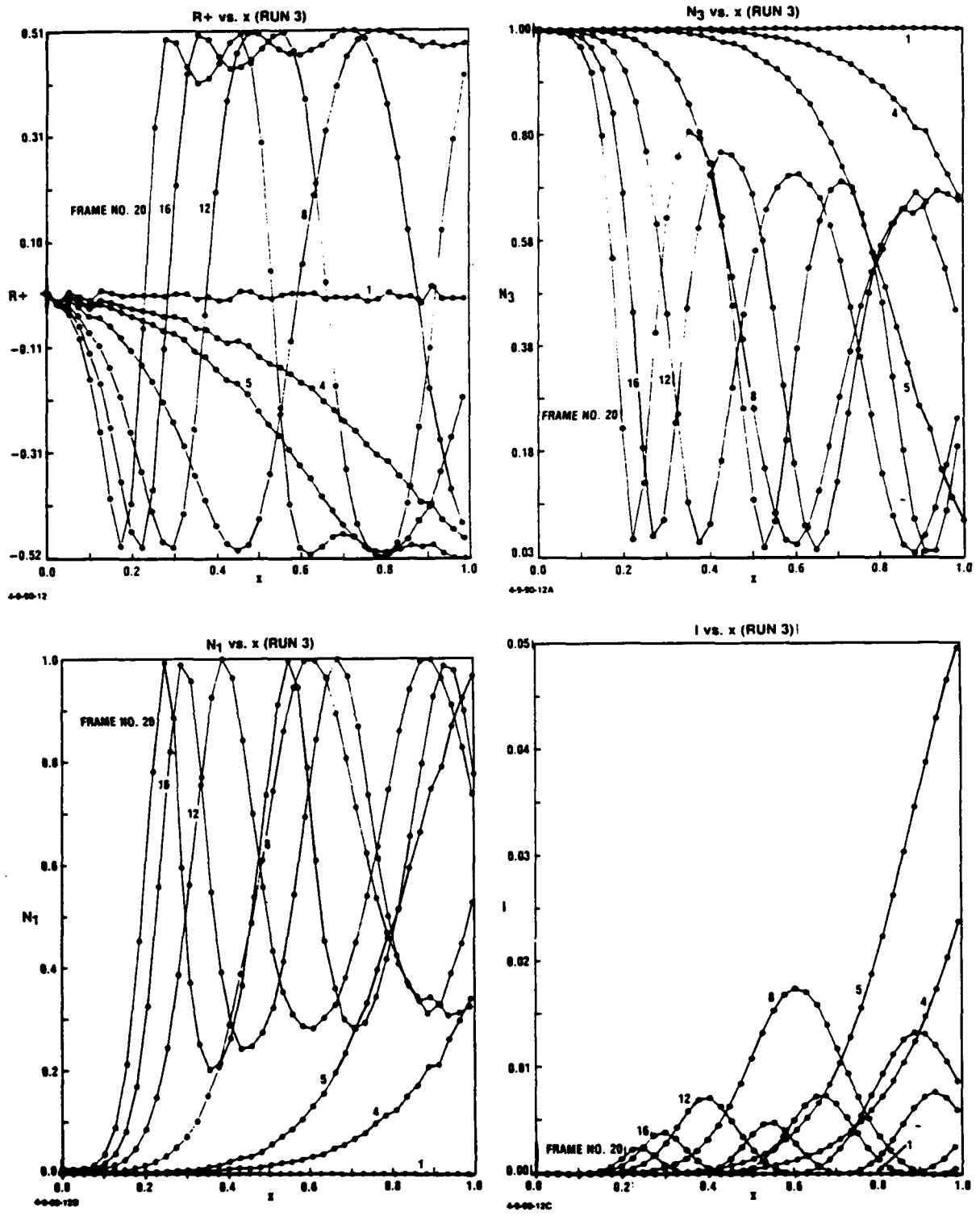

Figure 23. Plot of the Spatial Variation of the Polarization $R^+(x)$, Number Density $N_3(x)$, Field $N_1(x)$, and Intensity $I(x)$ at Different Times Indicated by Frame Numbers. The times corresponding to frame numbers are given by 3.75 τ_{SF} x (frame number) and the pulse corresponding to these data (Run 3) as shown in Fig. 15. ($\gamma = 1$, $\Gamma = 10^{-4}$, $\mu = 0$, $N = 10^3$)

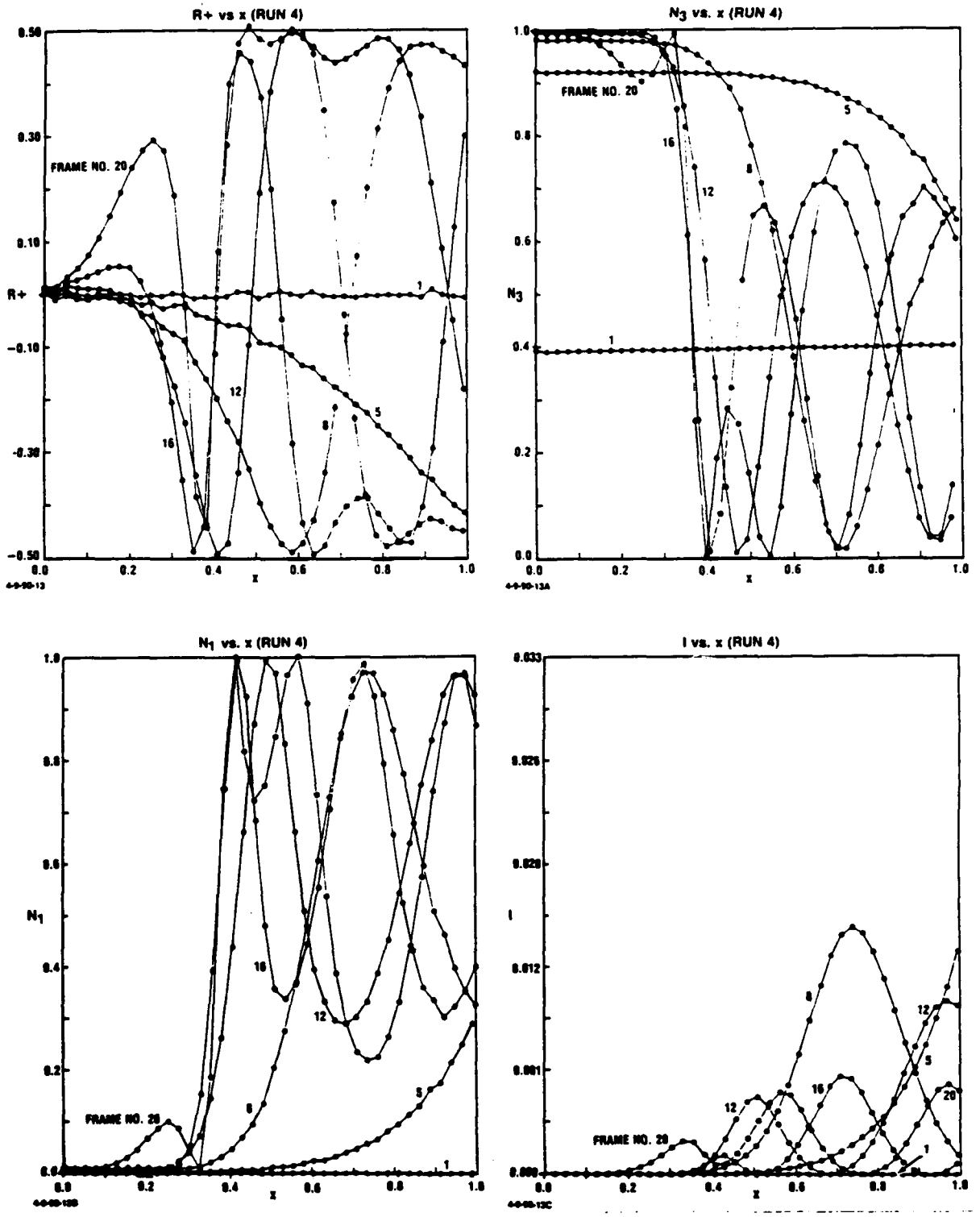

Figure 24. Plot of the Spatial Variation of the Polarization $R^+(x)$, Number Density $N_3(x)$, Field $N_1(x)$, and Intensity $I(x)$ at Different Times Indicated by Frame Numbers. The times corresponding to frame numbers are given by $5.0\ \tau_{SF}$ x (frame number) and the pulse corresponding to these data (Run 4) as shown in Fig. 16. ($\gamma = 0.1$, $\Gamma = 10^{-4}$, $\mu = 0$, $N = 10^3$)

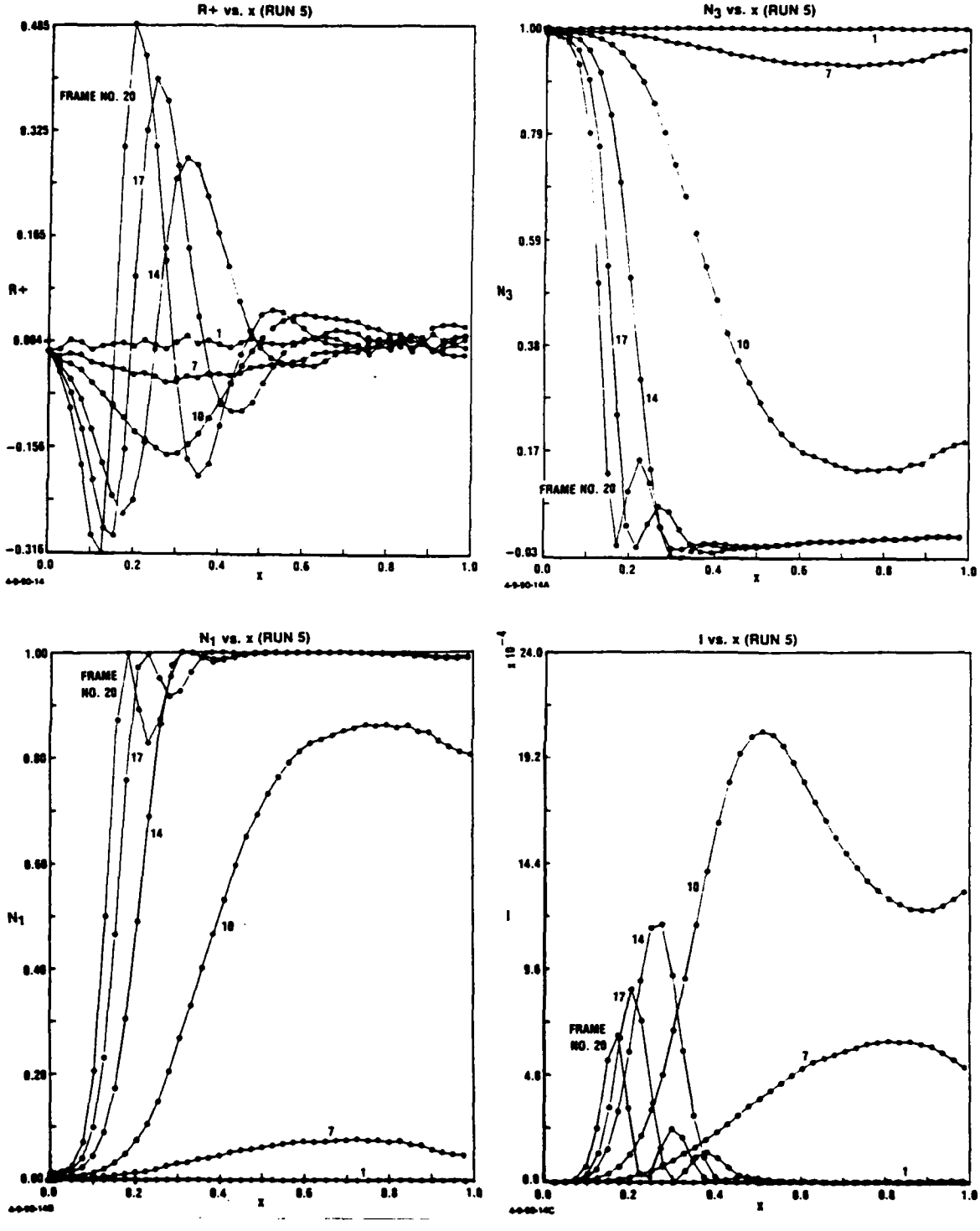

Figure 25. Plot of the Spatial Variation of the Polarization $R^+(x)$, Number Density $N_3(x)$, Field $N_1(x)$, and Intensity $I(x)$ at Different Times Indicated by Frame Numbers. The times corresponding to frame numbers are given by 7.5 τ_{SF} x (frame number) and the pulse corresponding to these data (Run 5) as shown in Fig. 17. ($\gamma = 10$, $\Gamma = 10^{-4}$, $\mu = 10$, $N = 10^3$)

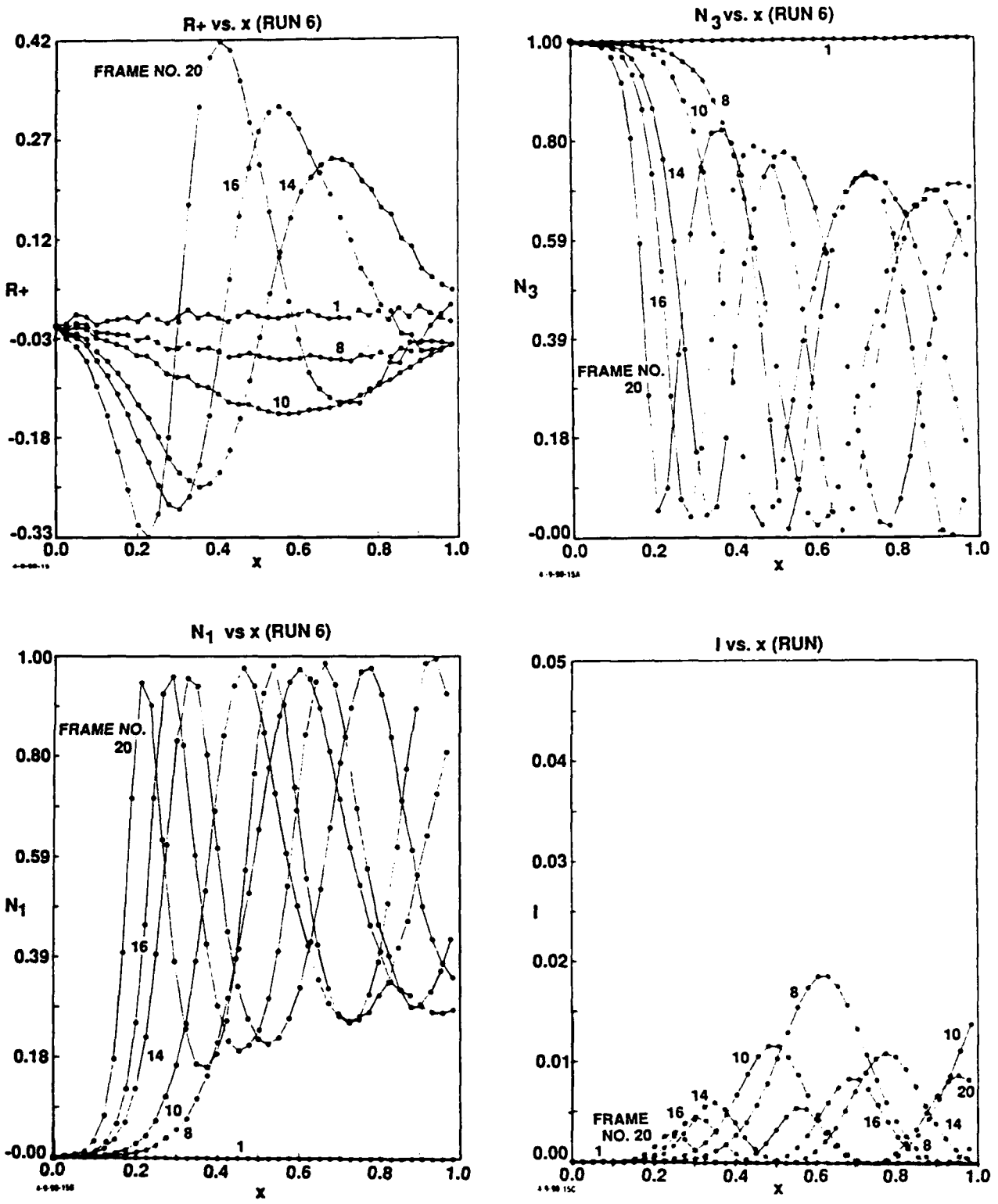

Figure 26. Plot of the Spatial Variation of the Polarization $R^+(x)$, Number Density $N_3(x)$, Field $N_1(x)$, and Intensity $I(x)$ at Different Times Indicated by Frame Numbers. The times corresponding to frame numbers are given by 3.75 τ_{SF} x (frame number) and the pulse corresponding to these data (Run 6) as shown in Fig. 18. ($\gamma = 10$, $\Gamma = 10^{-4}$, $\mu = 5$, $N = 10^3$)

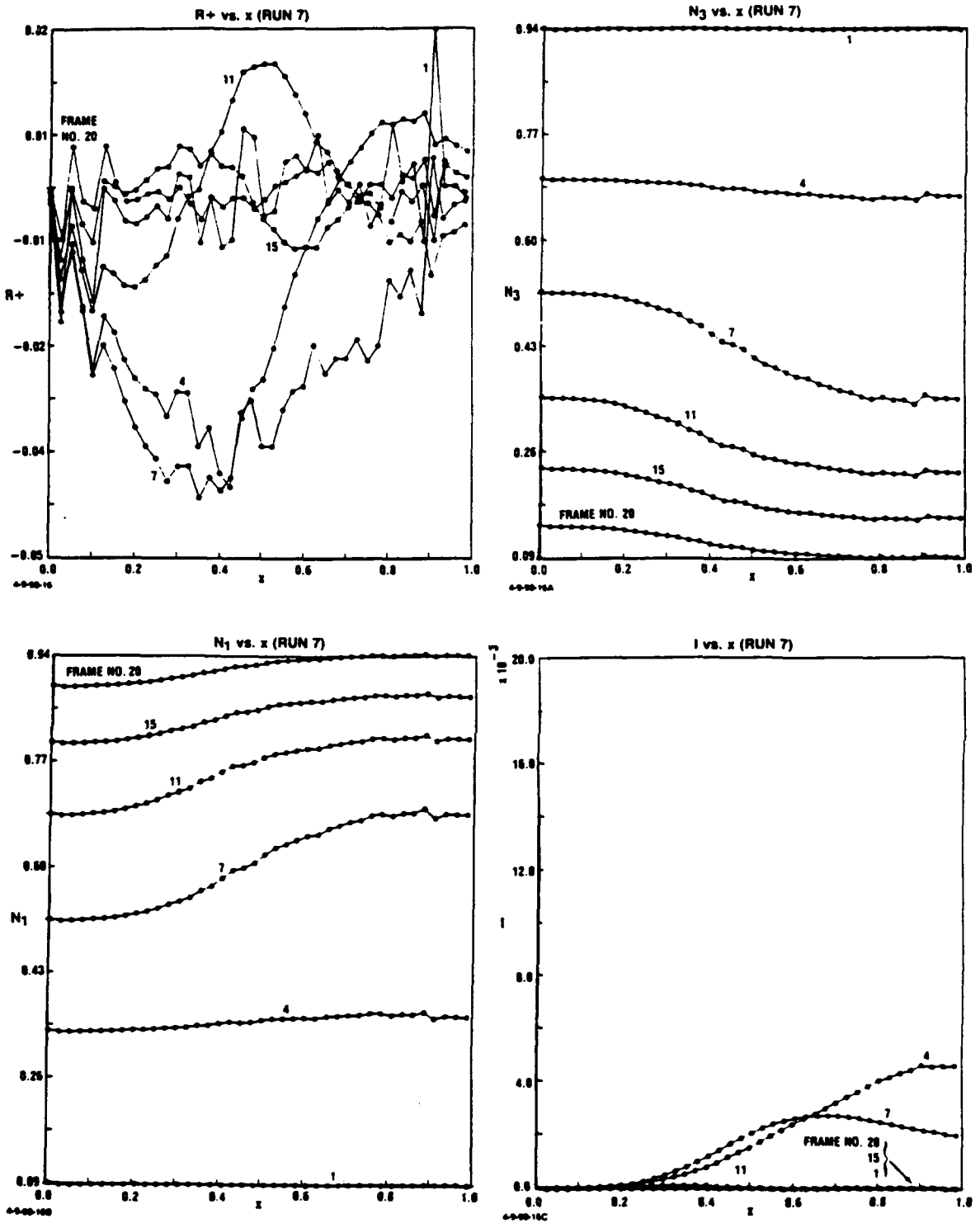

Figure 27. Plot of the Spatial Variation of the Polarization $R^+(x)$, Number Density $N_3(x)$, Field $N_1(x)$, and Intensity $I(x)$ at Different Times Indicated by Frame Numbers. The times corresponding to frame numbers are given by 4.0 τ_{SF} x (frame number) and the pulse corresponding to these data (Run 7) as shown in Fig. 19. ($\gamma = 1$, $\Gamma = 10^{-2}$, $\mu = 5$, $N = 10^3$)

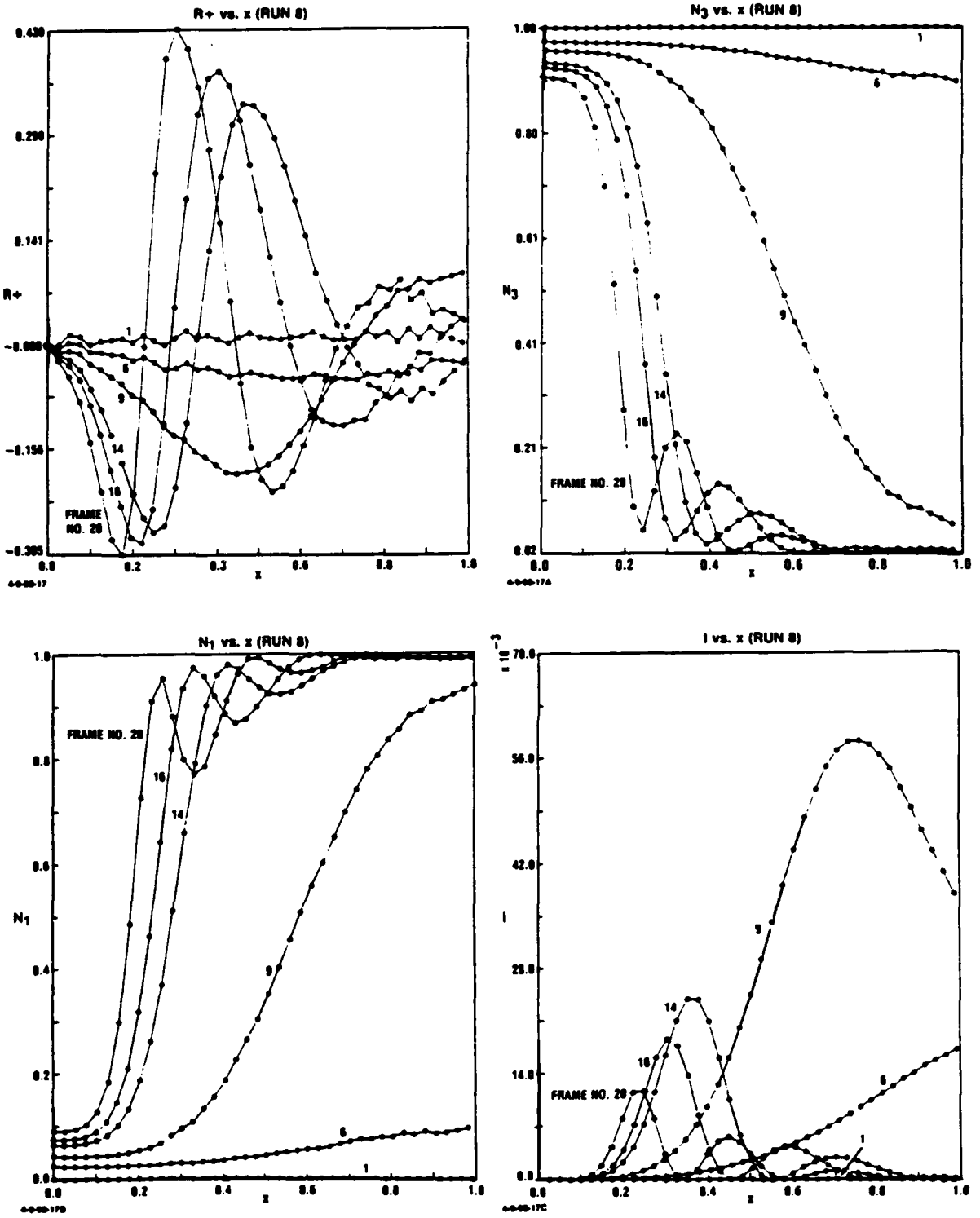

Figure 28. Plot of the Spatial Variation of the Polarization $R^+(x)$, Number Density $N_3(x)$, Field $N_1(x)$, and Intensity $I(x)$ at Different Times Indicated by Frame Numbers. The times corresponding to frame numbers are given by 5.0 τ_{SF} x (frame number) and the pulse corresponding to these data (Run 8) as shown in Fig. 20. ($\gamma = 10$, $\Gamma = 10^{-3}$, $\mu = 5$, $N = 10^3$)

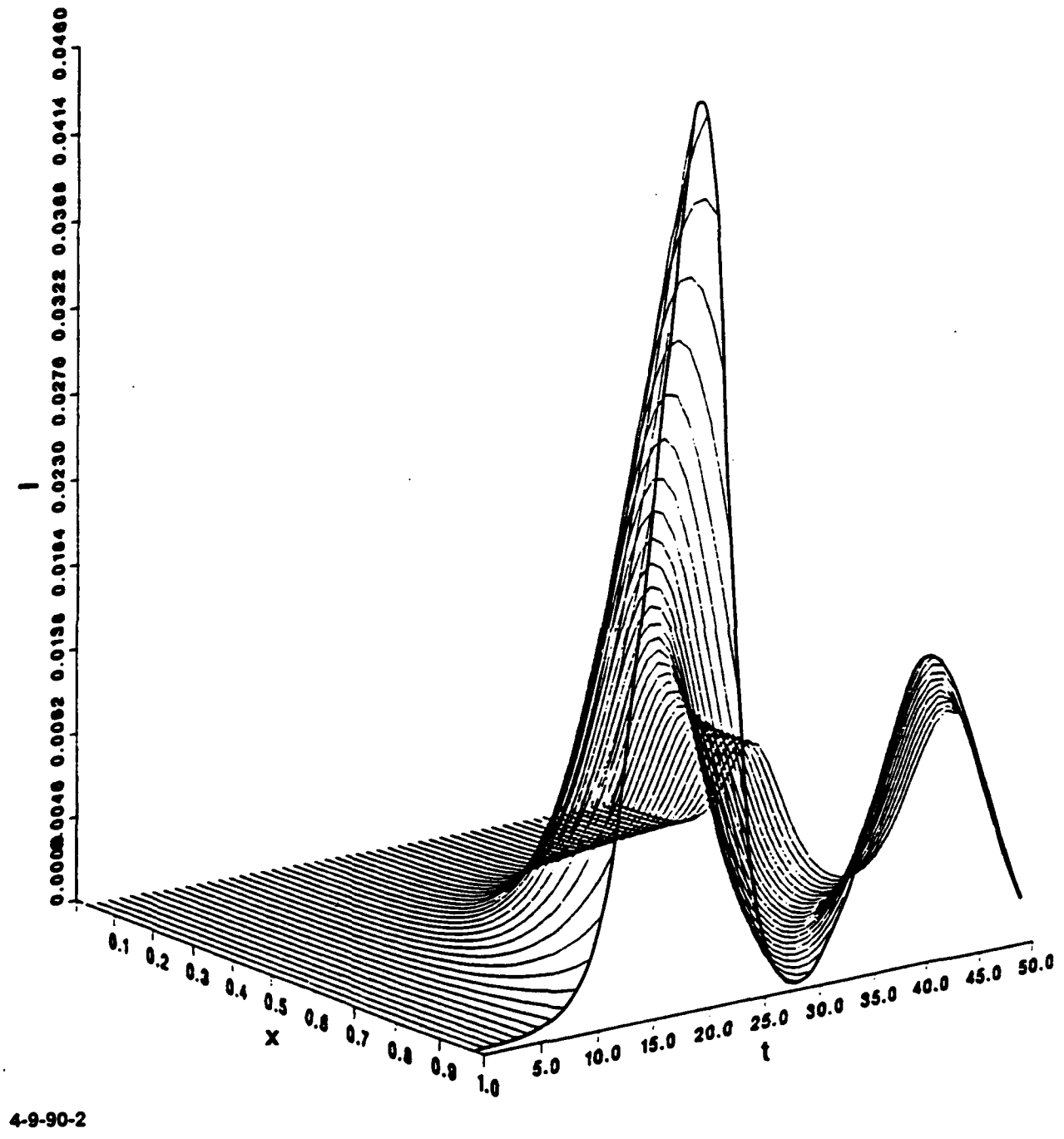

Figure 29. Intensity as a Function of Space and Time for Run 1. ($\gamma = 10$, $\Gamma = 10^{-4}$, $\mu = 0$, $N = 10^3$) The time axis is labeled in frame numbers (50 frames = 50 τ_{SF}).

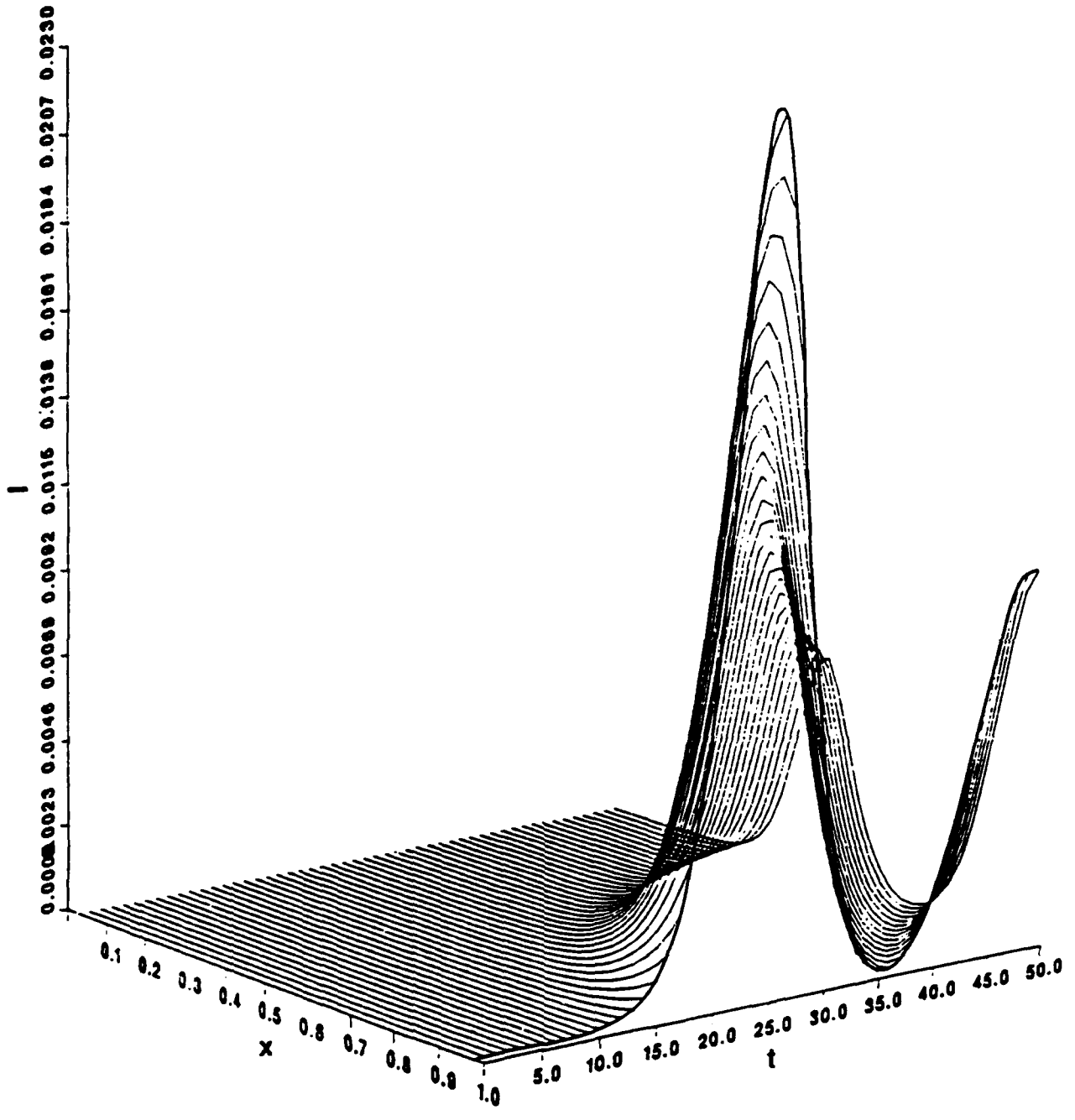

Figure 30. Intensity as a Function of Space and Time for Run 2. ($\gamma = 10$, $\Gamma = 10^{-4}$, $\mu = 0$, $N = 10^6$) The time axis is labeled in frame numbers (50 frames = 75 τ_{SF}).

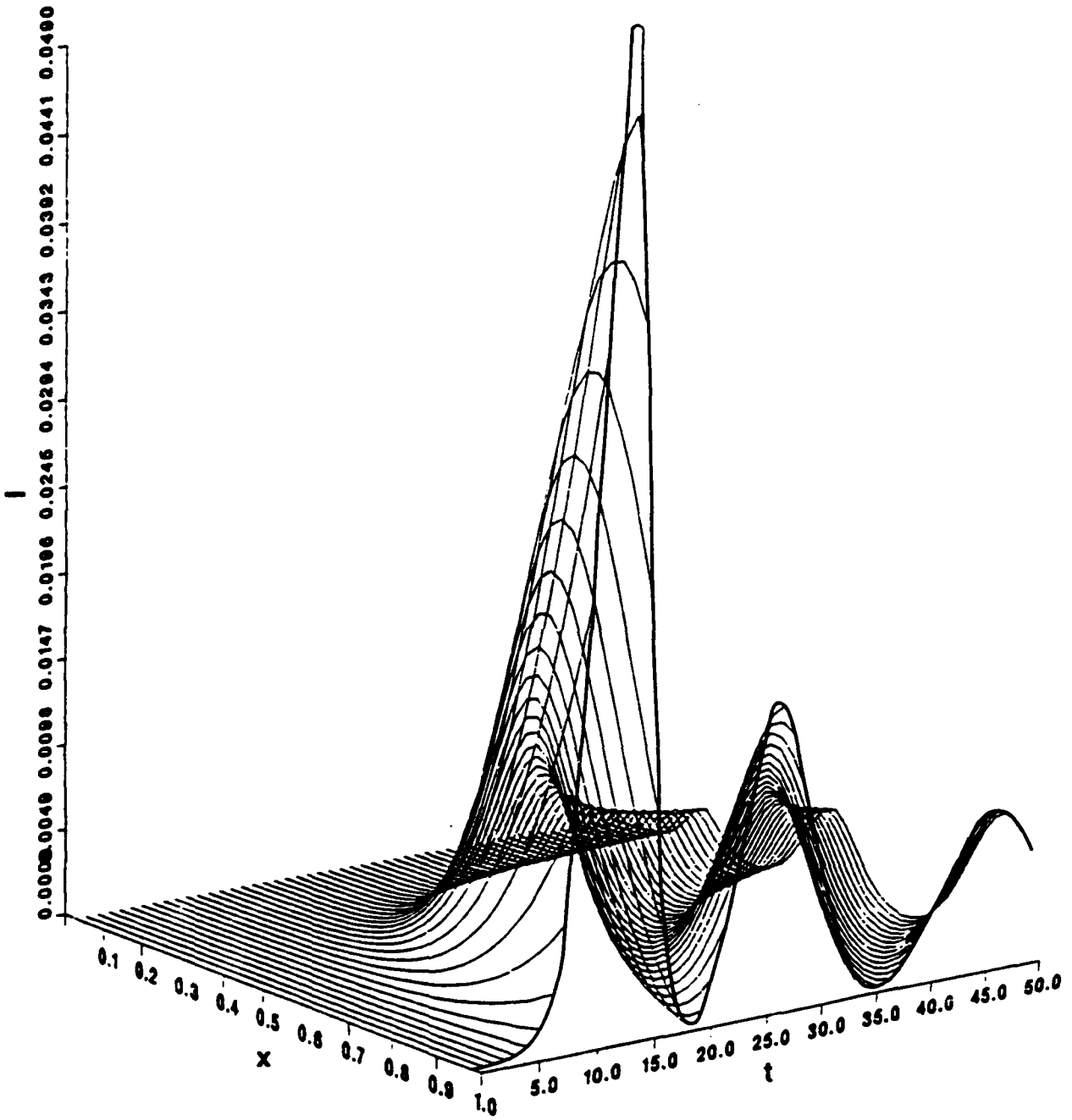

4-9-90-4

Figure 31. Intensity as a Function of Space and Time for Run 3.
($\gamma = 1$, $\Gamma = 10^{-4}$, $\mu = 0$, $N = 10^3$)
The time axis is labeled in frame numbers (50 frames = 75 τ_{SF}).

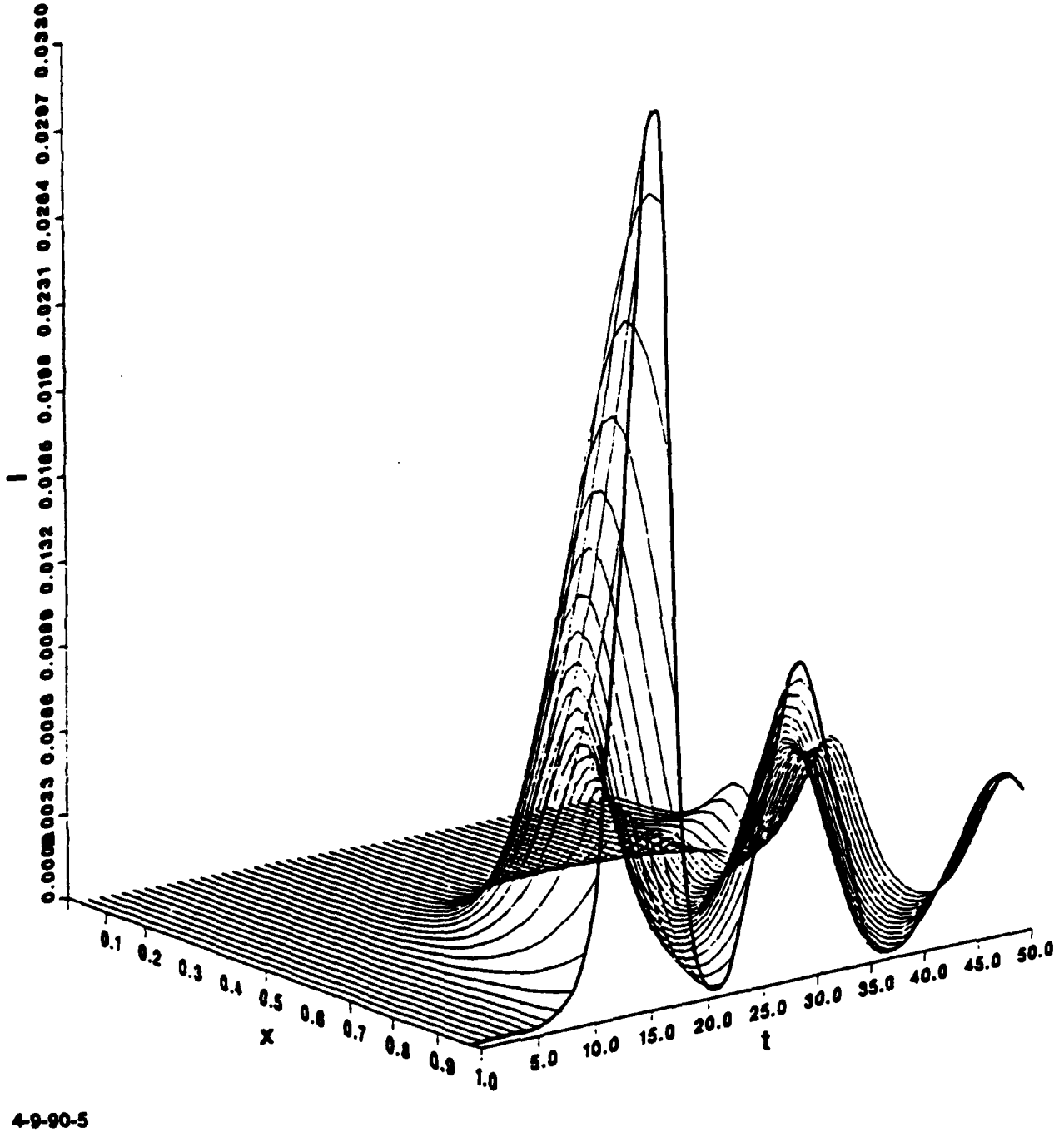

Figure 32. Intensity as a Function of Space and Time for Run 4. ($\gamma = 0.1$, $\Gamma = 10^{-4}$, $\mu = 0$, $N = 10^3$) The time axis is labeled in frame numbers (50 frames = 100 τ_{SF}).

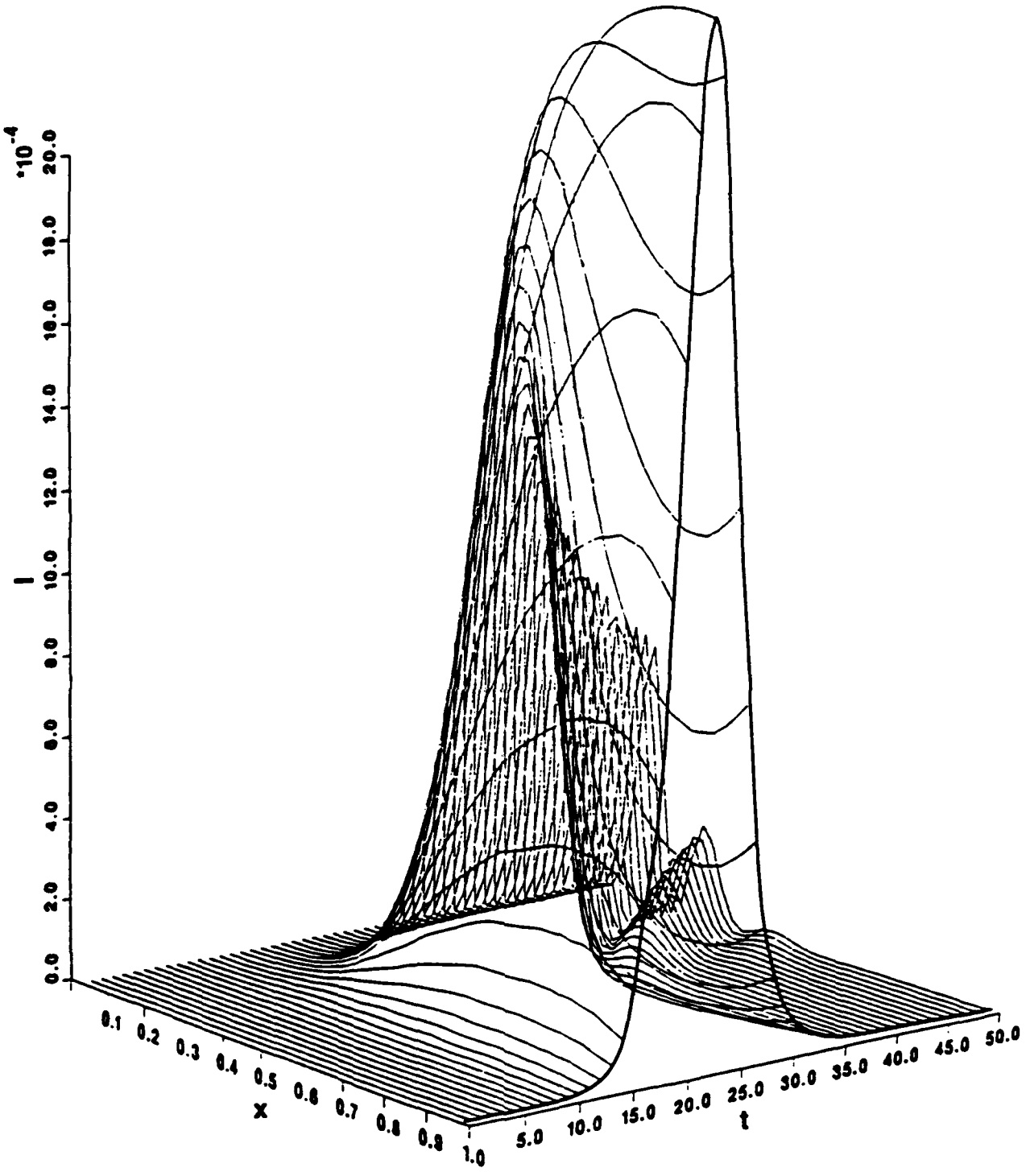

4-9-90-6

Figure 33. Intensity as a Function of Space and Time for Run 5. (γ = 10, Γ = 10^{-4}, μ = 10, N = 10^3) The time axis is labeled in frame numbers (50 frames = 150 τ_{SF}).

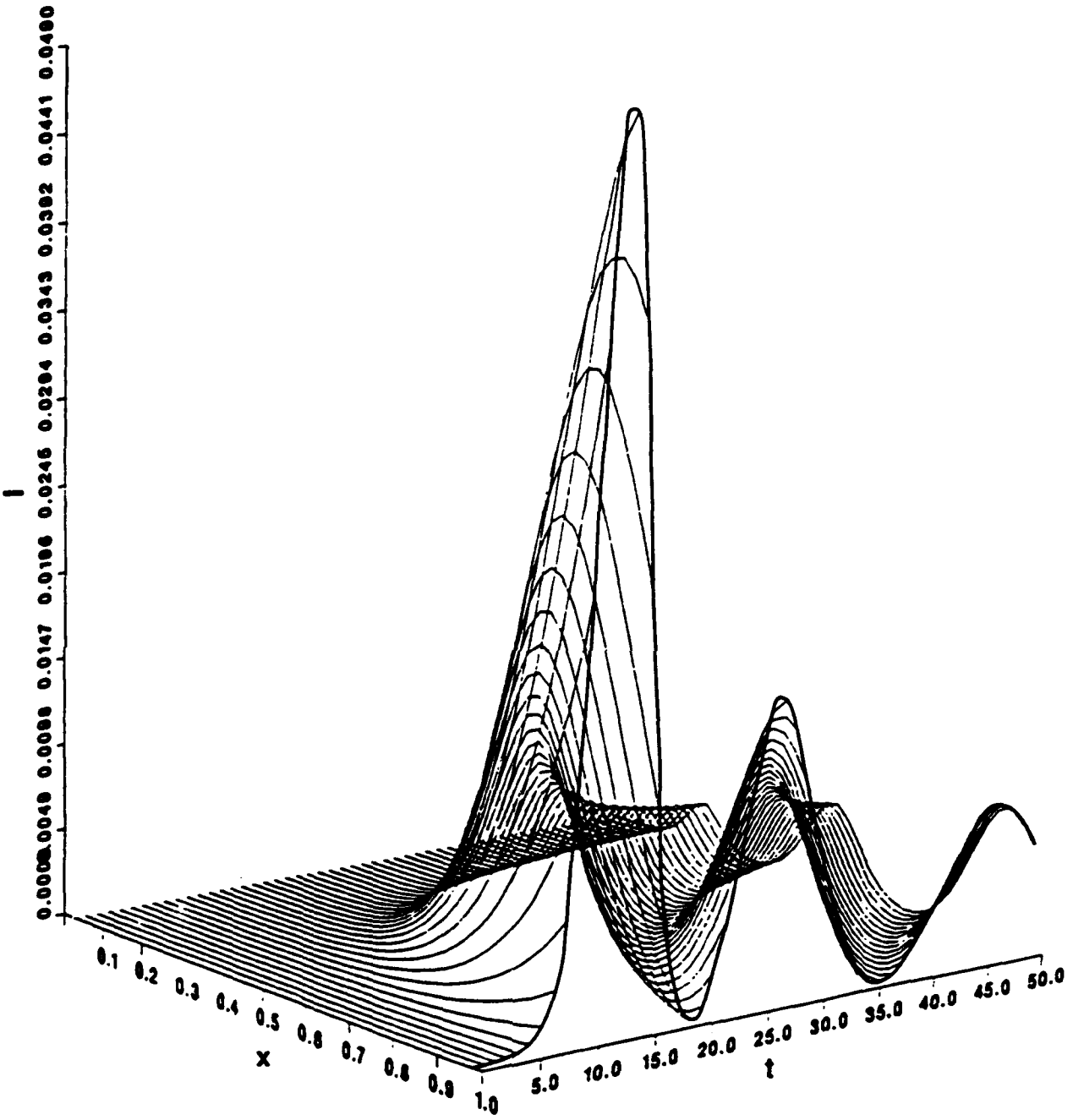

4-9-90-4

Figure 34. Intensity as a Function of Space and Time for Run 6. ($\gamma = 10$, $\Gamma = 10^{-4}$, $\mu = 5$, $N = 10^3$) The time axis is labeled in frame numbers (50 frames = 75 τ_{SF}).

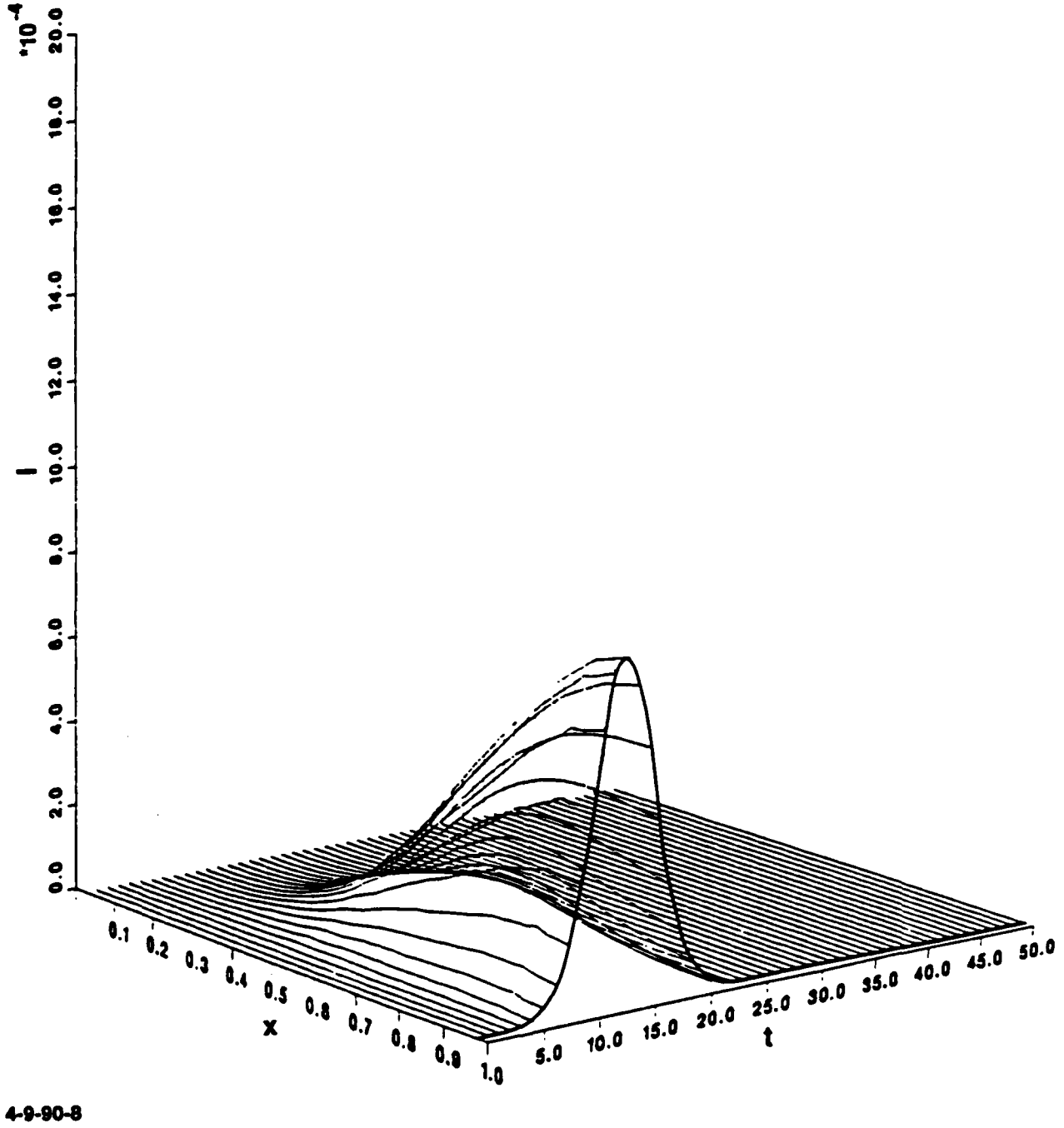

Figure 35. Intensity as a Function of Space and Time for Run 7. ($\gamma = 1$, $\Gamma = 10^{-2}$, $\mu = 5$, $N = 10^3$) The time axis is labeled in frame numbers (50 frames = 200 τ_{SF}).

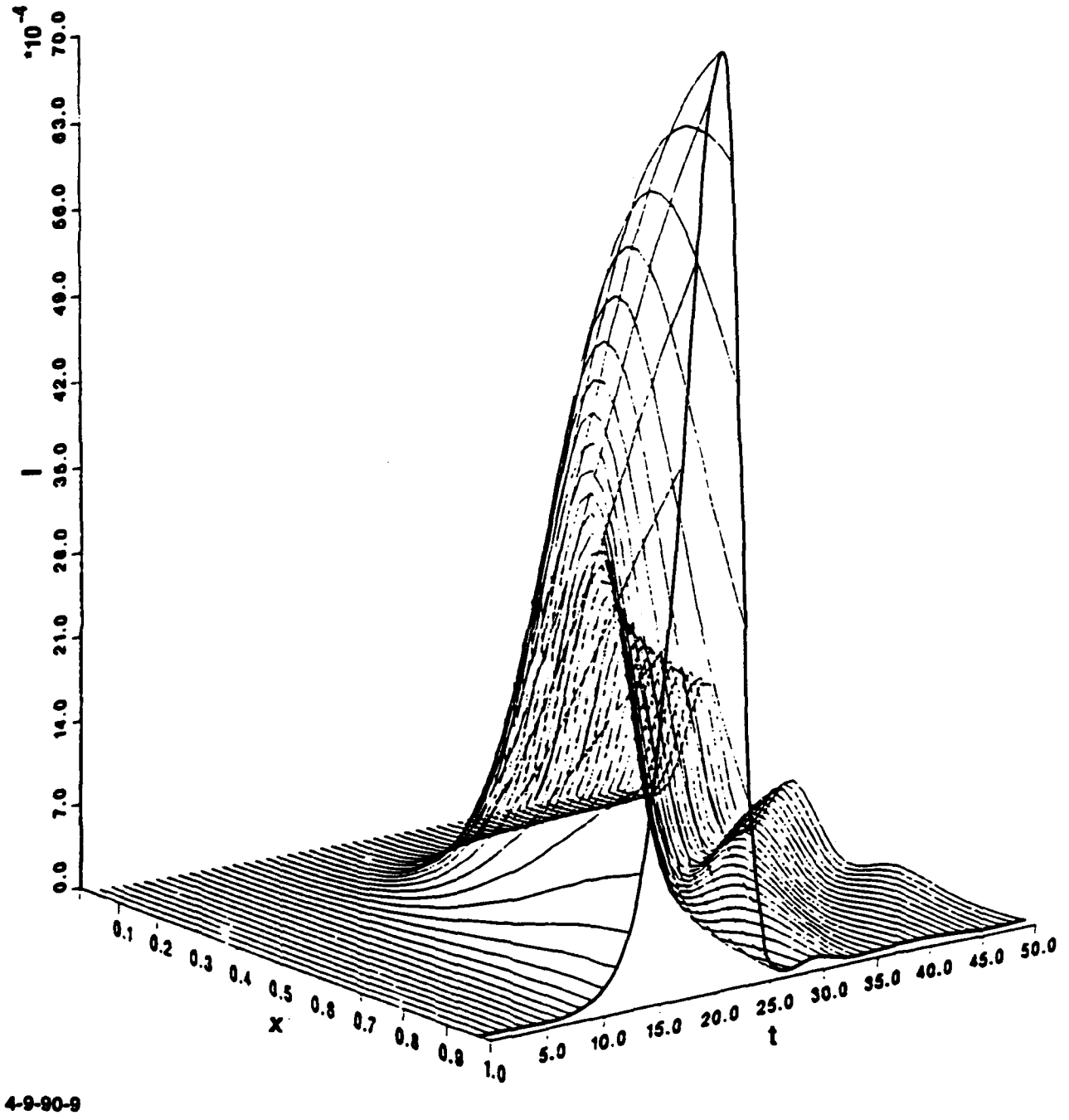

Figure 36. Intensity as a Function of Space and Time for Run 8.
(γ = 10, $\Gamma = 10^{-3}$, μ = 5, N = 10^3)
The time axis is labeled in frame numbers (50 frames = 100 τ_{SF}).

F. CONCLUSIONS

This paper considers a generalized version of the Haake-Reibold model of SF in a multilevel system of emitters, having up to five energy levels. The generalized version takes into account finite pumping rates, spatial attenuation of the electromagnetic field, dephasing, and population depletion due to processes such as internal conversion and spontaneous, but noncollective, transverse emission.

In this paper we studied the dependence of emitted pulse shapes on the statistics and time dependence of the noise sources. Monte Carlo results obtained by averaging 25 to 100 pulses, which seem to be adequate samples, also depend upon the noise source variance.

The spatial attenuation parameter μ reduces the pulse peak and shifts it to longer times. The peak will decrease gradually but will not disappear if no dephasing mechanisms that reduce the dipole built up by the noise source exist and no population depletion mechanisms destroy the inversion.

Small values of the dephasing factor have no effect on the emitted pulse delay time or intensity, but when the dephasing rate Γ_ϕ is comparable to the SF decay $1/\tau_{SR}$ rate the delay time starts to increase with increasing values of the dephasing factor until it reaches a maximum, after which it decreases rapidly.

Because of spatial attenuation, for maximum intensity of the pulse radiated out of the active region the choice of the region's length should be governed by the values of the attenuation factor μ and the coupling constant g_1 associated with coupling between the emitters and the electromagnetic field. The optimum length will depend on details of the propagating electromagnetic field inside the active region.

II. AN ANALYSIS OF THE EFFECTS OF INHOMOGENEOUS BROADENING AND TIME-DEPENDENT INTERACTIONS ON SUPERFLUORESCENT EMISSION

A. INTRODUCTION

If a "gamma-ray laser" is developed it may emit in a superradiant (SR) or superfluorescent (SF) mode instead of a stimulated emission (SE) mode (Refs. 4, 14). There are some characteristic features of superfluorescent decay which may provide ways of overcoming specific nuclear problems (Ref. 3) which at present prevent CW or pulsed laser (SE) action. In another paper (Ref. 3) we have investigated the possibility of nuclear superfluorescence and described the interrelationship of the pertinent nuclear and solid-state parameters that govern the experimental realization of this phenomenon. We also contrasted the nuclear SF problem with the atomic and molecular SF problem and described several special issues that differentiate the two.

The differences are due to (a) the shorter wavelength of the emitted nuclear radiation, (b) the subsequent large recoil energy compared to the natural linewidth, (c) the generally higher multipolarity of the nuclear radiation, (d) the common occurrence of completing transitions in nuclear processes, (e) the relatively high electronic attenuation for this nuclear radiation compared to the resonant cross-section, (f) the difficulty of pumping, requiring finite pumping times for nuclear systems, (g) the difficulty of providing desired geometrical shapes for the active medium, and (h) inhomogeneous broadening which can destroy the resonant condition when narrow nuclear lines are involved.

All of these issues are of secondary interest in atomic SF or SR studies but they present critical problems to the development of nuclear SF or SR, as well as lasing, or amplified spontaneous emission (ASE).

In a recent paper we discussed SF at wavelengths shorter than the interatomic spacing (Ref. 15), the effect of competing transitions and electronic attenuation on the SF pulse generation, and analyzed the effect of finite pumping times on the generation of the SF pulse (Ref. 3). In this paper we discuss how inhomogeneous broadening affects the

generation of a SF pulse and how the effect can be reduced through electronic relaxation or time-dependent hyperfine interactions.

In this paper we discuss the calculation of the emission line shape under dynamic conditions (the existence of time-dependent hyperfine interactions) and then generalize the procedure to a system of many nuclei. We calculate the emission pulse shape for a system of nuclei in slightly different environments, which causes inhomogeneous broadening, and then study the effect of time-dependent perturbations on the line shape and pulse generation.

B. SINGLE NUCLEUS EMISSION LINESHAPE

Consider a two-state nuclear system with energy levels α and λ as shown below connected by an electromagnetic transition:

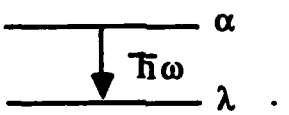

The probability for the emission of a single photon with energy $\hbar\omega$, wave vector $\vec{k}$ and polarization p is given by the Wigner-Weisskopf formula

$$P_{\lambda\alpha}(\vec{k}\omega p) = \frac{|<\alpha|V^{(+)}|\lambda>|^2}{\left[\omega - \left(E_\alpha - E_\lambda\right)\right]^2 + \left(\frac{\Gamma}{2}\right)^2} \quad , \tag{6}$$

where Γ is the natural line width for the transition from state α with energy E_α to state λ with energy E_λ and $V^{(+)}(\vec{k}\omega p)$ is the Hamiltonian for the emission of a photon with parameters $\vec{k}$, ω, p.

At this point we can make some modification to Eq. (6) which will allow us to use well-known results and convenient formalisms to deal with multiatom (or nuclear) emissions in a time-dependent environment. The first step is to rewrite Eq. (6) in terms of amplitudes and the second is to transform it into the time domain. Equation (6) can be rewritten in terms of the amplitude $A_{\lambda\alpha}$ for the process of interest as follows:

$$P_{\lambda\alpha} = A^*_{\lambda\alpha} A_{\lambda\alpha} \quad , \tag{7}$$

where

$$A_{\lambda\alpha} = \frac{<\lambda | V^{(-)} | \alpha>}{\left(\omega + E_\alpha - E_\lambda\right) - i\frac{\Gamma}{2}} \quad . \tag{8}$$

Now using

$$\frac{1}{\left(\omega + E_\alpha - E_\lambda\right) - i\frac{\Gamma}{2}} = i\int_0^\infty dt' \, e^{-i(\omega + E_\alpha - E_\lambda)t' - \frac{\Gamma}{2}t'} \quad , \tag{9}$$

we take the second step and get

$$\begin{aligned} A_{\lambda\alpha} &= i\int_0^\infty dt' <\lambda | V^{(+)} | \alpha> e^{-i(\omega + E_\alpha - E_\lambda)t' - \frac{\Gamma}{2}t'} \\ &= \int_0^\infty dt' <\lambda | e^{iHt'} V^{(+)} e^{-iHt'} | \alpha> e^{-i\omega t' - \frac{\Gamma}{2}t'} \\ &= \int_0^\infty dt' <\lambda | V^{(+)}(t') | \alpha> e^{-i\omega t' - \frac{\Gamma}{2}t'} \quad , \end{aligned} \tag{10}$$

where

$$\begin{aligned} V^{(-)}(t') &= e^{i(E_\lambda - E_\alpha)t'} V^{(-)} = e^{iE_\lambda t} V^{(-)} e^{-iE_\alpha t} \\ &= e^{iHt'} V^{(-)} e^{-iHt'} \quad , \end{aligned} \tag{11}$$

since

$$H | \lambda> = E_\lambda | \lambda> \text{ and } H | \alpha> = E_\alpha | \alpha> \quad .$$

To obtain a lineshape for a single resonance (transition $\alpha \rightarrow \lambda$) from a single emitting atom at position i we write

$$\begin{aligned} P_i(\vec{k}\omega p) &= A^*_{\lambda\alpha i} A_{\lambda\alpha} \\ &= \int_0^\infty dt' \int_0^\infty dt'' \, e^{i\omega(t'-t'') - \frac{\Gamma}{2}(t'-t'')} <\lambda | V^{(-)}(t') V^{+}(t'') | \alpha> \quad . \end{aligned} \tag{12}$$

Generalizing to multiple level systems with allowance for transitions between levels we write

$$P_i(\vec{k}\omega p) = \int_0^\infty dt' \int_0^\infty dt'' \; e^{i\omega(t'-t'') - \frac{\Gamma}{2}(t'+t'')} < V^{(-)}(t'')\, V^{(+)}(t') > \quad , \tag{13}$$

where

$$V^{(\pm)}(t) = e^{iHt} V^{(\pm)} e^{-iHt}$$

and the bracket pair notation means

$$< A > = \mathrm{tr} < \rho A > = \sum_{\lambda,\,\lambda'} < \lambda \,|\, \rho \,|\, \lambda' > < \lambda' \,|\, A \,|\, \lambda > \ ,$$

so that

$$< V^{(-)}(t'')\, V^{(+)}(t') > = < V^{(-)} V^{(+)}(t' - t'') > \ .$$

Introducing a change of variables $\tau = t' - t''$ and integrating with respect to t'' one gets a convenient form for the emission lineshape assuming V(t) is a stationary process

$$P_i(\vec{k}\omega p) = \frac{2}{\Gamma}\ \mathrm{Re} \int_0^\infty d\tau\ e^{i\omega\tau - \frac{\Gamma}{2}\tau} < V^{(-)}\, V^{(+)}(\tau) > \ . \tag{14}$$

This form is a starting point for a description of dynamic effects (relaxation) in Mossbauer emission and absorption experiments. Such experiments are usually modeled assuming nuclei emitting noncooperatively. An example of line shape calculations for a specific relaxation mechanism will be presented in Section F below.

C. EMISSION FROM A SYSTEM OF N NUCLEI

For N atoms using Eqs. (11) and (10) we get

$$P_{\lambda\alpha}(\omega) = A^2_{\lambda\alpha} = \left| \sum_i A_{\lambda\alpha i} \right|^2$$

$$= \left| \sum_i \int_0^\infty dt' < \lambda_i \,|\, e^{iH_i t'} V^{(-)} e^{-iH_i t'} \,|\, \alpha_i > e^{+i\omega t' - \frac{\Gamma}{2} t'} \right|^2 \ . \tag{15}$$

Subscript i is used to indicate that even though the states are the same, the energies can be slightly different for different nuclei, resulting in inhomogeneous

broadening of the line shape for the total system (Ref. 16). For a stationary case we use $H_i \mid \alpha_i > = E_{\alpha i} \mid \alpha_i >$ to get

$$A^2_{\lambda\alpha} = \left| \sum_i \int_0^\infty dt' < \lambda_i \mid V^{(-)} \mid \alpha_i > e^{i(E_{\lambda i} - E_{\alpha i})\, t' + i\omega t' - \frac{\Gamma}{2} t'} \right|^2$$

$$= \sum_i \int_0^\infty dt' \int_0^\infty dt'' \; < \lambda_i \mid V^{(-)} \mid \alpha_i > < \alpha_i \mid V^{(+)} \mid \lambda_i >$$

$$\times e^{i\omega_i (t' - t'') + i\omega (t' - t'') - \frac{\Gamma}{2} (t' + t'')}$$

$$+ \sum_{i,\, j \neq i} \int_0^\infty dt' \int_0^\infty dt'' \; < \lambda_i \mid V^{(-)} \mid \alpha_i > < \alpha_j \mid V^{(+)} \mid \lambda_j >$$

$$\times e^{i\omega_i t' - i\omega_j t'' + i\omega (t' - t'') - \frac{\Gamma}{2} (t' + t'')}$$

$$= \sum_i^N \hat{I}(\omega, \omega_i) + \sum_{i,\, j \neq i}^N \hat{I}(\omega; \omega_i, \omega_j) = \hat{I}_{N^1} + \hat{I}_{N^2} \quad . \tag{16}$$

The first term in Eq. (16) gives the lineshape for spontaneously emitted photons from the N nuclei acting independently and is equal to $\sum_i^N P_i (\vec{k}\omega p)$ of Eq. (14). The second term gives the lineshape for the collective emission. Each term in the sum is a Lorentzian with slightly different resonance energy ω_i. The sum gives an inhomogeneously broadened line which usually is assumed to have a Gaussian or Lorentzian envelope and with slight modifications is appropriate to describe both Mössbauer absorption and emission experiments (Refs. 17, 18). In the special case of a single nucleus, Eq. 1 is the starting point for Blume's discussion of the effect of time dependent hyperfine interactions on the Mössbauer lineshape (Ref. 19). In the case of N nuclei with appropriate normalization, it represents the source lineshape and also the absorption cross-section in the calculation of the effect of inhomogeneous broadening on Mössbauer experiments.

D. CALCULATION OF THE EMISSION PULSE SHAPE

For discussing SF emission we are primarily interested in the total intensity as a function of time rather than the lineshape or photon energy distribution. After inversion is accomplished, the delay time τ_D and the emission time τ_{SF}, both shorter than the natural lifetime of a single atom or nucleus, characterize the SF process.

With this in mind we consider the second term of Eq. (16)

$$\hat{I}_{N^2}(\omega) = \sum_{i,j\neq i}^{N} I(\omega; \omega_i, \omega_j) = \sum_{i,j\neq i}^{N} \int_0^\infty dt' \int_0^\infty dt'' < \lambda_i \,|\, V^{(-)} \,|\, \alpha_i >$$

$$x < \alpha_j \cdot V^{(+)} \cdot \lambda_j > e^{i\omega_i t' - i\omega_j t'' + i\omega(t'-t'') - \frac{\Gamma}{2}(t'+t'')} \quad . \tag{17}$$

We integrate $I_{N^2}(\omega)$ over ω, which produces a delta function in $(t' - t'')$ and allows us easily to compute the integral over t", for the total emission intensity.

$$\bar{I}_{N^2} = \sum_{i,j\neq i}^{N} \int_0^\infty dt' < \lambda_i \left| V^{(-)} \right| \alpha_i >< \alpha_j \left| V^{(+)} \right| \lambda_j > e^{i(\omega_i - \omega_j)t' - \Gamma t'} \quad .$$

Accordingly, for the emission intensity as a function of time we assume

$$I_{N^2}(t) = \sum_{i,j\neq i}^{N} < \lambda_i \,|\, V^{(-)} \,|\, \alpha_i > < \alpha_j \,|\, V^{(+)} \,|\, \lambda_j > e^{i(\omega_i - \omega_j)t - \Gamma t} \quad . \tag{18}$$

As can be seen from Eq. (18) the effect of inhomogeneous broadening from the difference $\omega_i - \omega_j$ in the exponential is to introduce a phase change between different radiators. This lowers the intensity of the emitted SF pulse. In Mössbauer spectroscopy the effect of inhomogeneous broadening is thought of as a reduction in overlap of source and absorber lines due to shifting in the individual resonances by detuning or different resonance energies at different sites. This is discussed in Ref. 17.

In discussions of lasing the effect of inhomogeneous broadening is used to describe the reduction of the stimulation cross-section and consequently the loss of gain in the operation of a laser. However, in the SF phenomena, as pointed out by Eberly (Ref. 13) it is the phase change introduced by the inhomogeneous broadening that controls the emission and not the reduction of overlap of resonance lines. For treating SF emission it is

the phase change introduced by different resonant energies ω_i at different sites i that describes the effect of inhomogeneous broadening on the emission.

At this point it is instructive to compare Eberly's derivation of the SF emission as effected by the inhomogeneous broadening and our results given in Eq. (16). Eberly shows that the intensity of emitted radiation as a function of time t and the wave vector $\vec{k}$ is given by

$$I(\vec{k},t) = I_o(\vec{k}) \sum_{m=1}^{N} <\chi | R_m^+ R_m^- | \chi >$$

$$+ I_o(\vec{k}) \sum_{e}^{N} \sum_{m \neq e}^{N} <\chi | R_m^+ R_m | \chi >$$

$$e^{i(\gamma_m - \gamma_e) T + \phi_m - \phi_e} \quad , \tag{19}$$

where in Eberly's notations R_m^+, R_m^- are the usual raising and lowering operators for the mth nucleus or atom, $|\chi>$ is the atomic (or nuclear) state in the interaction picture so that $|\chi> = U(T, 0) |\psi_H>$ with U(T, 0) as the unitary operator and $|\psi_H>$ the Heisenberg state. The detuning frequencies γ_m are obtained from $\gamma_m = \nu_m - \omega$ where ν_m is the transition frequency.

The first sum in Eq. (19) gives the single nucleus emission and is related to the first part of Eq. (16). The second sum in Eq. (19) gives the SF emission with the characteristic focused angular distribution and shortened emission time following an initial delay. We will now concentrate on the second sum and consider the effect of inhomogeneous broadening.

Eberly shows that

$$\sum_{l} \sum_{m \neq l} e^{i(\omega_m - \omega_l) t} = \left| \sum_{m} e^{i\omega_m t} \right|^2 - N$$

and the sum squared term can be written as

$$\left|\sum_m e^{i\omega_m t}\right|^2 = N^2 \left|\frac{1}{N}\sum_m e^{i\omega_m t}\right|^2 = N^2 \left|\left\{e^{i\omega_m t}\right\}_{ave}\right|^2$$

$$= N^2 \left|\int_0^\infty e^{i\gamma} g(\gamma)\, d\gamma\right|^2 , \qquad (20)$$

where $g(\gamma)$ is the inhomogeneously broadened lineshape function normalized to unity. In the case when $g(\gamma)$ can be modeled by a Lorentzian lineshape, the Fourier transform in Eq. (20) leads to exponential damping, and the SF intensity term, the N^2 part of Eq. (16), becomes

$$I_{N^2}(t) = N^2 |< V >|^2 e^{-2t/T_2^* - \Gamma t} . \qquad (21)$$

T_2^* is the inverse of the inhomogeneously broadened line width. For fast pumping, essentially completed near t = 0 (such that $t_{pump} << \tau_{SF} << T_2^* < \frac{1}{\Gamma}$), inhomogeneous broadening has little effect on the emission because the nuclei have not had time to dephase. Only after a relaxation time T_2^* does the phase difference between different nuclei i, j, $(\omega_i - \omega_j)t$, become large enough to affect the emission or to prevent the SF pulse from occurring.

Thus inhomogeneous broadening affects SF pulse emission differently from the way it affects lasing or amplified spontaneous emission (ASE). The difference between lasing and superfluorescence can be understood in terms of the different times during the evolution of a system that they dominate the emission and the kinds of processes that they resemble. SF is like an emission process that is cooperative in nature, whose characteristic is described by a delay time τ_D and the SF emission time τ_{SF}. Lasing is a process like absorption that is characterized by a cross-section, the stimulation cross-section σ_s. SF (under appropriate conditions) can occur early in the evolution of a system before complete dephasing, while lasing can occur even after dephasing if the gain coefficient is greater than zero (i.e., amplification is possible). This difference in the effect of inhomogeneous broadening on lasing (ASE) and SF has implications for γ-ray laser feasibility.

Both of the processes have to be considered in a complete study of γ-ray lasers. Candidate selection should be made using the criteria for both ASE and SF pulse generation. If inversion can be accomplished quickly and the inversion density is high

enough to initiate SF before dephasing sets in, $\tau_{SF} << T_2^* < \frac{1}{\Gamma}$, SF will occur. Otherwise, if the gain is high enough, ASE will occur. The transition region has been observed experimentally (Ref. 20) in atomic systems.

For lasing to occur it is necessary that the photon gain per unit length, K, be greater than zero (Refs. 21, 22).

$$K = \sigma_R \Delta n^* - \mu \quad , \tag{22}$$

and

$$\sigma_R = \frac{\lambda^2 \beta f g_N}{2\pi(1+\alpha)(1+a)} \quad , \tag{23}$$

with λ the wavelength of the photon emitted in the resonant transition, f the recoilless fraction, g_N the coupling constant, α the internal conversion coefficient, β the branching ratio, and μ is the linear attenuation coefficient. Inhomogeneous broadening is included through the term (1 + a) and the parameter a can be 10^6 or higher for isomeric nuclei of interest.

Thus when considering lasing or ASE the stimulation cross-section is assumed to be reduced by a time-independent factor $\frac{1}{1+a}$, while in SF the reduction of the intensity is characterized by a time-dependent phase factor which reflects the dynamic nature of the process and the evolution of the inverted state. The dephasing process can be described in terms of the dephasing time T_2^* as in Eq. (21).

E. TIME-DEPENDENT PERTURBATIONS

If the system under consideration is subjected to time-dependent perturbing effects, Eq. (14) can still be used to calculate the emission and absorption lineshapes for resonators acting independently. Assuming a time-dependent field acting on the nuclear spins we can write $H(t) = H_o + HI_z f(t)$,where f(t) is a random process. The lineshape is given by

$$P(k\omega p) = \frac{2}{\Gamma} \mathrm{Re} \int_0^\infty dt\, e^{i\omega t - \frac{\Gamma}{2} t \overline{\langle V^{(-)} V^{(+)}(\tau) \rangle}} \, ,$$

where the bar indicates an average over all functions f(t).

Let's assume that $f(t) = \pm 1$, selected at random for different t, and $H = H_o = \mu_o g_o h$ for the ground state and $H = H_1 = \mu_1 g_1 h$ for the excited state, with μ_i, g_i the respective magnetic moments and geomagnetic ratio, and h is the strength of the field, and let $\hbar = 1$ for convenience. Blume (Ref. 19) has computed the indicated average to be

$$< V^{(-)} V^{(+)} (t) > = e^{i(E_o - E_1)t} \left(\frac{1}{2I_1 + 1} \right) \sum_{m_o m_1} | < I_o m_o | V^{(+)} | I_1 m_1 > |^2$$

$$\times \left\langle e^{i(g_o m_o - g_1 m_1)\mu h \int_o^t f(t')\, dt'} \right\rangle_{ave} . \qquad (24)$$

The average on the right-hand side of (24) can be calculated as follows:

$$\left\langle e^{i\alpha \int_o^t f(t')\, dt'} \right\rangle_{ave} = \left(\cos x\, \Omega t + \frac{1}{x} \sin \Omega t \right) e^{-\Omega t} , \qquad (25)$$

where

$$x = \left| \frac{\left(g_o m_o - g_1 m_1 \right)^2 \mu^2 h^2}{\Omega^2} - 1 \right|^{\frac{1}{2}} . \qquad (26)$$

In the above, Ω is the relaxation rate or probability of jumping or flipping between values of $f(t) = +1$ and -1, with equal probabilities of finding the system in either $+1$ or -1. For a more general case assuming different probabilities of finding the system in state $f(t) = +1$ and -1, Balko and Hoy (Ref. 23) have calculated the Mössbauer lineshape to be

$$I(\omega) = \frac{(\alpha\Delta^+ - \Delta^-)\left[\Gamma\omega + \Omega(\Delta^+ - \alpha\Delta^-)\right] - (1+\alpha)\,\gamma\left(\Delta^+\Delta^- + \frac{1}{2}\Gamma\gamma\right)}{\left(\Delta^+\Delta^- + \frac{1}{2}\Gamma\gamma\right)^2 + \left[\Gamma\omega + \Omega(\Delta^+ - \alpha\Delta^-)\right]^2} , \qquad (27)$$

where

$$\Delta^+ = \omega + \delta, \quad \Delta^- = -\omega + \delta, \quad \gamma = (\alpha + 1)\,\Omega + \left(\frac{1}{2}\Gamma\right),$$

$$\alpha = (\Gamma/\Omega) + k .$$

To determine the effect of time-dependent perturbations on the SF pulse we generalize Eq. (18) to multiple levels by introducing the density matrix formalism as in the discussion following Eq. (13).

Then

$$\hat{I}_{N^2}(\omega) = \sum_{i,j\neq i}^{N} \int_0^\infty dt' \int_0^\infty dt'' \langle\lambda_i| V^{(-)} |\alpha_i\rangle\langle\alpha_j| V^{(+)} |\lambda_j\rangle$$

$$\times e^{i(E_{\lambda i}-E_{\alpha i})t} e^{-i(E_{\lambda j}-E_{\alpha j})t} e^{+i\omega(t'-t'') - \frac{\Gamma}{2}(t'+t'')}$$

becomes

$$\hat{I}_{N^2}(\omega) = \sum_{i,j\neq i}^{N} \int_0^\infty dt' \int_0^\infty dt'' \langle\lambda_i| e^{iE_{\lambda i}t'} V^{(-)} e^{-E_{\alpha i}t'} |\alpha_i\rangle\langle\alpha_j| e^{iE_{\alpha j}t''} V^{(+)} e^{iE_{\lambda j}t''} |\lambda_j\rangle$$

$$\times e^{+i\omega(t'-t'') - \frac{\Gamma}{2}(t'+t'')}$$

$$= \sum_{i,j\neq i} \int_0^\infty dt' \int_0^\infty dt'' \langle\lambda_i| V^{(-)}(t') |\alpha_i\rangle\langle\alpha_j| V^{(+)}(t'') |\lambda_j\rangle e^{i\omega(t'-t'') - \frac{\Gamma}{2}(t'+t'')} \quad . (28)$$

The matrix elements can be rewritten using Eq. (11) to show explicitly the time dependence, and the stochastic average can be taken as in Eq. (23), using the Hamiltonian of Eq. (22).

The matrix elements are

$$\langle\lambda_i| V_i^{(-)}(t) |\alpha_i\rangle = \langle\lambda_i| e^{i\int_0^t H(t')\,dt'} V_i^{(-)} e^{-i\int_0^t H(t')\,dt'} |\alpha_i\rangle$$

$$= \sum_{\lambda_i', \alpha_i'} \langle\lambda_i| e^{i\int_0^t H(t')\,dt'} |\lambda_i'\rangle\langle\lambda_i'| V_i^{(-)} |\alpha_i'\rangle\langle\alpha_i'| e^{-i\int_0^t H(t')'\,dt'} |\alpha_i\rangle$$

$$= \sum_{\lambda_i', \alpha_i'} \delta_{\lambda_i, \lambda_i'} e^{iE_i t' + ig_i\mu hm_i \int_0^{t'} f(t'')\,dt''} \langle\lambda_i'| V_i^{(-)} |\alpha_i'\rangle$$

$$\times \delta_{\alpha_i, \alpha_i'} e^{-iE_o t' - ig_o\mu hm_o \int_0^{t'} f(t'')\,dt''} .$$

Similarly

$$< \alpha_j | V(t'')^{(+)} | \lambda_j > = \sum_{\lambda_j', \alpha_j'} \delta_{\lambda_j, \lambda_j'} e^{+ iE_o t'' + ig_o\mu_o \int_o^{t''} f(t''') dt'''} < \alpha_j' | V_j^{(+)} | \lambda_j' >$$

$$\times \delta_{\alpha_j, \alpha_j'} e^{- iE_1 t'' - ig_1\mu hm_1 \int_o^{t''} f(t''') dt'''} .$$

We have used the condition that $V^{(\pm)}$ connects only the ground and excited states and our time-dependent Hamiltonian $H(t)$ only changes the energy of a state but doesn't induce transitions between states.

Integrating over ω, since we are interested in all energies, we get a $\delta(t' - t'')$ from the $e^{i\omega (t' - t'')}$. Performing the integral over t'', taking the average over initial states and the sum over final states, and concentrating our interest on a single nuclear transition, thus dropping the sum over α and λ, we get

$$I_{N^2}(t) = \sum_{i,\, j \neq i}^{N} < \lambda_i | V_i^{(-)}(0) | \alpha_i > < \alpha_j | V_j^{(+)} | \lambda_j > e^{-\Gamma t}$$

$$\times \overline{\left(e^{i\left(g_1\mu hm_1 - g_o\mu hm_o\right) \int_o^t f(t')\, dt'} \right)_i \left(e^{+i\left(g_o\mu hm_o - g_1\mu hm_1\right) \int_o^t f(t')\, dt'} \right)_j} , \qquad (29)$$

where on the right-hand side the bar over the two factors in parentheses indicates the average value.

The random variation of f(t') at nucleus i is independent of the variation of f(t') at nucleus j. Generally, one has to take into account at the same time,

(a) the independent fluctuations at nuclei i and j, and

(b) the variation in the two sites of the parameter α over an appropriate distribution.

The stochastic averages can then be taken as in Eq. (24) using the Hamiltonian of Eq. (22). We get

$$I_{N^2}(t) = \sum_{i,\, j \neq i}^{N} \sum_{\lambda,\, \alpha} < \lambda_i \left| V_i^{(-)} \right| \alpha_i >< \alpha_j \left| V_j^{(+)} \right| \lambda_j > G^2(\Omega, \alpha, t) e^{-\Gamma t} \qquad (30)$$

where

$$G(\Omega, \alpha, t) = \left(\cos x\,\Omega t + \frac{1}{x}\,\sin x\,\Omega t\right)e^{-\Omega t} \tag{31}$$

and

$$x = \left[\frac{\alpha^2}{\Omega^2} - 1\right]^{1/2}$$

$$\alpha = \left|g_1 \mu hm_1 - g_o \mu hm_o\right|$$

as expected for $\Omega >> \alpha$, $G(t) \approx 1$, and the inhomogeneous broadening and phase destruction of the superradiant pulse disappears, while for $\Omega << \alpha$, $G(t) \approx \frac{1}{2}\left(e^{i\alpha t} + e^{-i\alpha t}\right)$ and the maximum phase destruction occurs if $G(\Omega, \alpha, t)$ is calculated for a distribution of α's given by $g(\alpha)$ which represents the appropriate inhomogeneous broadening.

If we assume the distribution is gaussian with variance σ^2 then

$$g(\alpha,\sigma) = \frac{1}{\sigma\sqrt{2\pi}}\,e^{-\alpha^2/2\,\sigma^2} \tag{32}$$

and the average value

$$\overline{G}(\Omega, \sigma, t) = \int_0^\infty \gamma(\alpha, \sigma)\, G(\Omega, \alpha, t)\, d\alpha \tag{33}$$

should replace $G(\Omega, \alpha, t)$ in the expression Eq. (30) to obtain $I_{N2}(t)$.

In the following three figures we show some examples of the effectiveness of inhomogeneous broadening dephasing reduction factor $\overline{G}(\Omega, \sigma, \tau)$ as it depends on Ω and σ. In all cases $\Gamma = 1\ s^{-1}$ is assumed.

In Fig. 37 we show the function $\overline{G}(\Omega, \sigma, t)$ for parameters $\Omega = 0$, $\sigma = 1$, 10, and 100 as a function of time. The horizontal line labeled $\sigma = 0$ shows no reduction in the SF pulse intensity because there is no inhomogeneous broadening. The other three curves show the decrease in SF pulse intensity when different dephasing rates due to different amounts of inhomogeneous broadening are present. A SF pulse with a delay time of 1.6 sec, which would appear at the positions of the arrow labled ① when $\sigma = 0$, would be

reduced to about 1/2 of this value when $\sigma = 1$. A pulse appearing earlier (at arrow 2) would suffer less of a reduction. In Fig. 38 we show a plot of these results with the time axis on a logarithmic scale. For the three σ values the drop-off is clearly indicated at different times. Figures 39 and 40 show the reduction factor for $\sigma = 10^3$ and 10^4, respectively, and different values of the relaxation rate Ω. The curves decay rapidly for small values of Ω and slow down for higher values approaching the limit of 1.0 as Ω approaches infinity. The results of Figs. 39 and 40 indicate that time-dependent hyperfine interactions can reduce the effect of inhomogeneous broadening. As the relaxation rate Ω increases, the SF intensity also increases, and in the limit of $\Omega >> \sigma$ the SF pulse intensity approaches the value one obtains when σ=0. This SF pulse intensity is determined by the number of cooperating nuclei and the intensity of nuclear properties. Thus, if a candidate exists that when inverted would produce SF were it not for inhomogeneous broadening, our results show that it is still possible to get a SF emission if a fast enough relaxation of the levels producing the inhomogeneous broadening can be realized.

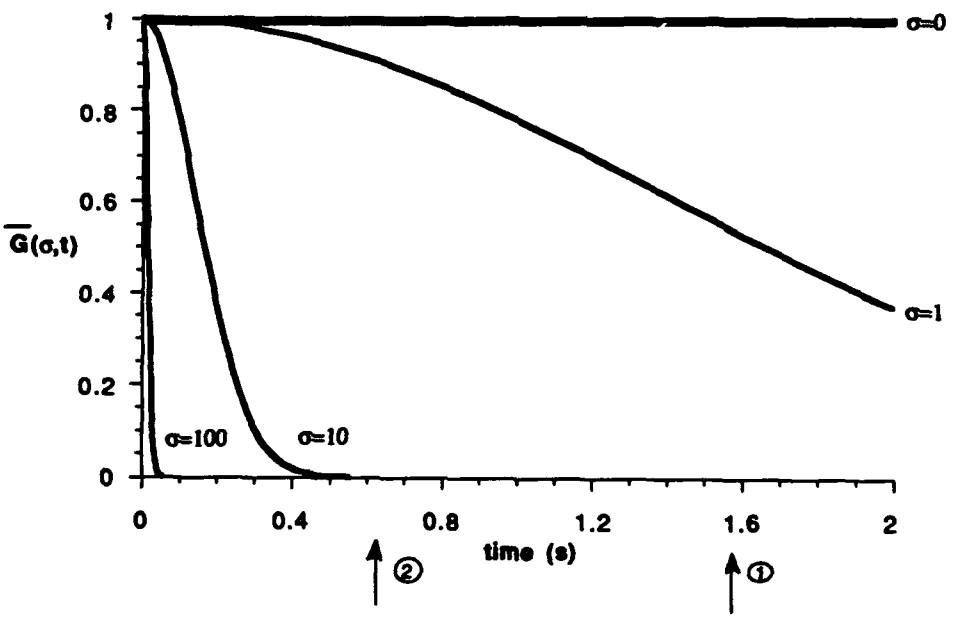

Figure 37. Reduction of SF Pulse Intensity by Inhomogeneous Broadening with Variance σ^2

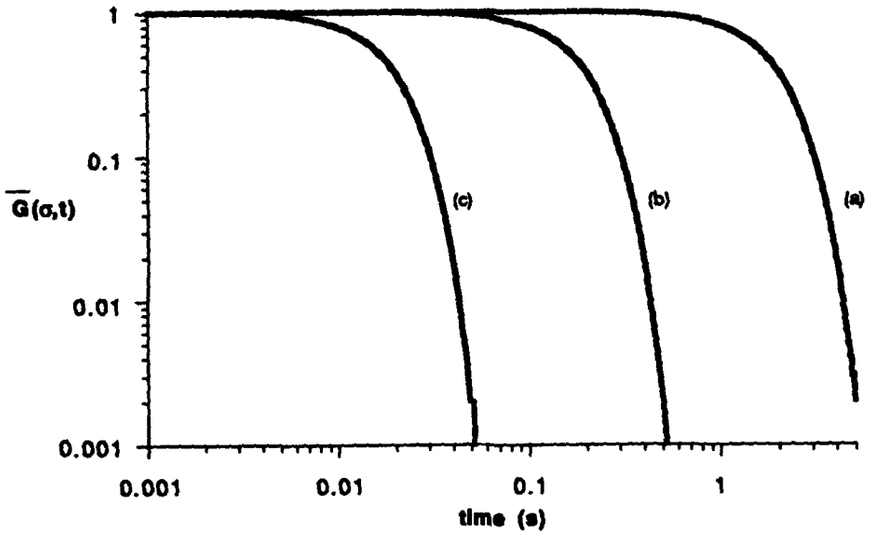

Figure 38. Semi-log Plot of the Results Shown in Figure 37. The drop-off times for different values of σ are clearly indicated. For (a) σ = 1, (b) σ = 10 and (c) σ = 100.

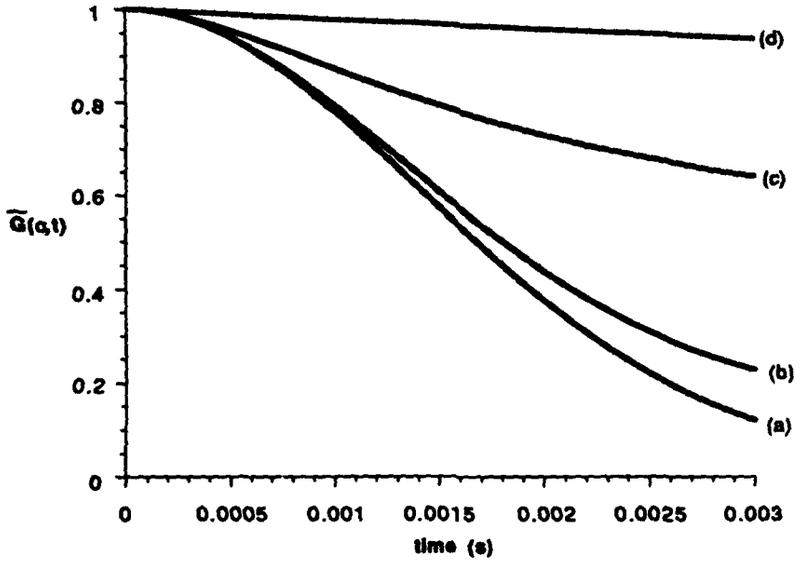

Figure 39. Recovery of SF Pulse Intensity by Relaxation in the Presence of Inhomogeneous Broadening with $\sigma = 10^3$. The relaxation rates are (a) $\Omega = 10$, (b) $\Omega = 10^2$, (c) $\Omega = 10^3$ and (d) $\Omega = 10^4$

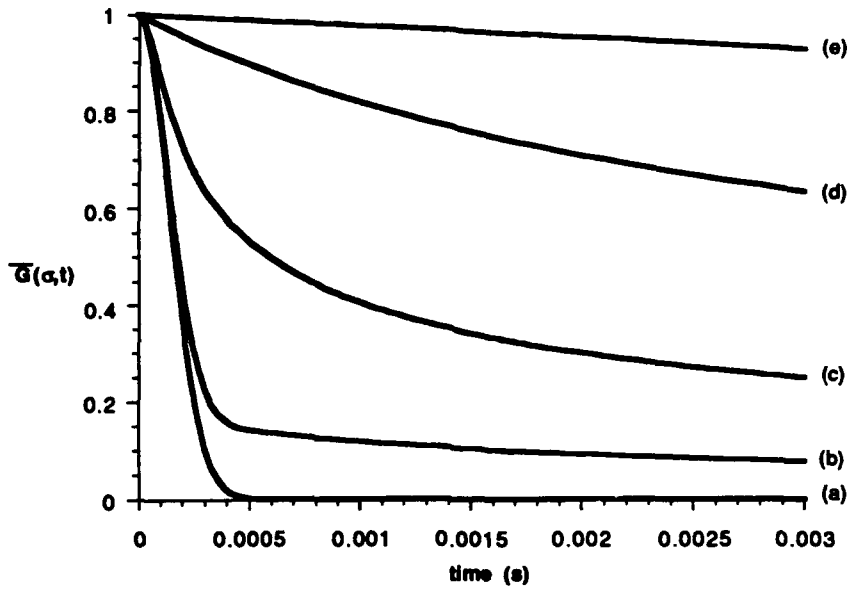

Figure 40. Recovery of SF Pulse Intensity by Relaxation in the Presence of Inhomogeneous Broadening with $\sigma = 10^4$. The relaxation rates are (a) $\Omega = 10$, (b) $\Omega = 10^3$, (c) $\Omega = 10^4$, (d) $\Omega = 10^5$ and (e) $\Omega = 10^6$.

F. CONCLUSIONS

Our calculations show that the effect of inhomogeneous broadening on SF emission is qualitatively different from that on ASE or lasing. The effect on SF is to cause dephasing of the different nuclear dipoles that are forming correlations. This dephasing is time dependent and has a time scale that goes inversely with the inhomogeneously broadened line. For times less than this, SF emission is less affected by this broadening than ASE or lasing. For the latter, the reduction is time independent and the stimulation cross-section is reduced by a factor of $\frac{1}{1+a}$ where $a = 2\sqrt{2ln2}\,\frac{\sigma}{\Gamma}\,\sigma$ is the variance of the distribution characterizing the inhomogeneous broadening and Γ is the natural line width.

We also show that time-dependent hyperfine interactions of the nucleus with the electrons can induce a reduction of the dephasing and an increase in the probability of SF over a large time range. These electronic relaxation effects are well known for their lineshape modification as observed in Mössbauer and nuclear magnetic resonance (NMR) experiments. For SF they provide a means of reducing the dephasing due to inhomogeneous broadening and thus may be useful in overcoming one of the more difficult obstacles to nuclear SF.

III. COHERENT EFFECTS AND INHOMOGENEOUS BROADENING

A. INTRODUCTION

In a recent publication (Ref. 24) we derived an expression for the inhomogeneously broadened lineshape expected in a Mössbauer absorption experiment. Assuming that the nuclei interacted incoherently, the expression for absorption was given as a product of intensity of incoming beam and the single nucleus absorption cross-section. We summarize the results here and then derive an expression assuming coherent processes for scattering of emissions from a multinuclear source by a multinuclear absorber. The calculation presented here was done to check the claims presented at a recent ultrashort wavelength laser review meeting that homogeneous broadening equally and intentionally produced in both source and absorber lines could produce an enhanced Mössbauer effect.

The experimental condition assumed for both calculations is shown in Fig. 41(a), and the lineshapes for both the inhomogeneously broadened source and absorber are depicted in Fig. 41(b).

B. INCOHERENT APPROACH

The detected loss in the total photon count, I_D, because of the presence of the absorber is given by

$$I_D = \int_{t_1}^{t_2} dt \int_{-\infty}^{+\infty} I(E, \Gamma, S)\, n\, \sigma(E, \Gamma)\, dE \qquad (34)$$

where n is the number of resonant nuclei in the beam per cm^2, and the measurement is performed during the time interval $t_2 - t_1$. $I(E, \Gamma, S)$ is the source radiation lineshape and $\sigma(E, \Gamma)$ is the resonant cross-section of the nuclei in the absorber.

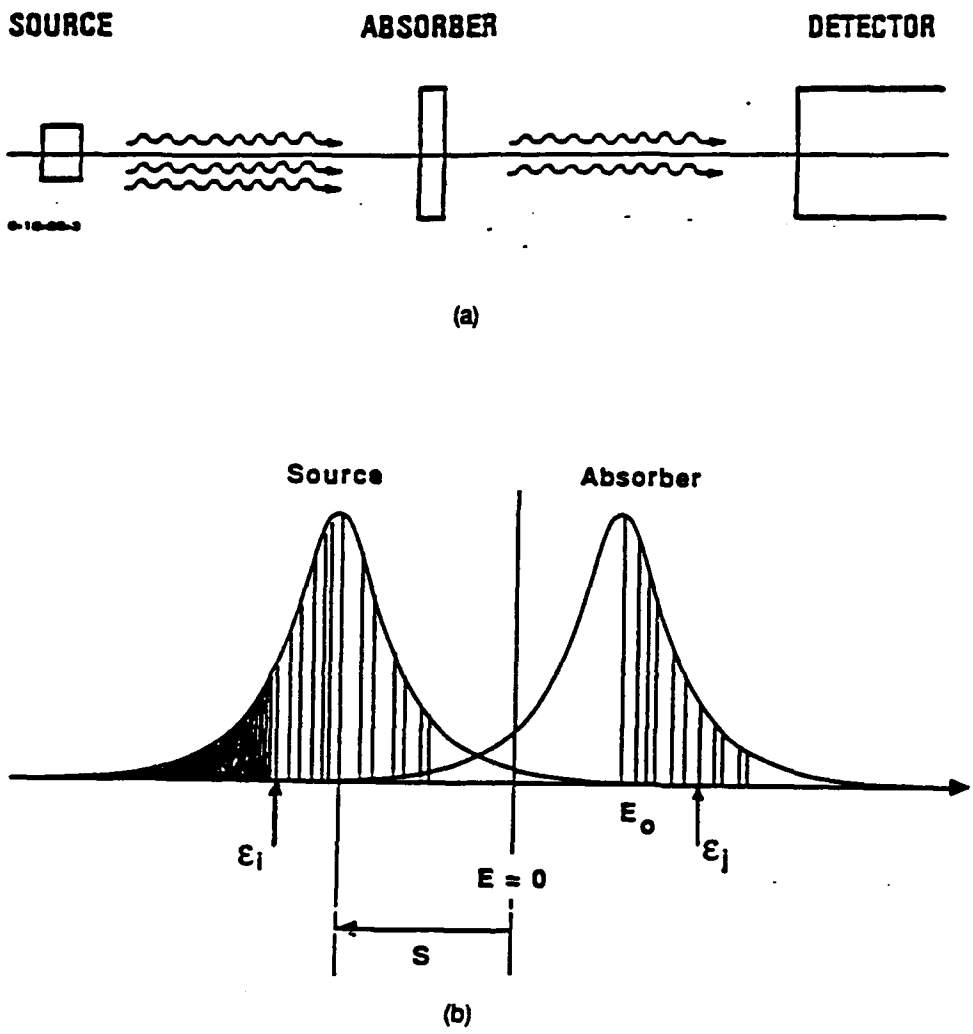

Figure 41. (a) A schematic showing the Mössbauer transmission experimental geometry. (b) A graphic representation of the source and absorber lineshapes. The vertical lines represent some of the natural lines of the different nuclei in the source and absorber whose envelopes are the inhomogeneously broadened lines. S represents the doppler shift of the source and ε_i and ε_j the resonance energies of nuclei i and j in the source and absorber, respectively.

The source lineshape is given by

$$I(E, \Gamma, S) = \sum_{i}^{N} P_i(\varepsilon_i) \frac{I_0 \left(\frac{\Gamma}{2\pi}\right) f_s}{[E-(E_0-\varepsilon_i)-S]^2 + (\Gamma/2)^2} \quad , \tag{35}$$

where I_0 is the flux of photons from the source in $cm^{-2}\,s^{-1}$ in the direction of the detector, E_0 is the resonant energy of an unperturbed nucleus, ε_i is the perturbation of the energy of nucleus i due to the environment, S is the Doppler shift due to the relative motion of the source and absorber nuclei and is given by S = v/c E, with velocity v where c is the speed of light, Γ is the natural linewidth[6] and f_s is the recoil-free fraction in the source. It is assumed in Eq. (34) that the integration time is short enough that I_0 can be taken as constant.

The distribution of nuclear environments is assumed to be normal with width Δ so that the probability of finding a nucleus with energy ε_i displaced from the resonance energy E_0 in a width $\Delta\varepsilon_i$ is given by

$$P_i(\varepsilon_i) = \frac{1}{\sqrt{\pi}\,\Delta} e^{-\varepsilon_i^2/\Delta^2} \Delta\varepsilon_i \quad . \tag{36}$$

Similarly, for the effective cross-section of the absorber we have

$$\sigma(E,\Gamma) = \sum_{i}^{N} P_i(\varepsilon_i) \frac{\sigma_o \Gamma_\gamma \Gamma f_a}{[E-(E_0-\varepsilon_i)]^2 + (\frac{\Gamma}{2})^2} \quad . \tag{37}$$

Where σ_0 is the cross-section on resonance and is given by

$$\sigma_0 = \frac{\lambda^2}{2\pi} \frac{2I_e+1}{2I_g+1} \frac{1}{1+\alpha} \quad .$$

I_e and I_g are the nuclear spin quantum numbers of the excited and ground states, respectively, α is the internal conversion coefficient of the transition, λ is the nominal wavelength of the gamma-ray, Γ_γ is the photon absorption partial width.

---

6 Γ is the total level width which is a sum of the level widths of all the processes contributing to the level decay.

Assuming the source lineshape, absorber cross-section, and distribution of nuclear environments as given by Eqs. (35), (37), and (36), respectively, the intensity of the beam I' absorbed by a thin absorber[7] ($E_o = 0$ without loss of generality) is given by

$$I'(\Gamma, \Delta, S) = \frac{I_o \sigma_o}{4\pi\Delta_1\Delta_2} n_a \sum_i^{N_s} \sum_j^{N_a} e^{-\epsilon_i^2/\Delta_1^2} e^{-\epsilon_j^2/\Delta_2^2} \Delta\epsilon_i \Delta\epsilon_j$$

$$\times \int_{-\infty}^{+\infty} dE \frac{(\Gamma/2\pi)}{(E-\epsilon_i-S)^2 + (\Gamma/2)^2} \frac{\Gamma_\gamma \Gamma}{(E-\epsilon_j)^2 + (\Gamma/2)^2} \qquad (38)$$

where N_s, N_a are the total number of sites with energy shifts ϵ_i and ϵ_j in the source and absorber, respectively, and where n_a is the number of nuclei per cm^2 in the absorber. Converting the sum to an integral, one has (see Ref. 24).

$$I'(\Gamma,\Delta,S) = \frac{\sqrt{2\pi}}{4} I_o \sigma_o (\Gamma_\gamma/\Delta) n_a \, \mathrm{Re}\,(e^{Z^2}) \, \mathrm{erfc}(Z) \qquad (39)$$

where

$$\Delta^2 \equiv (\Delta_1^2 + \Delta_2^2)/2 \text{ , and } Z \equiv (\Gamma + iS)/\sqrt{2}\,\Delta \quad .$$

The maximum normalized resonant absorption ($S = 0$) is given by

$$I''(\Gamma,\Delta) = I'(\Gamma,\Delta,S=0)/\left(\tfrac{1}{2} I_o n_a \sigma_o\right) \qquad (40)$$

$$= \frac{\sqrt{\pi}}{2} \left(\frac{\Gamma_\gamma}{\Gamma}\right) \left[x\, e^{x^2} \mathrm{erfc}\, x\right],$$

where

$$x = \frac{\Gamma}{\sqrt{2}\,\Delta} \quad .$$

Figure 42 shows the normalized plot of expression in Eq. (40).

---

7 A thin Mössbauer absorber is one for which the lineshape of the beam passing through the absorber is not sufficiently modified to show saturation effects. This is discussed in Appendix B, Ref. 24, where it is shown that for the Mössbauer thickness $b < 10$ the ratios of the intensities of the lines in the spectrum are close to their theoretical values and saturation effects are small. Under such conditions, it is appropriate to use Eq. (34) for the absorption calculations instead of the general expression given in Eq. (41), Ref. 24.

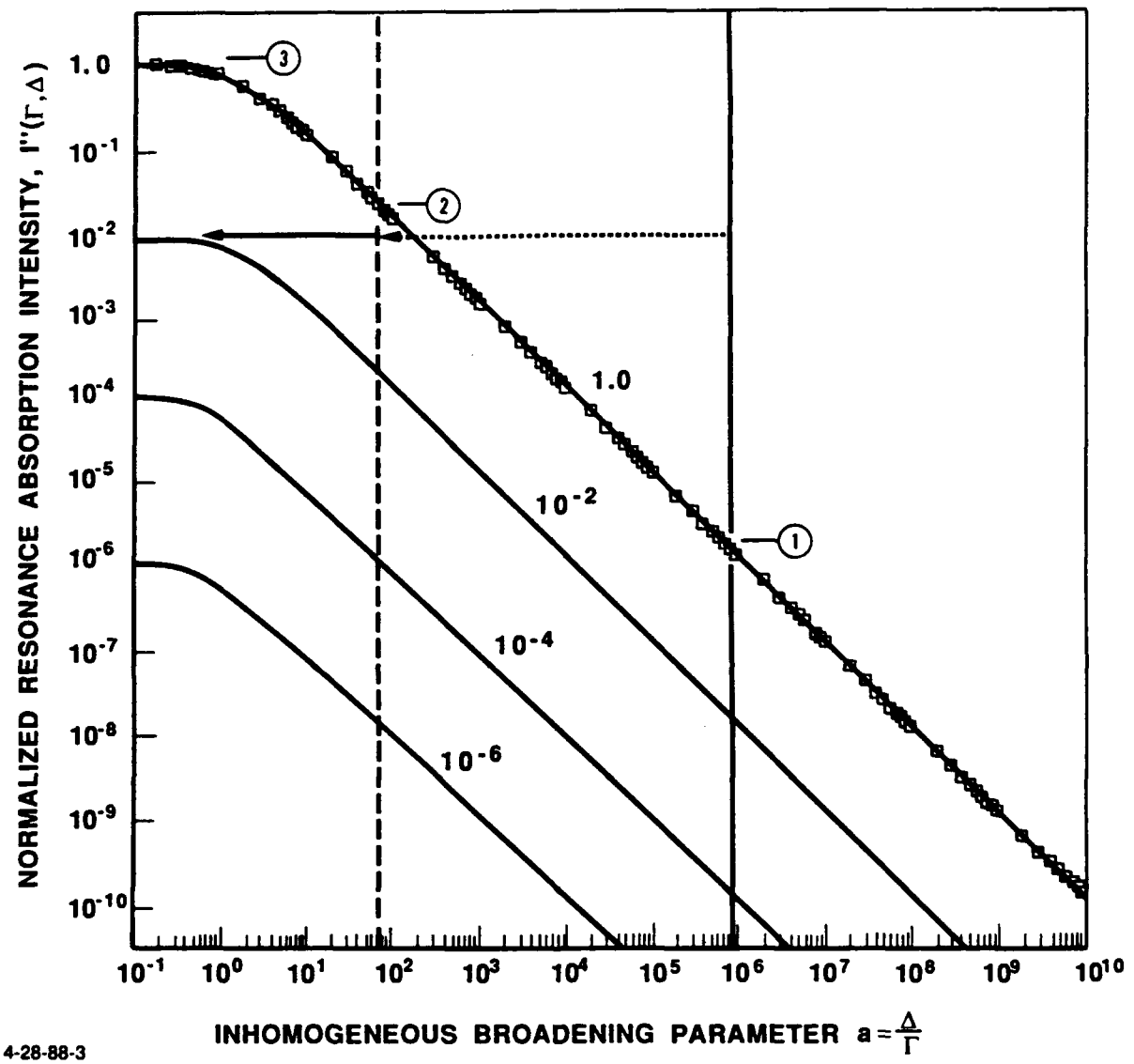

Figure 42. Plots of the Maximum Normalized Resonance Absorption Curves, $I''(\Gamma,\Delta)$, Calculated From Eq. (40) and Plotted as a Function of Δ/Γ. The numbers labeling the curves give the different values of Γ_γ/Γ. The dashed horizontal arrow shows the effect on the resonance expected from RF pulsing techniques and the solid arrow the reduction in inhomogeneous broadening expected from good crystal preparation techniques from ordinary isomeric samples with a broadening parameter of $a = 10^6$.

Note that there is a dependence on $x = \frac{\Gamma}{\sqrt{2}\,\Delta}$ through the exponential and error function terms and a dependence on Γ alone through the factor Γ_γ/Γ. When the inhomogeneous broadening is reduced by some means $\Delta \to 0$, $x \to \infty$, and I" approaches a maximum $1/2\ I_0\sigma_0 n_a\ (\Gamma_\gamma/\Gamma)$. When the lines are homogeneously broadened to obtain overlap $\Gamma \to \Delta$ or in the limit $\Gamma \to \infty$, $x \to \infty$ and the second term becomes maximum but then $(\Gamma_\gamma/\Gamma) \to 0$. Thus, although total overlap is achieved, the resonant effect disappears because the maximum radiative cross-section on resonance is reduced to keep the total integrated cross-section constant.

This does not happen when $\Gamma_\gamma/\Gamma = 1$, but this is highly unlikely in nuclear systems. Generally, the total width Γ is a sum of several parts including the radiative width Γ_γ, the internal conversion Γ_α, and other transitions Γ_i so that

$$\Gamma = \Gamma_\gamma + \Gamma_\alpha + \sum_i \Gamma_i \quad .$$

Under these more realistic conditions homogeneous broadening alone will not increase the resonant effect even though complete overlap of lines is achieved unless we go to the "motionally " narrowed limit and all the inhomogeneous effects are wiped out. (See Ref. 24, Fig. 24.)

C. COHERENT APPROACH

To treat the problem coherently, since we do not know which nucleus emitted and which is going to be excited, we have to sum over the amplitudes for all nuclear processes. The amplitudes have to be calculated for a scattering process since we also have to include the deexcitations coherently.

Consider the emission of a photon of energy E by the i^{th} nucleus in the source at a resonance energy, $E_o + \varepsilon_i$, where ε_i is the energy shift due to the environment. This shift is responsible for the inhomogeneous broadening of the system linewidth. The photon γ', scattered by the j^{th} nucleus in the absorber, has energy E'. The process is depicted in Fig. 43.

Heitler (Ref. 25) has shown how to calculate the differential scattering cross-section for a single resonator (nucleus or atom) using second-order perturbation theory. Boyle and Hall (Ref. 17) have generalized these results to a system of many nuclei.

Our discussion follows these two developments. Following Heitler and Boyle and Hall, the amplitude for the process depicted in Fig. 43 where the i^{th} nucleus in the source emits a photon of energy E and the j^{th} nucleus in the absorber absorbs the photon of energy E and emits a photon of energy E' is given by

$$A_{ij} = S_o P_i \frac{1}{\left[(E'-E) - i\frac{\gamma}{2}\right]} \frac{1}{\left[\left(E' - \varepsilon_j - E_0\right)\right] - i\frac{\Gamma}{2}} , \qquad (41)$$

where P_i is the probability nucleus i emits at energy E and all the energy independent terms have been lumped into S_o. For identical source and scatterer nuclear environments ($\varepsilon_i = \varepsilon_j = 0$) Eq. (41) reduces to

$$A_{ij} = S_o \frac{1}{\left[(E'-E) - i\frac{\gamma}{2}\right]} \frac{1}{\left[\left(E' - E_o\right) - i\frac{\Gamma}{2}\right]} . \qquad (42)$$

From Boyle and Hall's result we find that $S_o^2 = \frac{\gamma}{2\pi}\left(\frac{\Gamma^2}{4}\right)\sigma_o\left(\frac{\Gamma_\gamma}{\Gamma}\right)F(\theta)$ where γ is the width of the ground state due to the presence of radiation, Γ is the natural width of the transition and the angular term can be written in terms of Clebsh-Gordon coefficients and vector spherical harmonics as shown in References 26 and 27.

For a system of N source nuclei and M absorber nuclei we get for the total scattered intensity

$$I_{total} = \sum_i^N \left| \sum_j^M A_{ij} \right|^2 , \qquad (43)$$

of which the incoherent part is given by

$$I_{incoh} = \sum_{i,j}^{N,M} \left| A_{ij} \right|^2 , \qquad (44)$$

and the interference term by

$$I_{int} = \sum_i^N \sum_{\substack{j,k \\ j \neq k}}^{M,K} A_{ij} A_{ik}^* . \qquad (45)$$

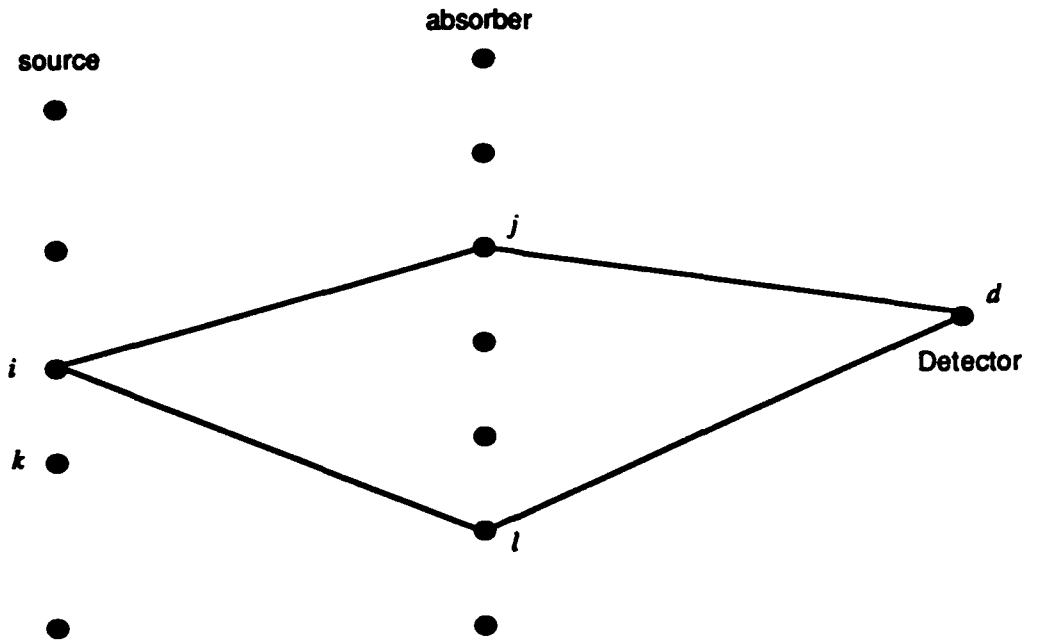

Figure 43. A Graphic Representation of the Scattering Process. Nuclei in the source emit photons that are scattered by the absorber and eventually detected. As on example, processes $i \rightarrow j$ and $i \rightarrow l \rightarrow d$ are possible contributors but not $k \rightarrow l \rightarrow d$.

Assuming a normal distribution of nuclear environment as given by Eq. (36) and converting the sums to integrals we get:

$$I_{total}(E) = \int_{-\infty}^{+\infty} d\varepsilon \int_{-\infty}^{+\infty} d\varepsilon_1 \int_{-\infty}^{+\infty} d\varepsilon_2 \, I_{beam}(E, \varepsilon) \, A(E, E', \varepsilon_1) \, A^*$$

$$\times (E, E', \varepsilon_2) \, P(\varepsilon) \, P(\varepsilon_1) \, P(\varepsilon_2) \, n_s n_a^2 \frac{d\Omega}{4\pi} dA \qquad (46)$$

with the incoming beam profile given by

$$Ibeam(E, \varepsilon) = \frac{\left(\frac{\Gamma}{2\pi}\right) f_a}{\left(E - E_0 - \varepsilon\right)^2 + \left(\frac{\Gamma}{2}\right)^2} \quad ,$$

$$A(E, E', \varepsilon') = S_o \frac{1}{\left[(E' - E) - i\gamma/2\right]} \frac{1}{\left[\left(E' - \varepsilon' - E_0\right) - i\Gamma/2\right]} \quad , \qquad (47)$$

$$P(\varepsilon) = \frac{1}{\sqrt{\pi}\,\Delta}\, e^{\frac{-\varepsilon^2}{\Delta^2}} \quad , \tag{48}$$

and n_s, n_a are the number densities of nuclei in source and absorber, respectively, and $d\Omega$ is the solid angle intercepting the absorber area dA. The factor $\frac{d\Omega}{4\pi} n_s$ picks out the nuclei emitting in the direction of the absorber and intercepting the absorber area dA.

For maximum effect S = E_0 = 0. Assuming E_0 = 0 and replacing S_o^2 by its definition we get

$$I_{tot}(E') = \frac{\gamma}{2\pi}\left(\frac{\Gamma^2}{4}\right)\left(\frac{\Gamma}{2\pi}\right)\sigma_0\,\frac{\Gamma_\gamma}{\Gamma}\,\frac{n_a^2\, n_s}{\sqrt{\pi}\,\Delta}\int_{-\infty}^{+\infty} dE\,\frac{1}{(E-\varepsilon)^2+\left(\frac{\Gamma}{2}\right)^2}$$

$$\times\frac{e^{-\varepsilon^2/\Delta^2}\,d\varepsilon}{\left[(E'-E)^2+\left(\frac{\gamma}{2}\right)^2\right]}\,\frac{1}{\sqrt{\pi}\,\Delta}\int_{-\infty}^{+\infty}\frac{e^{-\varepsilon_1^2/\Delta^2}\,d\varepsilon_1}{\left[(E'-\varepsilon_1)-i\frac{\Gamma}{2}\right]}\,\frac{1}{\sqrt{\pi}\,\Delta}\int_{-\infty}^{+\infty}\frac{e^{-\varepsilon_2^2/\Delta^2}\,d\varepsilon_2}{\left[(E'-\varepsilon_2)+i\frac{\Gamma}{2}\right]} \quad . \tag{46a}$$

If we look at Eq. (46a) and group $\sigma_0\,\Gamma^2/4$, $\gamma/2\pi$, and $\frac{\Gamma}{2\pi}$ with the resonant denominators containing Γ and γ, respectively, then these terms will be normalized like an absorption cross-section with maximum σ_0 in units of area and a beam with integrated intensity of one photon/area [compare Eq. (35) and Eq. (37)]. The maximum intensity will occur at energies when all terms are on resonance. The factor multiplying the overall expression will be $\frac{\Gamma_\gamma}{\Gamma}$. In general when the total cross-section Γ is increased to Δ to obtain overlap of resonance lines, the factor $\frac{\Gamma_\gamma}{\Gamma}$ will reduce the overall effect.

We first perform the integral over E in Eq. (46a) using the result of Appendix F (below) that

$$\int_{-\infty}^{+\infty} dE\,\frac{1}{(E-\varepsilon)^2+\left(\frac{\Gamma}{2}\right)^2}\,\frac{1}{(E'-E)^2+\left(\frac{\gamma}{2}\right)^2} = \frac{2\pi\left(\frac{1}{\Gamma}+\frac{1}{\gamma}\right)}{(E'-\varepsilon)^2+\left(\frac{\Gamma+\gamma}{2}\right)^2} \quad .$$

Equation (46a) can be written as

$$I_{tot}(E') = \frac{\gamma}{2\pi}\left(\frac{\Gamma^2}{4}\right)\sigma_0 \frac{\Gamma_\gamma}{\Gamma} \frac{n_a^2 n_s}{\sqrt{\pi}\ \Delta}\left(1+\frac{\Gamma}{\gamma}\right)\int_{-\infty}^{+\infty} \frac{e^{-\epsilon^2/\Delta^2} d\epsilon}{\left[(E'-\epsilon)^2 + \left(\frac{\Gamma+\gamma}{2}\right)^2\right]} \frac{1}{\sqrt{\pi}\ \Delta}$$

$$\times \int_{-\infty}^{+\infty} \frac{e^{-\epsilon_1^2/\Delta^2} d\epsilon_1}{\left[(E'-\epsilon_1) - i\frac{\Gamma}{2}\right]} \frac{1}{\sqrt{\pi}\ \Delta} \int_{-\infty}^{+\infty} \frac{e^{-\epsilon_2^2/\Delta^2} d\epsilon_2}{\left[(E'-\epsilon_2) + i\frac{\Gamma}{2}\right]} \quad . \tag{46b}$$

The right-hand side of Eq. (46b) can be evaluated further by noting that the expression breaks up into a product of three integrals of form

$$B_1(z, \Delta, \Gamma) = \int_{-\infty}^{+\infty} \frac{e^{-x^2/\Delta^2} dx}{(E'-x)^2 + (\Gamma/2)^2} = \frac{\pi}{\Gamma} e^{z^2} \operatorname{erfc} z \tag{49}$$

$$B_2(z_1, \Delta, \Gamma) = \int_{-\infty}^{+\infty} \frac{e^{-x^2/\Delta^2} dx}{(E'-x) - i\left(\frac{\Gamma}{2}\right)} = i\frac{\pi}{2} e^{z_1^2} \operatorname{erfc} z_1 \tag{50}$$

$$B_3(z_2, \Delta, \Gamma) = i\pi e^{z_2^2} \operatorname{erfc} z_2 - 2\pi i e^{-z_2^2}$$

where

$$z = \frac{\Gamma + iE'}{2\Delta}\ ,\ z_1 = \frac{iE' - \frac{\Gamma}{2}}{\Delta} \text{ and } z_2 = \frac{-\left(iE' + \frac{\Gamma}{2}\right)}{\Delta} \quad . \tag{51}$$

The expression for B was obtained earlier [see Eq. (39) and Ref. 24]. The expressions for B2 and B3 are derived in Appendix D (below). Using expressions (49), (50), and (51) we can rewrite (46a) as

$$I_{tot}(E') = S_0^2\ n_s n_a^2 \frac{1}{\pi \frac{3}{2}\Delta^3} B_1(z, \Delta, \Gamma)\, B_2(z_1, \Delta, \Gamma)\, B_3(z_2, \Delta, \Gamma) \quad .$$

The total number of events at the detector is obtained by integrating over the scattered energy E' to get

$$I = \int_{-\infty}^{+\infty} I_{tot}(E')\, dE'$$

$$= \sigma_o \left(\frac{\Gamma_\gamma}{\Gamma}\right) \frac{n_s n_a^2}{\pi^{\frac{5}{2}}} \left(\frac{\Gamma}{2\Delta}\right)^3 \int_{-\infty}^{+\infty} dE'\, B_1(z, \Delta, \Gamma)\, B_2(z, \Delta, \Gamma)\, B_3(z_2, \Delta, \Gamma) \quad .$$

The integration has to be done numerically for arbitrary parameters but in the limit $\frac{\Gamma}{2\Delta} \to \infty$ we get an explicit result (see Appendix E, below) $I \to \sigma_o \left(\frac{\Gamma_\gamma}{\Gamma}\right) \frac{n_s n_a^2}{3\pi^2}$, which can be interpreted as follows: For $\Delta \to 0$ and Γ finite (i.e., the natural linewidth) the maximum effect is observed. For Δ = finite and $\Gamma \to \infty$ (i.e., large homogeneous broadening) the effect goes to zero because of the factor $\left(\frac{\Gamma_\gamma}{\Gamma}\right)$, in agreement with the incoherent calculation.

D. CONCLUSIONS

We have examined the effect of inhomogeneous broadening on nuclear resonance absorption in a Mössbauer experiment. As the broadening increases, the resonance effect between source and absorber decreases. Increasing the homogeneous broadening (i.e., the broadening of each resonance line in a system by the same amount in the source and absorber) increases the overlap of lines but *decreases* the overall Mössbauer effect. This is in contradiction to statements made at a recent ultrashort wavelength laser meeting. This happens in both an incoherent and a coherent calculation. Thus, the homogeneous broadening in both the source and absorber by itself will not in general improve the resonance effect.

REFERENCES

1. J.C. MacGillivray and M.S. Feld, "Theory of Superradiance in an Extended, Optically Thick Medium," *Phys. Rev. A*, **14**, No. 3 (1976), pp. 1169-1189.

2. G.C. Baldwin, J.C. Solem, and V.I. Gol'danskii, "Approaches to the Development of Gamma-Ray Lasers," *Rev. Mod. Phys.*, **53**, No. 4 (1981), pp. 687-744.

3. B. Balko et al., *IDA Gamma-Ray Laser Annual Summary Report (1988): Investigation of the Feasibility of Developing a Laser Using Nuclear Transitions*, Institute for Defense Analyses, IDA Paper P-2175 (1990).

4. G.T. Trammel and J.P. Hannon, *Opt. Commun.*, **15**, No. 3 (1975), pp. 325-329.

5. G.C. Baldwin and M.S. Feld, *J. App. Phys.*, **59** (1986), p. 3665.

6. M.S. Feld and J.C. McGillivray in *Coherent Nonlinear Optics, Recent Advances*, edited by M.S. Feld and V.S. Letokhov, Chaper 2, Springer Verlag (1980).

7. R. Bonifacio and L.A. Lugiato, "Cooperative Radiation Processes in Two-level Systems: Superfluorescence," *Phys. Rev. A*, **11**, No. 5 (1975), pp. 1507-1521; "Cooperative Radiation Processes in Two-level Systems: Superfluorescence II," *Phys. Rev. A*, **12**, No. 2 (1975), pp. 587-598.

8. H.M. Gibbs, Q.H.F. Vrehen, and H.M.J. Hikspoors, *Phys. Rev. Lett.*, **39** (1977), p. 547.

9. M. Feld, "Superradiance and Laser-Controlled Gamma Emission," *Proceedings of the IST/IDA Gamma-Ray Laser Workshop*, Eds. B. Balko, L. Cohen, and F.X. Hartmann, Institute for Defense Analyses, IDA Memorandum Report M-162, January, 1986.

10. J. Mostowski and B. Sobolewska, "Initiation of Superfluorescence from a Sphere," *Phys. Rev. A*, **28**, No. 5 (1983), pp. 2943-2952; "Three Dimensional Theory of Initiation of Superfluorescence," *Phys Rev. A*, **30**, No. 3 (1984), pp. 1392-1400.

11. F. Haake and R. Reibold, "Interplay of Superfluorescence and Incoherent Processes in Multilevel Systems," *Phys. Rev. A*, **29**, No. 6 (1984), pp. 3208-3217.

12. D. Polder, M.F.H. Schuurmanns, and Q.H.F. Vrehens, "Superfluorescence: Quantum-Mechanical Derivation of Maxwell-Bloch Description with Fluctuating Field Source," *Phys. Rev. A*, **19**, No. 3 (1979), pp. 1192-1203.

13. J.H. Eberley, *ACTA Phys. Polonica* **A39**, 633 (1971).

14. J.H. Terhune and G.C. Baldwin, *Phys. Rev. Lett.*, **14**, (1965), pp. 589-591.

15. I. Kay, Chapter II in Ref. 3.

16. B. Balko, L. Cohen, and F.X. Hartmann, *IDA Gamma-Ray Laser Annual Summary Report (1985), Investigation of the Feasibility of Developing a Laser Using Nuclear Transitions (Revised Edition)*, Institute for Defense Analyses, IDA Paper P-2021 (Rev.) (1985)

17. A.J.F. Boyle and H.E. Hall, *Rep. Prog. Phys.* **25**, 441 (1962), and Ref. 14.

18. B. Balko and G.R. Hoy, *Phys. Rev. B* **10**, 4523 (1974), and *Phys. Rev. B* **10**, 36 (1974).

19. M. Blume in *Hyperfine Structure and Nuclear Radiations*, edited by E. Matthias and D.A. Shirley, North Holland, Amsterdam (1968).

20. J. Okada, K. Ikeda, M. Mutsuoka, *Optics Comm.* **27**, No. 3, 321 (1978).

21. Chapter I and Appendix B in Ref. 3.

22. B. Balko in "Gamma-Ray Lasers," a special issue of the *J. Quant. Spectrosc. Radiat. Transfer* edited by B. Balko, L. Cohen, D. Sparrow, Vol. **40** #6, 1988.

23. B. Balko and G.R. Hoy, *Phys. Rev. B* **10**, 36 (1974).

24. B. Balko, L. Cohen, and J. Nicoll, *IDA Gamma-Ray Laser Summary Report (1987), Investigation of the Feasibility of Developing a Laser Using Nuclear Transitions*, Institute for Defense Analyses, IDA Paper P-2083, December 1985.

25. W. Heitler, *Quantum Theory of Radiation*, Oxford (Clarendon) Press (1954), pp. 196-204.

26. G.R. Hoy and S. Chandra, *J. Chem. Phys.* **47**, 961 (1967).

27. B. Balko, G.R. Hoy, *Phys. Rev. B*, 10, 36 (1974).

APPENDIX A

A MONTE CARLO SOLUTION OF THE MAXWELL-BLOCH EQUATIONS

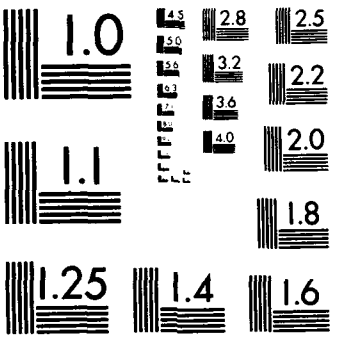
1.0
1.1
1.25
1.4
1.6
1.8
2.0
2.2
2.5
2.8
3.2
3.6
4.0
4.5
5.0
5.6
6.3

APPENDIX A
A MONTE CARLO SOLUTION OF THE MAXWELL-BLOCH EQUATIONS

The Maxwell-Bloch equations considered in this appendix are:

$$\frac{\partial N_4}{\partial t} = -\gamma N_4$$

$$\frac{\partial N_3}{\partial t} = -\left(E_{31}^{+} R_{31}^{+} + E_{31}^{-} R_{31}^{-}\right) - \Gamma_3 N_3 + \gamma N_4$$

$$\frac{\partial N_1}{\partial t} = +\left(E_{31}^{+} R_{31}^{+} + E_{31}^{-} R_{31}^{-}\right) - \Gamma_1 N_1 + \Gamma_3 N_3$$

$$\frac{\partial R_{31}^{+}}{\partial t} = (N_3 - N_1) E_{31}^{-} - \frac{\Gamma_3 + \Gamma_1 + \Gamma_\varphi}{2} R_{31}^{+} + \xi_{31}^{+} \qquad \text{(A-1)}$$

$$\frac{\partial R_{31}^{-}}{\partial t} = (N_3 - N_1) E_{31}^{+} - \frac{\Gamma_3 + \Gamma_1 + \Gamma_\varphi}{2} R_{31}^{-} + \xi_{31}^{-}$$

$$\frac{\partial E_{31}^{+}}{\partial x} = g_1 R_{31}^{-} - \frac{1}{2}\mu E_{31}^{+}$$

$$\frac{\partial E_{31}^{-}}{\partial x} = g_1 R_{31}^{+} - \frac{1}{2}\mu E_{31}^{-} \quad .$$

If the initial state $|0>$ is defined as the vacuum state for the electromagnetic field and an eigenstate for the operators N_1, N_3, N_4, with eigenvalues 0, 0, 1, then initial and boundary conditions are

$$E_{31}^{+}(x, 0)\,|0> = E_{31}^{-}(x, 0)\,|0> = N_1(x, 0)\,|0> = N_3(x, 0)\,|0> = 0$$

and (A-2)

$$E_{31}^{+}(0, t) = E_{31}^{-}(0, t) = 0 \quad .$$

The quantities g_1 and μ are both positive. It then follows from Eq. (A-2) and the last two equations of (A-1) that

$$R_{31}^{+}(x, 0)\,|0> = R_{31}^{-}(x, 0)\,|0> = 0 \quad . \qquad \text{(A-3)}$$

The terms ξ^+ and ξ^- appearing in the third and fourth equations of (A-1) are stochastic, independent, Gaussian distributed functions with zero means and the second moments

$$\langle \xi^+_{31}\, \xi^+_{31} \rangle = \langle \xi^-_{31}\, \xi^-_{31} \rangle = \langle \xi^-_{31}\, \xi^+_{31} \rangle = 0$$

$$\langle \xi^+_{31}(x, t)\, \xi^-_{31}(x', t') \rangle = (1/N) \langle N_4(t) \rangle\, \delta(x-x')\, \delta(t-t') \qquad \text{(A-4)}$$

$$= (1/N)\, e^{-\gamma t}\, \gamma\, \delta(x-x')\, \delta(t-t') \quad .$$

The statistical parameters given by (A-4) reflect the fact that ξ^+ and ξ^- are Hermitian conjugate operators.

Acording to the last two equations,

$$R^+ = (1/g_1)\left(\frac{\partial E^-}{\partial x} + \frac{1}{2}\mu E^-\right) \text{and } R^- = (1/g_1)\left(\frac{\partial E^+}{\partial x} + \frac{1}{2}\mu E^+\right) \quad . \qquad \text{(A-5)}$$

Substituting from (A-5) into the fourth and fifth equations of (A-1) leads to the differential equations

$$E^+_{xt} + \frac{1}{2}\mu E^+_t = g_1 (N_3 - N_1) E^+ - \frac{\Gamma_3 + \Gamma_1 + \Gamma_\varphi}{2} (E^+_x + \frac{1}{2}\mu E^+) + \xi^-$$

and (A-6)

$$E^-_{xt} + \frac{1}{2}\mu E^-_t = g_1 (N_3 - N_1) E^- - \frac{\Gamma_3 + \Gamma_1 + \Gamma_\varphi}{2} (E^-_x + \frac{1}{2}\mu E^-) + \xi^+ \quad .$$

In the spirit of the Haake-Reibold approximations the initial-boundary value problem for the Maxwell-Bloch system of differential equations (A-1), with the population of level 4 totally inverted initially, can be treated classically (i.e., as if the operators were all c-numbers). For this purpose the c-number initial and boundary values

$$E^+_{31}(x, 0) = E^-_{31}(x, 0) = N_1(x, 0) = N_3(x, 0) = 0,\ N_4(x, 0) = 1$$

(A-7)

$$E^+_{31}(0, t) = E^-_{31}(0, t) = 0$$

replace the operator initial and boundary values in (A-2). Also, a corresponding classical ensemble average replaces any expectation value; e.g., the radiation intensity

$$I(t) = \langle E^-(1, t)\, E^+(1, t) \rangle$$

is interpreted as a second moment of the stochastic electric field satisfying the substituted classical initial-boundary value problem.

The c-number substitutes for the operator quantities appearing in (A-1) will all be real functions; hence, a single function E will replace the Hermitian conjugate operators E^+ and E^-, a single function R will replace the Hermitian conjugate operators R^+ and R^-, and a single function ξ will replace the Hermitian conjugate operators ξ^+ and ξ^-. Thus,

$$E_{xt} + \frac{1}{2}\mu E_t = g_1 (N_3 - N_1) E - \frac{\Gamma_3 + \Gamma_1 + \Gamma_\varphi}{2} (E_x + \frac{1}{2}\mu E) \qquad \text{(A-8)}$$

replaces both equations in (A-6), and similarly modified, single c-number equations will replace the two equations in (A-5) as well as the second and third equations in (A-1).

For numerical calculations the corresponding difference equations are:

$$\begin{aligned}
&N_4 (x, t) = N_4 (x, t_o) - h\gamma N_4 (x, t_o) \quad , \\
&N_3 (x, t) = N_3 (x, t_o) - 2hE (x, t_o) R (x, t_o) - h\Gamma_3 N_3 (x, t_o) + h\gamma N_4 (x, t_o) \quad , \\
&N_1 (x, t) = N_1 (x, t_o) - 2hE (x, t_o) R (x, t_o) - h\Gamma_1 N_1 (x, t_o) + h\Gamma_3 N_3 (x, t_o) \quad , \\
&E (x, t) = E (x, t_o) + E (x_o, t) - E (x_o, t_o) - \frac{1}{2}\Delta\mu [E (x_o, t) - E (x_o, t_o)] \quad , \\
&\quad + h\Delta g_1 [N_3 (x_o, t_o) - N_1 (x_o, t_o)] E (x_o, t_o) - \frac{1}{2} h\Delta\mu (\Gamma_1/2) E (x_o, t_o) \quad , \\
&\quad - h (\Gamma_1/2) [E (x, t_o) - E (x_o, t_o)] + g_1 h\Delta\xi (x_o, t_o) \quad ,
\end{aligned} \qquad \text{(A-9)}$$

along with

$$R(x, t) = (1/\Delta g_1) [(1 + \frac{1}{2}\mu\Delta) E (x, t) - E(x_o, t)] \quad , \qquad \text{(A-10)}$$

which comes from (A-5). The quantities h and Δ are the difference equation time and distance increments: $(t - t_o)$, $(x - x_o)$.

The stochastic noise function $\xi(x,t)$, which, in the form $\xi(x_o, t_o)$, appears only in the last equation of (A-9). It is calculated by selecting a random number from a normal distribution with mean zero and a variance given by

$$\sigma^2 = (1/N) e^{-\gamma t} \quad , \qquad \text{(A-11)}$$

which comes from (A-4), the delta functions having been integrated out in the last equation of (A-9).

As indicated, for every grid point (x_o, t_o) an independent random number is selected, from which ξ is obtained. The random number ξ can be calculated as follows, in

terms of two random numbers, u_1 and u_2, chosen independently from a uniform distribution over the interval (0,1).

First, the number ξ_o given by

$$\xi_o = \sqrt{-2 \ln u_1} \cos (2\pi u_2) \qquad \text{(A-12)}$$

is a random number from a Gaussian distribution with mean zero and a variance of 1. This can be seen from the fact that the modulus of a complex number for which the real and imaginary parts are independent, normally distributed random variables with identical means and variances is Rayleigh distributed over the interval $(0,\infty)$, and the phase of the complex number is uniformly distributed over the interval $(0,2\pi)$. Then ξ is given by

$$\xi = \sigma\xi_o \quad , \qquad \text{(A-13)}$$

where σ is determined by (A-11).

LISTING OF CODE

```
                    5/29/92
      double precision n1(201),n3(201),e31p(201),e31m(201)
      double precision e1(250),e2(250),e3(250),e4(250),e5(250),e6(250)
      double precision a1(250),a2(250),a3(250),a4(250),a5(250),a6(250)
      double precision n1t(201),n3t(201),e31pt(201),e31mt(201)
      double precision eii(201),r31p(201),r31m(201)
      double precision xns1(201),xns2(201)
        double precision dn3dt(201),tempn3(201)
        real abc(250),abcv(250)
        double precision pi,sd,t,gma,gm1,gm3,ff,cf,xf,g1,alpha
        double precision f0,scale,bta,d,h,y1,y2,rn1,rn2,rn3
        double precision e,ef,ef1,ef2,ee,f,gm10,r,tp,tf,bta1,bta2,tjp
        double precision cbeta
        double precision tjn1,tjn2,aa,x
        double precision s5w,s6w,e0
        double precision et
        double precision ffff,aaa
        integer iseed,n,m,nf,issw,isssw,is4w,is5w,is6w,ksel,is,iss,np,
     'isw,it1,it0,nout,nx,nt,nd,nxv,ntv,ii,m8
        common/a/e1,e2,e3
        common/b/e4,e5,e6
        common/c/a1,a2,a3
        common/d/a4,a5,a6

        open(unit=3,file='xio',status='new',form='formatted')
        open(unit=16,file='fp6',status='new',form='formatted')

        pi = dble(4.*atan(1.))
        n = 40
        m = 2000
        t = 100.d0
        gma = 10.d0
        gm1 = 1.d-6
        gm3 = 1.d-4
        ff = 1.d-3
        cf = 0.d0
        nf = 10
        bta1 = 0.d0
        bta2 = 0.d0
        scale = .1d0
        iseed = 1029384567
        issw = 1
        aaa = 1.d4
        isssw = 0
        cbeta = 0.d0
        is4w = 0
        s5w = 1.d0
        s6w = 1.d0
        e0 = 0.0d0
        is5w = 0
        alpha = 0.d0
        is6w = 0
        ksel = 0
        sd = 1.d0
        is = 100
        iss = 1
        xf = 1.d0
        g1 = 1.0d0
        f0 = 1.d0
```

```
      np = 250
      isw = 0
      tjn1 = 2.d0
      tjn2 = 3.d0
      tjp = t + 1.d0
      it0 = m + 2
      it1 = m + 4
      nout = n
      write(3,*) 'iseed,sd=',iseed,sd
      write(3,*) 'n,m =    ',n,m
      write(3,*) 'is,iss=  ',is,iss
      write(3,*) 'xf,t  =  ',xf,t
      write(3,*) 'gma   =  ',gma
      write(3,*) 'gm1,gm3= ',gm1,gm3
      write(3,*) 'g1,ff  = ',g1,ff
      write(3,*) 'nf,f0  = ',nf,f0
      write(3,*) 'cf,np  = ',cf,np
      write(3,*) 'scale,isw = ',scale,isw
      write(3,*) 'it0,it1 = ' ,it0,it1
      write(3,*) 'nout = ',nout
      write(3,*) 'bta1,bta2,tjp',bta1,bta2,tjp
      if (isssw.ne.0) write(3,*) 'isssw,cbeta = ',isssw,cbeta
      write(3,*) 'issw = ',issw
      if(issw.gt.0) write(3,*) 'tjn1,tjn2,aa = ',tjn1,tjn2,aa
      if (is4w.ne.0) write(3,*) 'is4w = ',is4w
      if (is5w.ne.0) write(3,*) 'is5w, alpha =',is5w,alpha
      cf = cf/2.d0
      write(3,*) 's5w,s6w,e0 = ',s5w,s6w,e0
      write(3,*) 'is6w,ksel = ',is6w,ksel
      d = t/dble(float(m))
      h = xf/dble(float(n))
      nx = np
      nt = 1
      dt = .1
      t0 = 0.
      nd = m/np
      do 11 i=1,np
11    abc(i) = sngl(t*float(i-1)/np)
      write(16,997) nx
      write(16,997) nt
997   format(1x,i4)
      write(16,998) dt
      write(16,998) t0
998   format(1x,f10.4)
      write(16,996) (abc(i), i=1,np)
996   format(1x,f13.6)
      nxv = n
      ntv = m/is
      dtv = t/float(ntv)
      t0v = 0.
      do 111 i=1,n
111   abcv(i) = float(i-1)*sngl(h)
      e0 = e0*d
      do 1000 nn=1,nf
      do 1 j=1,n+1
      n1(j) = 0.d0
      n3(j) = 0.d0
      n3t(j) = 0.d0
      n1t(j) = 0.d0
      e31p(j) = 0.d0
```

```
            e31pt(j) = 0.d0
            e31mt(j) = 0.d0
            e31m(j) = 0.d0
            if (is6w.eq.2.and.j.eq.ksel) then
             e31p(j) = e0
             e31pt(j) = e0
             e31mt(j) = e0
             e31m(j) = e0
            endif
    1       continue
            if (is6w.eq.1) then
               if (nn.eq.1) e0 = e0/d
               e31p(1) = e0
               e31m(1) = e0
               e31pt(1) = e0
               e31mt(1) = e0
            endif
            ii = 0
            do 100 i=1,m
            if (is5w.ne.0) g1=dexp(-i*d*alpha*gm3/2.d0)
            if(issw.eq.0) then
            r = dexp(-gma*float(i-1)*d/2.)*dsqrt(gma*ff)
            if ((it0.lt.i.and.i.lt.it1).and.isw.eq.1) r = 0.
            if (isw.eq.2) r = sqrt(gma*ff)
            endif
            if(issw.eq.1) then
               if(float(i-1)*d.lt.tjn1.or.float(i-1)*d.gt.tjn2) then
                  r = dexp(-gma*float(i-1)*d/2.)*dsqrt(gma*ff)
               else
                  r = dsqrt((dexp(-gma*float(i-1)*d) + aa)*(gma*ff))
               endif
            endif
            if(issw.eq.2) then
               if(float(i-1)*d.lt.tjn1.or.float(i-1)*d.gt.tjn2) then
                  ffff = dexp(-gm3*float(i-1)*d)
                  r = dsqrt((1.d0-dexp(-gma*float(i-1)*d))*(gm3*ff))*ffff
               else
                  r = dsqrt(((1.d0-dexp(-gma*float(i-1)*d)) + aa)*(gm3*ff))
               endif
           endif
            if(issw.eq.3) then
                  r = dsqrt((dexp(-gma*float(i-1)*d)*gma +
           ,           (1.d0-dexp(-gma*float(i-1)*d))*
           .            aaa*gm3*dexp(-gm3*float(i-1)*d))*ff)
            endif
            ee = 0.d0
            ef = 0.d0
            do 2 j=1,n
            if (dble(float(i))*d.lt.tjp) then
              bta = bta1
            else
              bta = bta2
            endif
            if (isssw.ne.0) bta = bta*dexp(-cbeta*d*dble(float(i)))
            if (is4w.eq.1.and.i.ge.2) then
               bta = bta*gm3/(gm3+2.d0*dabs(tempn3(n)))
            endif
            if (is4w.eq.2.and.i.ge.2) then
               bta = bta*gm3/(gm3+2.d0*dabs(tempn3(j)))
            endif
```

```
      e = s5w*(d/h)*(e31p(j)*(e31m(j+1)-e31m(j))
     .   +        e31m(j)*(e31p(j+1)-e31p(j)))/g1
     .   +        cf*(e31p(j) + e31m(j))**2*d/(2.d0*g1)
      ee = ee + e*e
      ef1 = - gm1*n1(j)*d + gm3*n3(j)*d
      ef2 = - gm3*n3(j)*d + gma*dexp(-gma*(i-1)*d)*d*f0
      ef = ef + ef1*ef1 + ef2*ef2
      n1t(j) = n1(j) + e + ef1
      n3t(j) = n3(j) - e + ef2
      if (n1t(j).gt.1.d0) n1t(j) = 1.d0
      if (n3t(j).gt.1.d0) n3t(j) = 1.d0
      y1 = dble(urand(iseed))
      y2 = urand(iseed)
      rn1 = f(y1,sd)*r
      rn1 = dcos(y2*2.d0*pi)*rn1
      rn3 = rn1
      xns1(j) = rn1
      xns2(j) = rn1
      gm10 = gm3*(1.d0 + bta + alpha)
       rn1 = s6w*rn1
       rn3 = s6w*rn3
      tp = (1.d0 + cf*h/2.d0)
      tm = (1.d0 - cf*h/2.d0)
      e31pt(j+1) = (e31pt(j)*tm + e31p(j+1)*tp - e31p(j)*tm)
     .           + ((n3(j)-n1(j))*e31p(j))*d*h*g1
     . -(gm10/2.d0)*(e31p(j+1)-e31p(j)+cf*h*e31p(j))*d + rn3*d*h*g1
        e31pt(j+1) = e31pt(j+1)/tp
        if((is6w.eq.2.or.is6w.eq.5).and.j+1.eq.ksel) then
          if (is6w.eq.5) then
           et = dsqrt(6.5d-10)*dsqrt(n3t(j)*h*gm3*5.d0)*d
          else
           et = e0
          endif
         e31pt(j+1)=e31pt(j+1)+dexp(-gm3*d*dble(float(i))/2.d0)*et
        endif
        if(is6w.eq.3.or.is6w.eq.4) then
         et = n3t(j)*h*gm3
         if(is6w.eq.4) et = -1.d0
         e31pt(j+1)=e31pt(j+1)+dexp(-gm3*d*dble(float(i))/2.d0)*et
        endif
      e31mt(j+1) = (e31mt(j)*tm + e31m(j+1)*tp - e31m(j)*tm)
     .           + ((n3(j)-n1(j))*e31m(j))*d*h*g1
     . -(gm10/2.d0)*(e31m(j+1)-e31m(j)+cf*h*e31m(j))*d + rn1*d*h*g1
        e31mt(j+1) = e31mt(j+1)/tp
        if((is6w.eq.2.or.is6w.eq.5).and.j+1.eq.ksel) then
          if (is6w.eq.5) then
           et = dsqrt(6.5d-10)*dsqrt(n3t(j)*h*gm3*5.d0)*d
          else
           et = e0
          endif
         e31mt(j+1)=e31mt(j+1)+dexp(-gm3*d*dble(float(i))/2.d0)*et
        endif
        if(is6w.eq.3.or.is6w.eq.4) then
         et = n3t(j)*h*gm3
         if(is6w.eq.4) et = -1.d0
         e31mt(j+1)=e31mt(j+1)+dexp(-gm3*d*dble(float(i))/2.d0)*et
        endif
2     continue
      e31p(1) = e31pt(1)
      e31m(1) = e31mt(1)
```

```
          if ((i/500)*500.eq.i) write(6,*) nn,i,ee,ef
          do 3 j=1,n
          n1(j) = n1t(j)
          n3(j) = n3t(j)
          e31p(j+1) = e31pt(j+1)
          e31m(j+1) = e31mt(j+1)
          tempn3(j) = e31pt(j)*(e31pt(j+1) - e31pt(j))/h
 3        eii(j) = e31pt(j)*e31mt(j)
          do 333 j=1,n
          r31p(j) = (e31p(j+1) - e31p(j))/h
 333      r31m(j) = (e31m(j+1) - e31m(j))/h
          if ((i/is)*is.eq.i) then
          e31p(1) = scale + e31p(1)
          eii(1) = scale + eii(1)
          r31p(1) = scale + r31p(1)
          e31p(1) = -scale + e31p(1)
          eii(1) = -scale + eii(1)
          r31p(1) = -scale + r31p(1)
           endif
          if (((i-1)/nd)*nd.eq.i-1) then
           e1(ii+1) = n1(nout-1)
           e2(ii+1) = e31p(nout)
           e3(ii+1) = n3(nout-1)
           e4(ii+1) = f0*dexp(-gma*float(i)*d)
            e5(ii+1) = r31p(nout-2)
           e6(ii+1) = e31p(nout)*e31m(nout)
           ii = ii + 1
          endif
          if(mod(i,10).eq.0)write(*,*)i
 100      continue
          if (nn.eq.1) then
          do 30 i=1,np
           a1(i) = e1(i)
           a2(i) = e2(i)
           a3(i) = e3(i)
           a4(i) = e4(i)
           a5(i) = e5(i)
 30        a6(i) = e6(i)
          else
           do 31 i=1,np
           a1(i) = a1(i) + e1(i)
           a2(i) = a2(i) + e2(i)
           a3(i) = a3(i) + e3(i)
           a4(i) = a4(i) + e4(i)
           a5(i) = a5(i) + e5(i)
 31        a6(i) = a6(i) + e6(i)
          endif
 1000     continue
          do 35 i=1,np
           a1(i) = a1(i)/float(nf)
           a2(i) = a2(i)/float(nf)
           a3(i) = a3(i)/float(nf)
           a4(i) = a4(i)/float(nf)
           a5(i) = a5(i)/float(nf)
 35        a6(i) = a6(i)/float(nf)
           m8 = (m+1)/is
          write(16,999) (a6(i), i=1,np)
          write(16,999) (a6(i), i=1,np)
 999      format(1x,f20.15)
 97       format(2e15.6)
```

```
 99      format(5e13.5)
         x = 0.d0
         do 777 i=1,np
 777     x = x + a6(i)
         x = x*t/dble(float(np))
         write(3,*) 'integral of intensity = ',x
         write(6,*) 'iseed, int of int = ', iseed,x
         stop
         end
          double precision function f(y,s)
         double precision y,s
         f = s*dsqrt(2.*dlog(1.d0/y))
         return
         end
       FUNCTION URAND (IY)
       INTEGER  IY
C
C*************************************************************
C
C                                                 ROBERT RENKA
C                                        NORTH TEXAS STATE UNIV.
C                                                (817) 565-2767
C
C   THIS FUNCTION RETURNS A UNIFORMLY DISTRIBUTED RANDOM
C NUMBER IN THE INTERVAL [0,1).  THE INTEGER SEED IY IS BOTH
C AN INPUT AND OUTPUT PARAMETER.  IT SHOULD BE INITIALIZED
C TO AN ARBITRARY INTEGER PRIOR TO THE FIRST CALL, AND
C SHOULD NOT BE ALTERED BETWEEN SUBSEQUENT CALLS UNLESS THE
C SEQUENCE OF RANDOM NUMBERS IS TO BE REPEATED.
C   URAND IS A MODIFICATION OF THE CODE IN FORSYTHE, MAL-
C COLM, AND MOLER, AND IS INTENDED ONLY FOR EXECUTION ON THE
C IBM PC OR A COMPATIBLE MACHINE.  THE ORIGINAL VERSION
C FAILS WHEN COMPILED WITH THE MICROSOFT VERSION 3.2 COMPI-
C LER BECAUSE OVERFLOW IN INTEGER MULTIPLICATION IS TREATED
C AS AN EXCEPTION AND RESULTS IN THE (HEX) VALUE 80000000
C RATHER THAN THE TRUE PRODUCT MODULO 2**32.
C
C INTRINSIC FUNCTIONS CALLED BY URAND -- DBLE, FLOAT, MOD
C
C*************************************************************
C
      INTEGER IAH, IAL, IC, IYH, IYL, IY1, IY2, K, KD2, MIC,
     .        M2
      REAL    S
C
      DATA IAH/12867/, IAL/63149/, IC/453816693/, K/65536/,
     .     KD2/32768/, MIC/1693666955/, M2/1073741824/
C
C A SEQUENCE OF RANDOM INTEGERS IS GENERATED BY IY =
C   (IA*IY + IC) MODULO M, WHERE IA AND IC ARE CHOSEN TO
C   SATISFY THE PROPERTIES RECOMMENDED BY KNUTH (VOL. 2),
C   AND M = 2**31 IS THE LARGEST REPRESENTABLE INTEGER
C   (PLUS 1).  IAL AND IAH ARE THE LOW AND HIGH ORDER HALVES
C   OF IA, M2 = M/2, AND MIC = M - IC.
C COMPUTE A SCALE FACTOR S FOR CONVERTING IY TO TYPE REAL.
C   S IS THE CLOSEST FLOATING POINT NUMBER TO 1/M.
C
      S = .5D0/DBLE(M2)
C
C SET IY TO IA*IY MOD M (OR IA*IY MOD M - M), AVOIDING
```

```
C   OVERFLOW.  IY1 IS IN (-M,M) AND IY2 IS IN [0,M).
C
      IYH = IY/K
      IYL = IY - K*IYH
      IF (IYL .EQ. 0) THEN
        IY = K*MOD(IAL*IYH,KD2)
        GO TO 1
      ENDIF
      IY1 = 2*(IYL*31574-M2) + IYL
      IY2 = KD2*MOD(MOD(IAH*IYL,K) + 2*MOD(IAL*IYH,KD2),K)
      IF (IY1/2 + IY2/2 .LT. M2) THEN
        IY = IY1 + IY2
        IF (IY .LT. 0) IY = (IY + M2) + M2
      ELSE
        IY = (IY1 - M2) + (IY2 - M2)
      ENDIF
C
C THE FOLLOWING STATEMENT IS DESIGNED TO AVOID OVERFLOW IN
C   THE FOLLOWING INTEGER ADDITION.
C
    1 IF (IY .GE. MIC) IY = (IY - M2) - M2
C
C SET IY TO (IY+IC) MOD M AND MAP IY TO THE UNIT INTERVAL.
C
      IY = IY + IC
      URAND = FLOAT(IY)*S
      RETURN
      END
```

NOTATION FOR MONTE CARLO CODE ST18

In Paper	In Code	Interpretation
N1	n1	normalized population of lower level
N3	n2	normalized population of upper level
N4	exp $(-\gamma t)$	normalized population of storage level
R_{31}^{+}	r31p	polarization
E_{31}^{+}	e31p	electric field
R_{31}^{-}	r31m	polarization
E_{31}^{-}	e31m	electric field
γ	gma	pumping rate
Γ_1	gm1	decay rate of lower level
Γ_3	gm3	decay rate of upper level
N	1/ff	number of cooperating nuclei
g1	g1	coupling constant
μ	cf	attenuation coefficient
ξ_{31}^{+}	rn1, xns1	noise source
ξ_{31}^{-}	rn2, xns2	noise source
	t	total time interval
	xf	length of space interval
	n	number of space steps
	m	number of time steps

In Paper	In Code	Interpretation
	p, np	number of points in graphs
	sd	standard deviation in noise generator
	iseed	seed for random noise generation
	is	time steps skipped between i/o
	issw	issw = 0, pump noise only (Haake-Reibold), $F_1(t)$,
		issw = 1, regular pump noise plus additional non decaying term, $F_1(t) + G_1(t)$
		issw = 2, spontaneous decay noise only, $F_2(t)$
		issw = 3, pump noise plus spontaneous decay noise, $F_1(t) + F_2(t)$
a	alpha	inhomogeneous broadening parameter
b	bta	homogeneous broadening parameter
	bta1	b value on (0, tjp)
	bta2	b value on (tjp,t)
A	aa	for issw $\neq$ 0, term for modifying noise
	tjn1, tjn2	if issw $\neq$ 0, noise changed on (tjn1, tjn2)
	cbeta	exponential degradation coefficient of bta1 or bta2
	isssw	isssw = 0, no exponential degradation of bta1 or bta2
		isssw = 1 for exponential degradation of bta1 or bta2 value on (tjp, t)
$\Gamma_\varphi = a\Gamma_3$		dephasing rate from inhomogeneous broadening
$\Gamma_\theta = b\Gamma_3$		dephasing rate from homogeneous broadening
N_o	f0	initial value of N_4
	isw	isw = 0, regular noise

	isw = 1, noise shut off for it0 through it1 time steps
	isw = 2, no exponential noise degradation
nout	space step at which data is collected (normally nout = n)
is5w	is5w = 0, no time dependence on g1
	is5w = 1, time dependence on g1 $\rightarrow$ g1 $e^{-a\Gamma_3 t/2}$
is6w	is6w = 0, noise used to initiate pulse,
	boundary condition on field at x = 0 $\varepsilon_0 = 0$
	is6w = 1, boundary condition on electric field at x = 0,
	$\varepsilon_0 \neq 0$
ε_0	boundary condition on electric field, $E = \varepsilon_0 e^{-\Gamma_3 t/2}$
s5w	s5w = 1.0, nonlinear ten in
	s5w = 0.0, nonlinear ten out
s6w	s6w = 1.0, noise active
	s6w = 0.0, noise not active

Input noise is generally a product of a term randomly varying in time and a constant factor or a term exponentially varying in time. The random term is obtained from a random function generator and the terms use for different values of ISSW are

$$F_1^2(t) = \frac{\gamma}{N} e^{-\gamma t}$$

$$F_2^2(t) = \left(1 - e^{-\gamma t}\right) A \frac{\Gamma_3}{N} e^{-\Gamma_3 t}$$

$$G_1^2(t) = A\frac{\gamma}{N}$$

INPUT PARAMETERS FOR SAMPLE RUN (ST18 CODE)

```
iseed . sd=      1029384567          1.00000000000000
n . m =                40                2000
is . iss=             100                   1
xf . t =       1 . 00000000000000                  100 . 000000000000
gma  =         10 . 0000000000000
gm1 . gm3=     1 . 00000000000000E-006             1 . 00000000000000E-004
g1 . ff    =   1 . 00000000000000                  1 . 00000000000000E-003
nf . f0    =             10    1 . 00000000000000
cf . np    =   0 . 00000000000000E-000                    250
scale . isw =    0 . 10000000000000E                              0
it0 . it1  =          2002          2004
nout   =              40
btal . bta2 . tjp      0 . 00000000000000E-000      0 . 00000000000000E-000
  101 . 000000000000
*isssw.cbeta           0             0
*is4w                  0
*is5w . alpha          0             0
*is6w . eo             0             0
issw   =               1
tjnl . tjn2 . aa  =    2 . 00000000000000           3 . 00000000000000
 0 . 00000000000000E-000
```

*parameters isssw.cbeta, is4w, is5w, alpha, is6w, eo printed out only if non zero

SF PULSE INTENSITY VS TIME
EXAMPLE

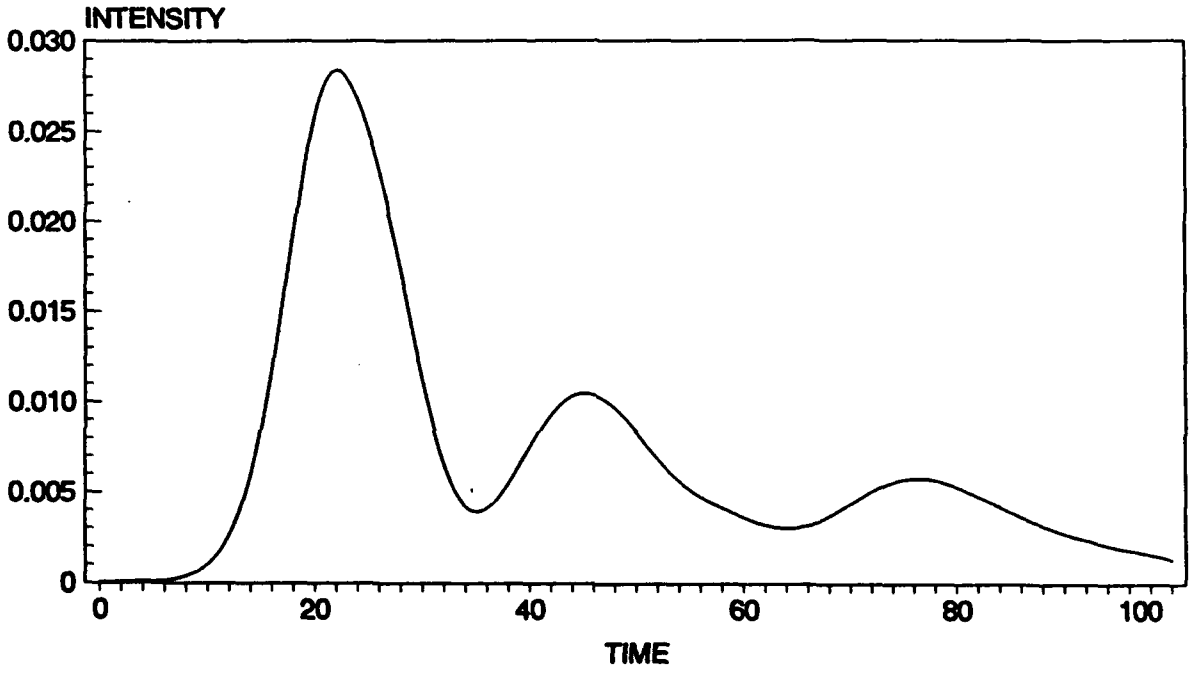

APPENDIX B

MEAN INTENSITY IN THE LIMIT OF FAST PUMPING

APPENDIX B
MEAN INTENSITY IN THE LIMIT OF FAST PUMPING

At early times the Maxwell-Bloch equations are effectively linear because of the initial conditions

$$E^+ (x, 0) \mid 0 > = R^- (x, 0) \mid 0 > = 0, \tag{B-1}$$

which make the nonlinear terms quadratically small. The resulting linearized equations are solvable in closed form.

With the boundary condition

$$E^+ (0, t) = E^- (0, t) = 0 \tag{B-2}$$

imposed at the left end of the active volume, taking into account the statistical properties of the stochastic source, the mean radiation intensity at the right end of the active volume is then given by

$$I(t) = \langle E\ (1, t)\, E^+ (1, t) \rangle$$

$$= (\gamma/N) \int_0^t dt' e^{-\gamma t'} \left[\{ I_0 (2[F(t, t')]^{1/2}) \}^2 - \{ I_1\ (2[F(t, t')]^{1/2}) \}^2 \right] , \tag{B-3}$$

where the $I_{0,1}(t)$ are modified Bessel functions and

$$F (t, t') = t - t' + (e^{-\gamma t} - e^{-\gamma t'})/\gamma \quad . \tag{B-4}$$

In the limit of fast pumping, $\gamma \rightarrow \infty$, the average intensity given by (B-3) becomes

$$I_\infty\ (t) = (1/N) \{ [I_0 (2\sqrt{t})]^2 - [I_1\ (2\sqrt{t})]^2 \} \quad . \tag{B-5}$$

For the time rate of change W(t) of the probability of finding the mean intensity I(t) above a reference level I_{Ref}, Haake and Reibold give the equation

$$W(t) = [\dot{I}(t)\, I_{Ref}/I(t)^2] \exp [- I_{Ref}/I(t)] \quad . \tag{B-6}$$

Haake and Reibold remark that W(t) should be a reasonable approximation to the probability density of the first passage time of I(t) above I_{Ref} and therefore at least a rough approximation to the delay time probability density.

The time at which the maximum value of W(t) occurs is then an estimate of the most probable delay time of the radiated pulse. Some typical delay time estimates based on B-6) with a value of 1 assigned to I_{Ref} and various values of N are given in Figs. (B-1)-(B-6), which illustrate the corresponding function W(t).

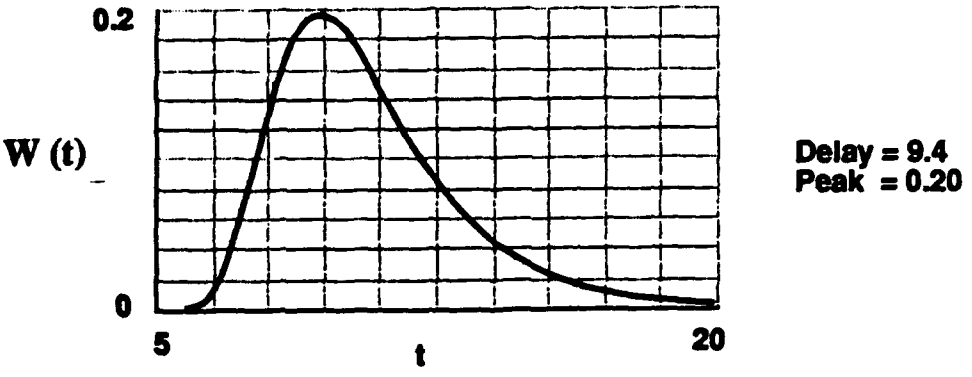

Figure B-1. Passage Time Probability Density in the Limit of Infinitely Fast Pumping: N = 1000

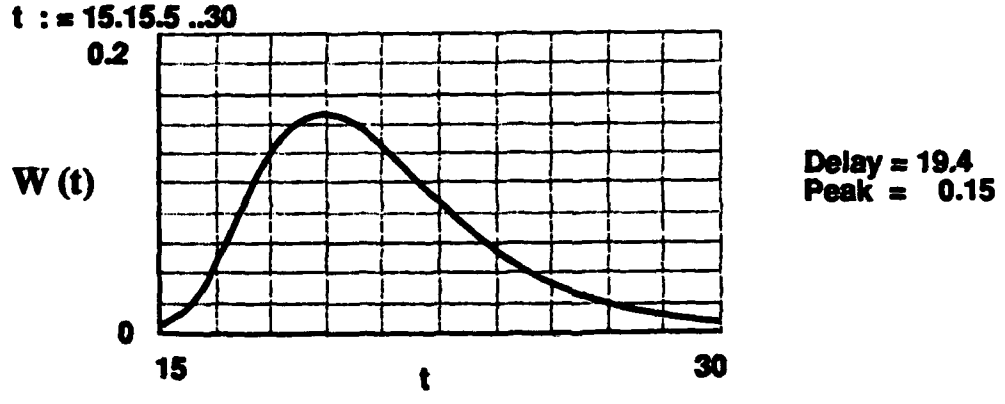

Figure B-2. Passage Time Probability Density in the Limit of Infinitely Fast Pumping: $N = 10^5$

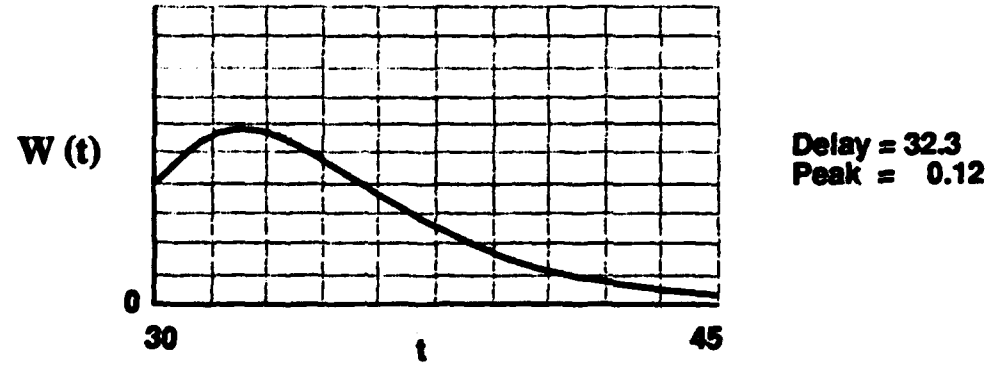

Figure B-3. Passage Time Probability Density in the Limit of Infinitely Fast Pumping: $N = 10^7$

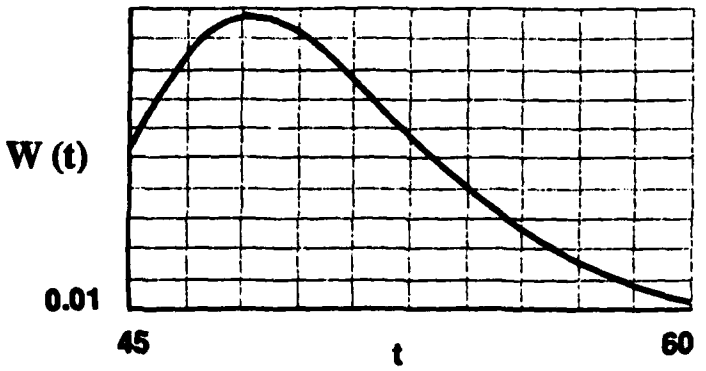

Figure B-4. Passage Time Probability Density in the Limit of Infinitely Fast Pumping: $N = 10^9$

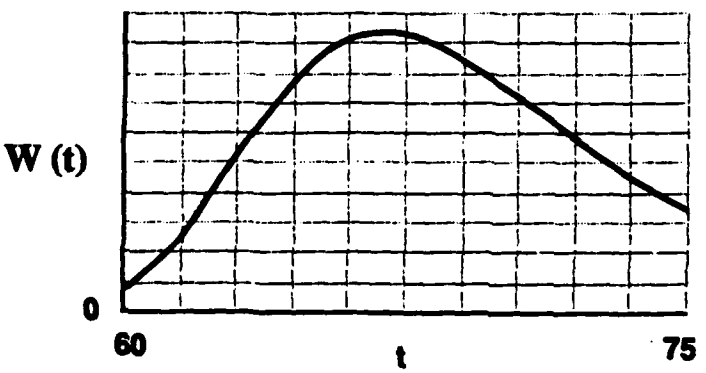

Figure B-5. Passage Time Probability Density in the Limit of Infinitely Fast Pumping: $N = 10^{11}$

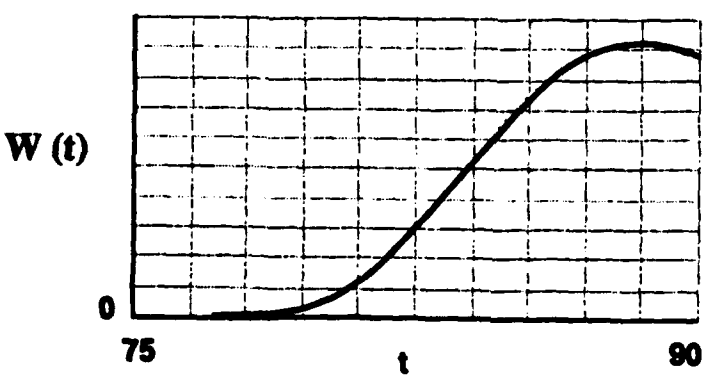

Figure B-6. Passage Time Probability Density in the Limit of Infinitely Fast Pumping: $N = 10^{13}$

APPENDIX C

AVERAGE OF A FUNCTION WITH A STOCHASTIC ARGUMENT

APPENDIX C
AVERAGE OF A FUNCTION WITH A STOCHASTIC ARGUMENT

This appendix details an investigation of the following problem: to calculate the stochastic average of the functional

$$\exp\left\{ i\int_0^t \left[\alpha g(t') + \beta h(t')\right] dt' \right\} \quad ,$$

where g(t) and h(t) are identical stochastic functions, each of which, as a stationary Markov process, independently takes on random values ± in successive infinitesimal time intervals Δt. The calculation is equivalent to finding the average

$$\left\{ \exp\left[i\int_0^t f(t')\, dt \right] \right\}_{av} \quad ,$$

where f(t) is a stochastic function of the same type as g(t) and h(t), but which can take on any of the values

$$\alpha_1 = \alpha - \beta,\ \alpha_2 = \alpha + \beta,\ \alpha_3 = -\alpha_2,\ \alpha_4 = -\alpha_1 \quad , \qquad \text{(C-1)}$$

with equal probability.

As in the case treated by Ref. C-1,

$$\left\{ \exp\left[i\int_0^t f(t')\, dt' \right] \right\}_{av} = \sum_{i=1}^{4} p_1 \langle i \,|\, \exp[(iF + W)t] \,|\, j \rangle \quad , \qquad \text{(C-2)}$$

where F is a 4th order diagonal matrix with the main diagonal elements α_1, given by (1) and W is the 4th order matrix

$$W = \begin{bmatrix} -2\Omega, & \Omega, & \Omega, & 0 \\ \Omega, & -2\Omega, & 0, & \Omega \\ \Omega, & 0, & -2\Omega, & \Omega \\ 0, & \Omega, & \Omega, & -2\Omega \end{bmatrix} \quad . \tag{C-3}$$

According to Ref. C-2, each off-diagonal element W_{ij} of W is the conditional probability per unit time of f(t) taking the value α_j, at time $t + \Delta t$, given that it had the value α_1 at time t.

The zero elements occur because the corresponding conditional probabilities are second order in Δt. The diagonal elements all have the value -2Ω because, as Ref. C-2 observes, the fact that for each condition the sum of conditional probabilities must be one implies that the sum of the corresponding probability rates must be zero.

The straightforward way to evaluate (C-2) is to diagonalize the matrix $iF + W$. The first step is to calculate its eigenvalues λ_1 by solving the equation

$$\det (iF + W - I) = 0 \quad , \tag{C-4}$$

where I is the 4^{th} order identity matrix.

As is evident from (C-3) and the definition of F, (C-4) is equivalent to

$$\det \begin{bmatrix} i\alpha_1 - \mu, & \Omega, & \Omega, & 0 \\ \Omega, & i\alpha_2 - \mu, & 0, & \Omega \\ \Omega, & 0, & i\alpha_3 - \mu, & \Omega \\ 0, & \Omega, & \Omega, & i\alpha_4 - \mu \end{bmatrix} = 0 \quad , \tag{C-5}$$

where

$$\mu = \lambda + 2 \quad . \tag{C-6}$$

Using (C-1), evaluating the determinant in (C-5) leads to the quartic equation in

$$\mu^4 + 2(\alpha^2 + \beta^2 - 2\Omega^2)\mu^2 + (\alpha^2 - \beta^2)^2 = 0 \quad , \tag{C-7}$$

which is also a quadratic equation in μ^2 and therefore explicitly solvable. All solutions of (C-7) are given by

$$\mu = \pm\left(\sqrt{\Omega^2 - \alpha^2} \pm \sqrt{^2 - \beta^2}\right) \quad ; \tag{C-8}$$

therefore according to (C-6) the required eigenvalues are the four quantities

$$\lambda = -2\Omega_1 \left(\sqrt{\Omega^2 - \alpha^2} \pm \sqrt{\Omega^2 - \beta^2} \right) \quad . \tag{C-9}$$

The next step is to calculate the eigenvector corresponding to each of the eigenvalues given by (C-9). The components T_{1k} of the eigenvector corresponding to the k^{th} eigenvalue will satisfy the system of equations

$$\begin{aligned}
(i\alpha_1 - 2\Omega)\, T_{1k} &+ \Omega\, T_{2k} &+ \Omega\, T_{3k} & &= \lambda_k\, T_{1k} \\
\Omega\, T_{1k} &+ (i\alpha_2 - 2\Omega)\, T_{2k} & &+ \Omega\, T_{4k} &= \lambda_k\, T_{2k} \\
\Omega\, T_{1k} & &+ (i\alpha_3 - 2\Omega)\, T_{3k} &+ \Omega\, T_{4k} &= \lambda_k\, T_{3k} \\
& \Omega\, T_{2k} &+ \Omega\, T_{3k} &+ (i\alpha_4 - 2\Omega) T_{4k} &= \lambda_k\, T_{4k} \, .
\end{aligned} \tag{C-10}$$

Subtracting the first equation in (C-10) from the last and using (C-6) leads to

$$T_{4k} = T_{1k}\, (i\alpha_1 - \mu) \,/\, (i\alpha_4 - \mu) \quad . \tag{C-11}$$

From the third equation it follows that

$$T_{3k} = -\,\Omega\, (T_{4k} + T_{1k}) \,/\, (i\alpha_3 - \mu) \quad , \tag{C-12}$$

and from the first that

$$T_{2k} = -\,T_{3k} - (i\alpha_1 - \mu)\, T_{1k} \,/\Omega \quad . \tag{C-13}$$

For each value of k the Eqs. (C-11)-(C-13) give T_{2k}, T_{3k}, and T_{4k} in terms of T_{1k}. Those assignments and the assignments of any arbitrary complex numbers for the T_{1k} will provide solutions for the system of Eqs. (C-10).

The T_{1k} satisfying (C-10) are elements of a diagonalizing transformation matrix T, such that

$$\exp\,[(iF + W)\, t] = T \exp(\Lambda t)\, T^{-1} \quad , \tag{C-14}$$

where Λ is the diagonal matrix for which the main diagonal elements are the eigenvalues λ_i. As just noted, for each k the solution vector of (C-10) will depend on an arbitrary choice of T_{1k}. If this number is chosen so that

$$\sum_{i=1}^{4} T_{ik}^2 = 1 \quad , \tag{C-15}$$

the inverse matrix T^{-1} of the corresponding T will be equal to the adjoint matrix T^{t}.

It then follows that (C-2) is equivalent to

$$\left\{ \exp\left[i \int_0^t f(t')\, dt' \right] \right\}_{av} = \sum_{i,\, j,\, k=1}^{4} p_i\, T_{ij} \exp(\lambda_j\, t)\, T_{kj} \quad . \tag{C-16}$$

Since the *a priori* probabilities p_1 of the four possible f(t) values are all equal, each $p_1 = 1/4$ in (C-16).

The relations (C-9), (C-11)-(C-13), and (C-15) provide the other quantities in (C-16). In the special case $\Omega = 0$, these relations lead immediately to the result

$$G(\alpha, \beta, t) = \cos(\alpha t) \cos(\beta t) \quad , \tag{C-17}$$

where

$$G(\alpha, \beta, t) = \left\{ \exp\left[i \int_0^t f(t')\, dt' \right] \right\}_{av}$$

is given by (C-16).

The function R(t) is an average reduction factor defined by

$$R(t) = K \int_0^{\infty} \int_0^{\infty} G(\alpha, \beta, t) \exp\left[-\left(\alpha^2 + \beta^2 \right) / \sigma^2 \right] d\, d\beta \quad , \tag{C-18}$$

where K is chosen so that

$$R(0) = 1 \quad .$$

For the special case $\Omega = 0$, it follows from (C-17) that

$$R(t) = \exp(-\sigma^2 t^2/4) \quad . \tag{C-19}$$

Figures C-1 to C-10 show R(t) for various values of Ω and σ.

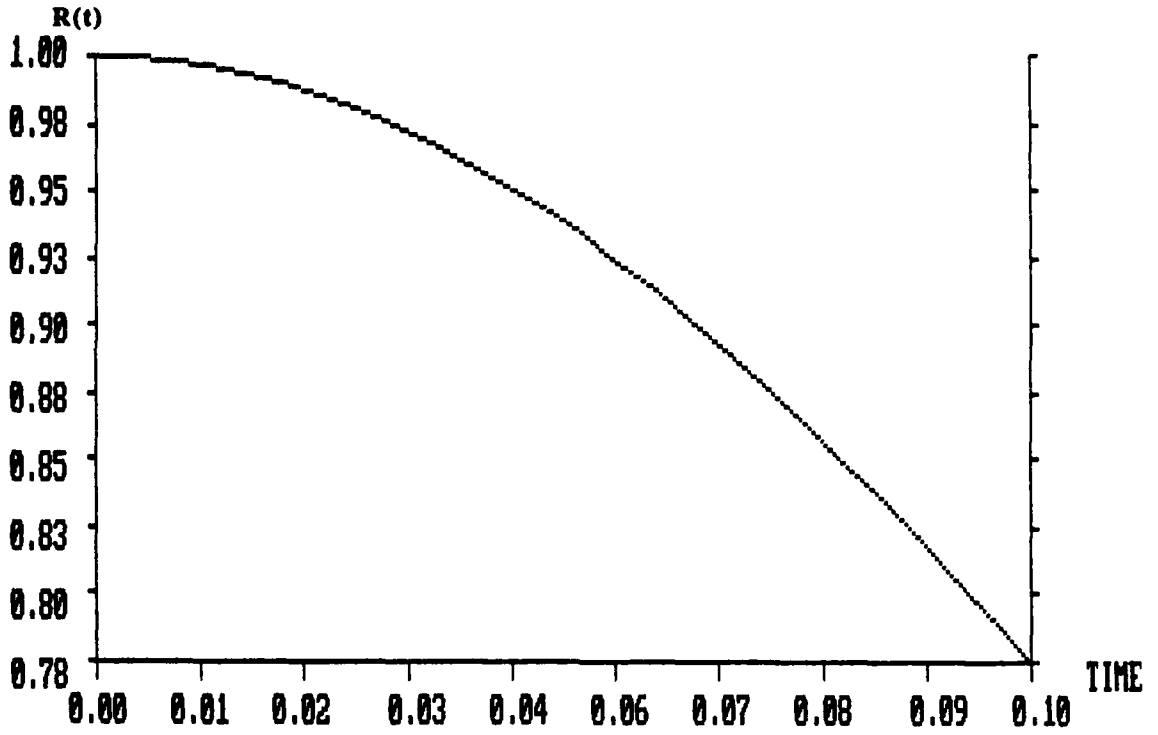

Figure C-1. Average Reduction Factor as a Function of Time After Inversion. $\Omega = 0$, $\sigma = 10$.

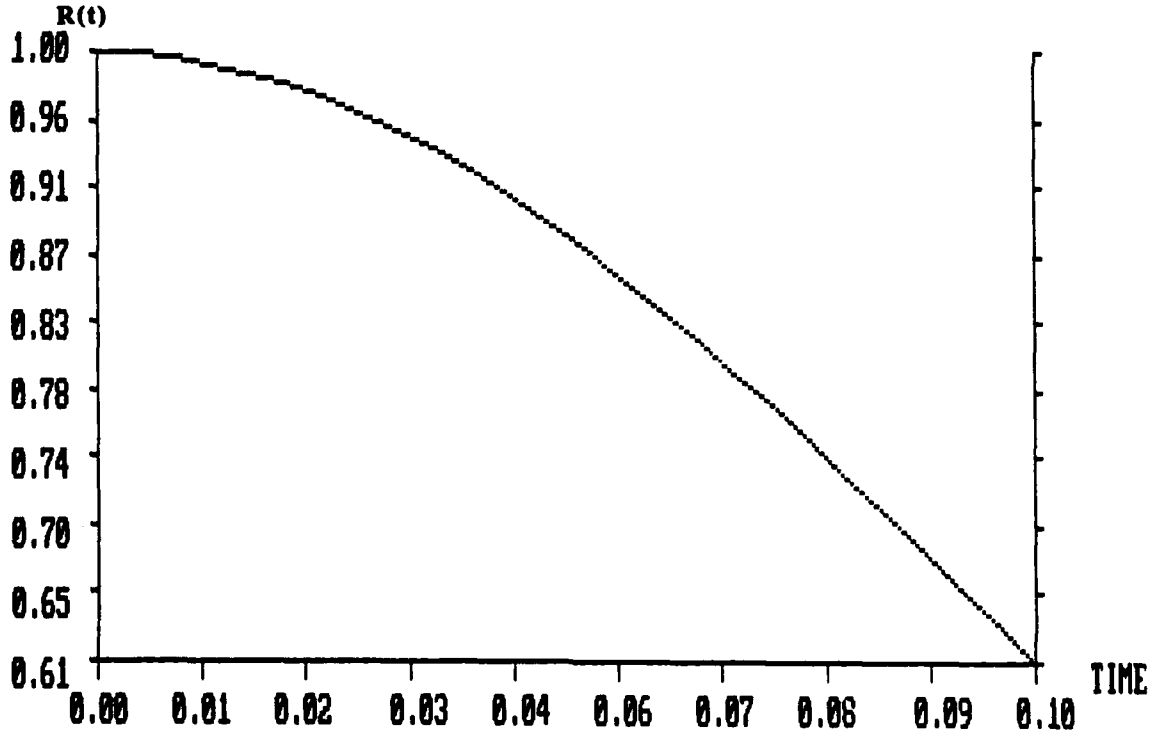

Figure C-2. Average Reduction Factor as a Function of Time After Inversion. $\Omega = 0.1$, $\sigma = 10$.

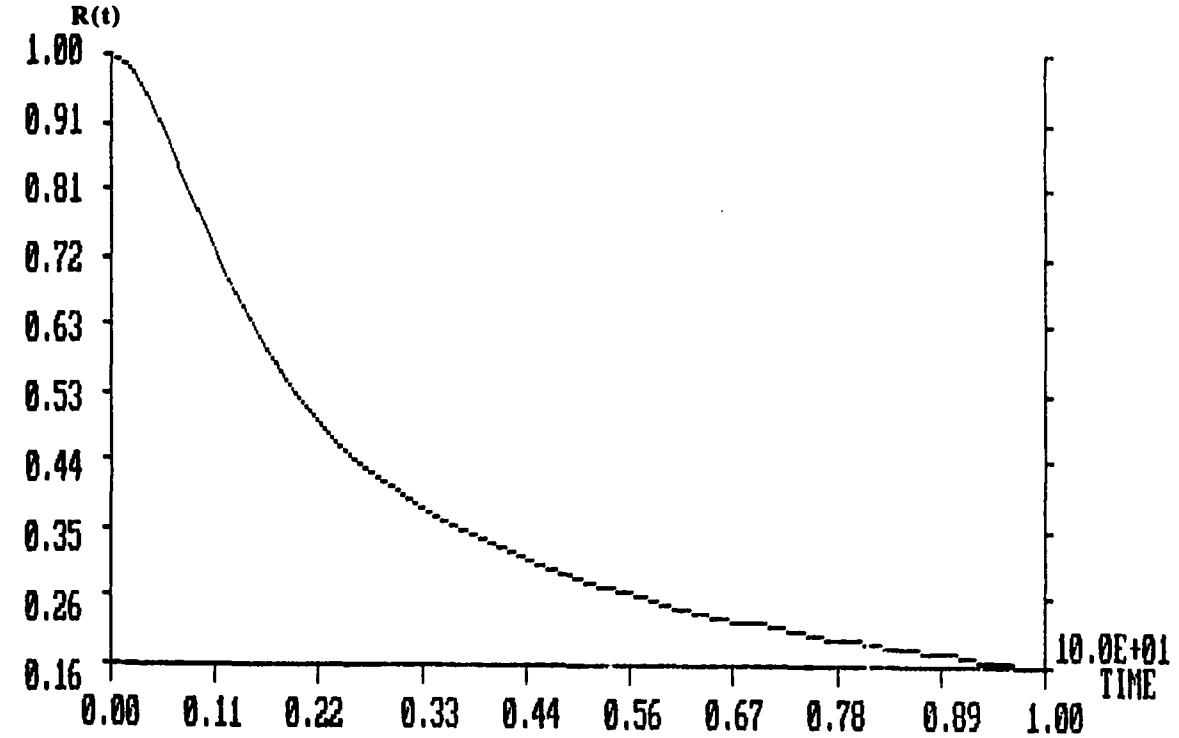

Figure C-3. Average Reduction Factor as a Function of Time After Inversion. $\Omega = 0.1$, $\sigma = 0.1$.

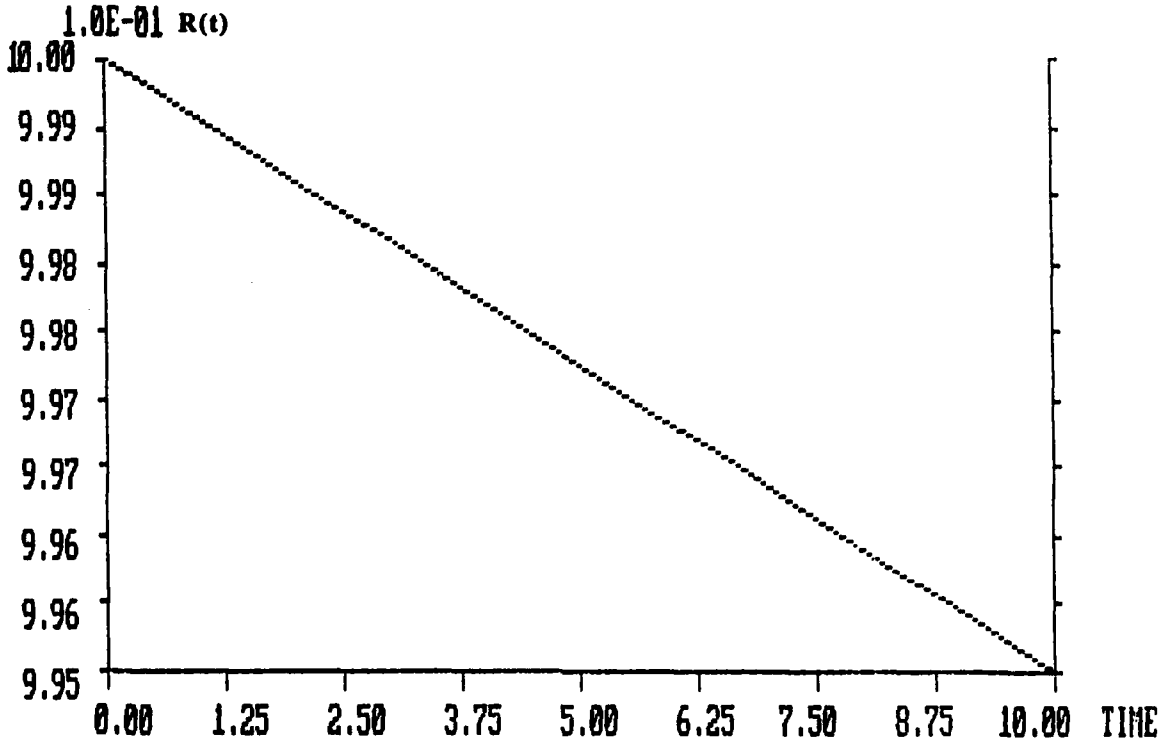

Figure C-4. Average Reduction Factor as a Function of Time After Inversion. $\Omega = 10$, $\sigma = 0.1$.

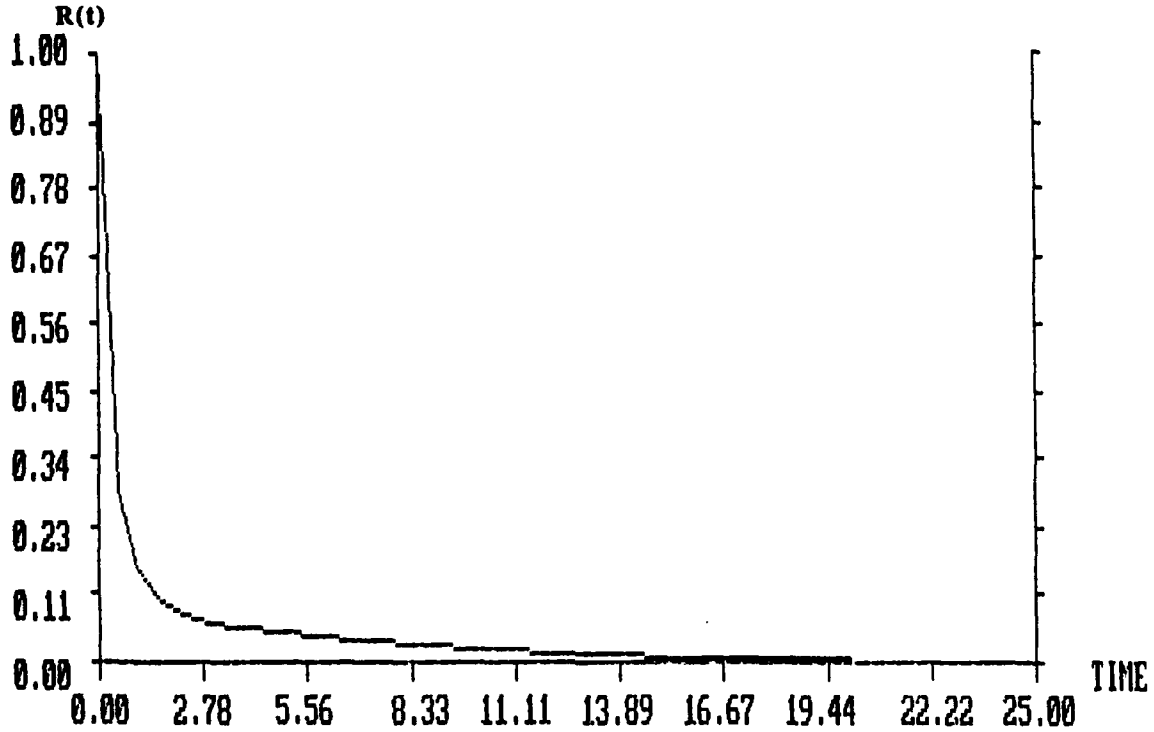

Figure C-5. Average Reduction Factor as a Function of Time After Inversion. $\Omega = 10$, $\sigma = 10$.

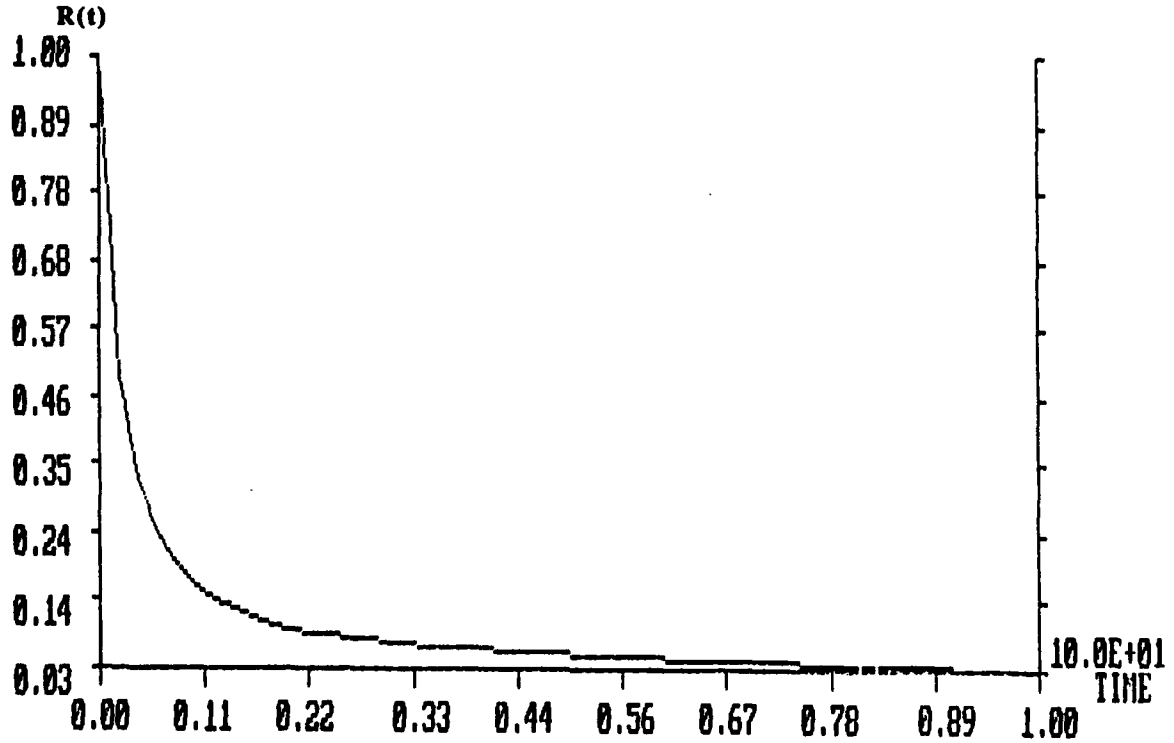

Figure C-6. Average Reduction Factor as a Function of Time After Inversion. $\Omega = 100$, $\sigma = 10$.

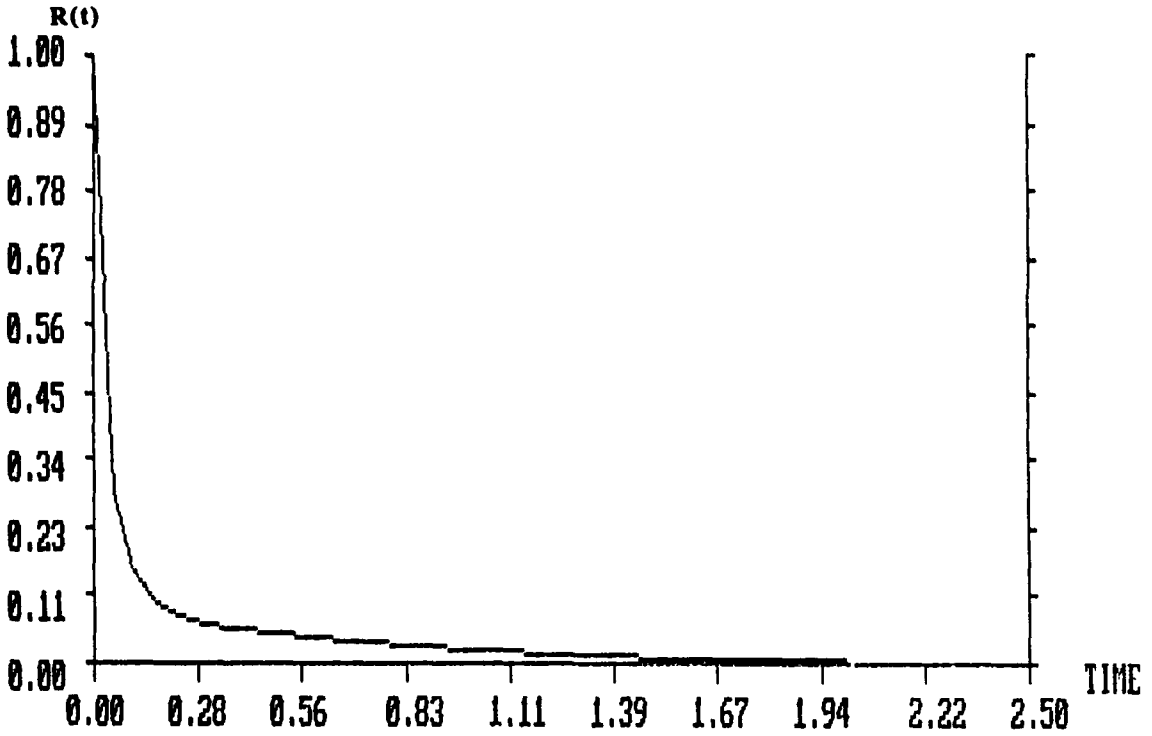

Figure C-7. Average Reduction Factor as a Function of Time After Inversion. Ω = 100, σ = 100.

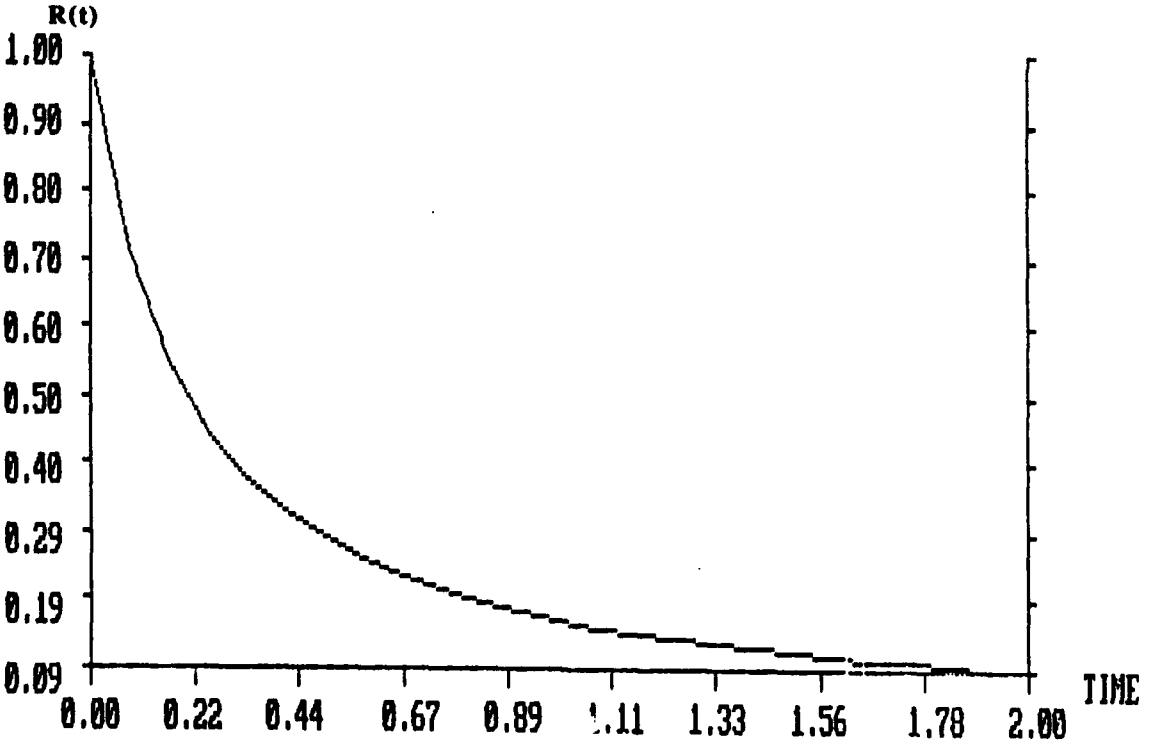

Figure C-8. Average Reduction Factor as a Function of Time After Inversion. Ω = 1E3, σ = 100.

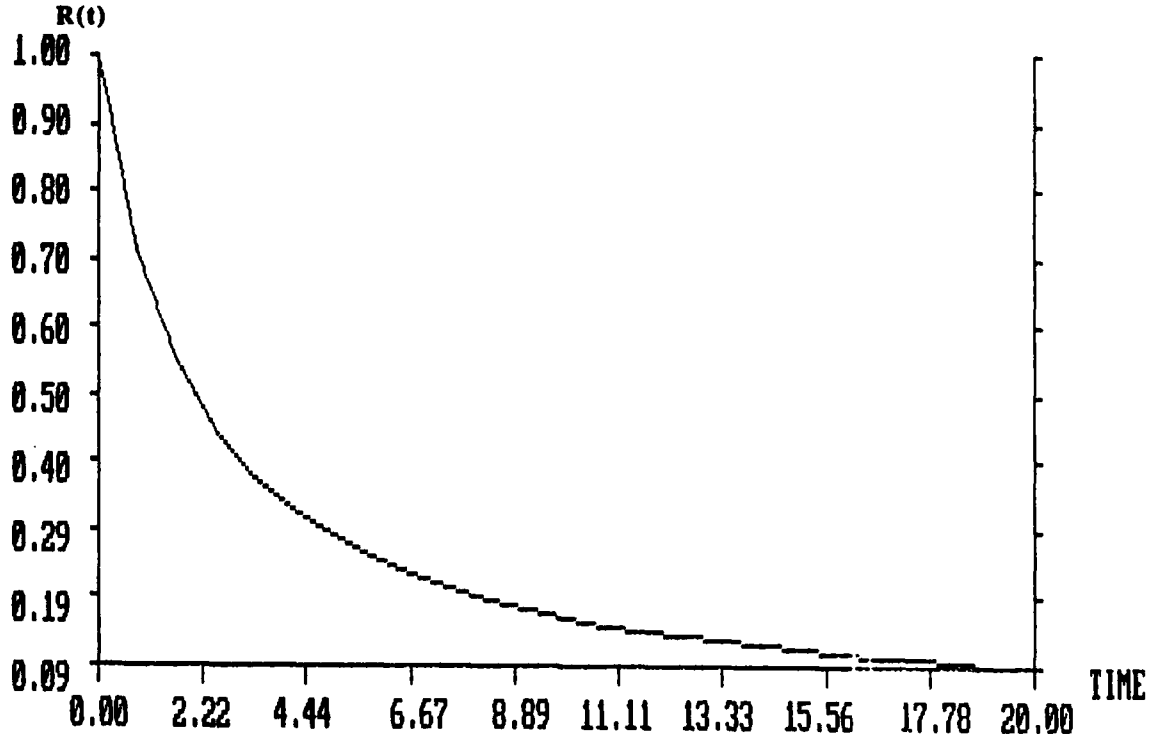

Figure C-9. Average Reduction Factor as a Function of Time After Inversion. Ω = 1E4, σ = 100.

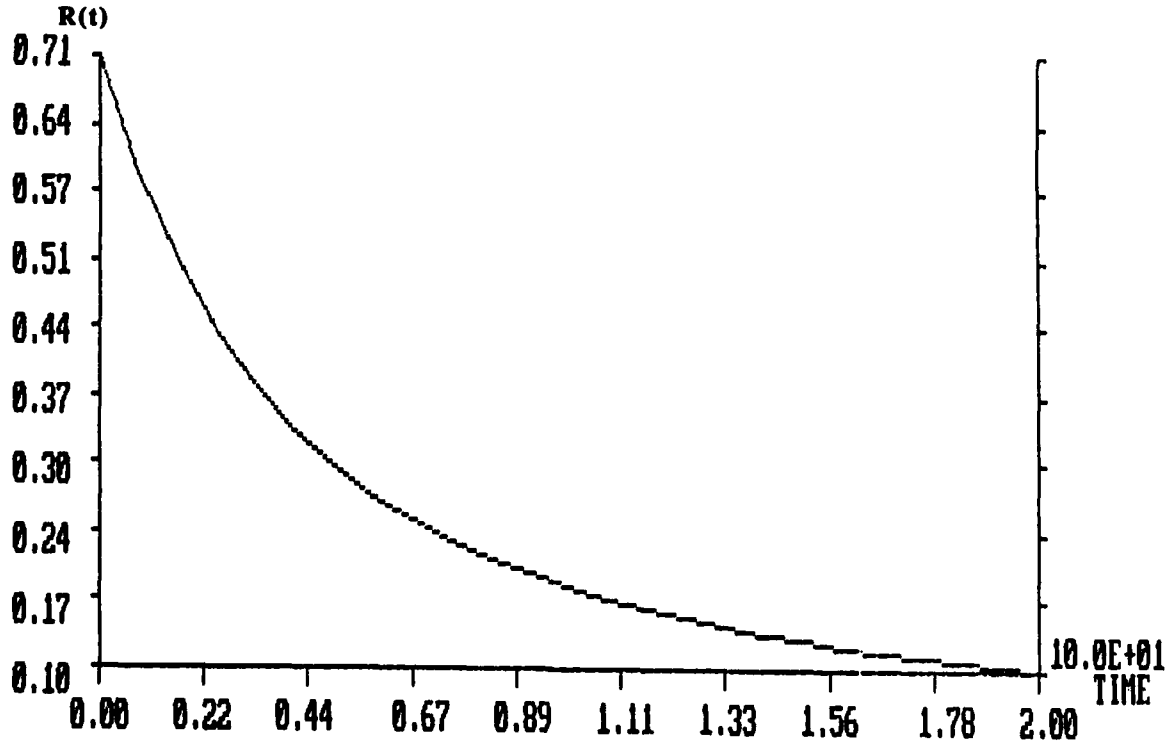

Figure C-10. Average Reduction Factor as a Function of Time After Inversion. Ω = 1E6, σ = 100.

REFERENCES--APPENDIX C

C-1. M. Blume and J.A. Tjon, "Mössbauer Spectra in a Fluctuating Environment," *Phys. Rev.*, Vol. 165, No. 2 (1968), pp. 446-455.

C-2. A. Abragam, *The Principles of Nuclear Magnetism*, Oxford (Clarendon) Press (1961), pp. 447-451.

APPENDIX D

NOTE ON A GAUSSIAN-LORENTZIAN INTEGRAL

APPENDIX D
NOTE ON A GAUSSIAN-LORENTZIAN INTEGRAL

The W(z) function defined in Ref. D-1 can be used to evaluate the integral

$$I(E,\Gamma) = \int_{-\infty}^{\infty} \frac{e^{-\frac{x^2}{\Delta^2}}}{(x-E) - i\frac{\Gamma}{2}}\, dx \ . \tag{D-1}$$

The W(z) function is defined by

$$W(z) = e^{-z^2}\, \mathrm{erfc}\,(-iz),\ \mathrm{Im}(z) > 0 \tag{D-2}$$

and has the integral representation

$$W(z) = \frac{1}{i\pi} \int_{-\infty}^{\infty} \frac{e^{-t^2}}{t-z}\, dt \tag{D-3}$$

for z in the upper half plane, so that

$$I(E,\Gamma) = i\,\pi\, e^{-z^2}\, \mathrm{erfc}\,(-iz)\ , \tag{D-4}$$

for

$$z = \frac{E + i\frac{\Gamma}{2}}{\Delta}\ .$$

In (D-4) the definition of z insures that it is in the upper half of the complex plane, as (D-3) requires. However, for the integral associated with I(E,−Γ), z is in the lower halfplane, which violates that condition.

On the other hand, deforming the integration contour in (D-3) leads to the conclusion that

$$I(E,-\Gamma) = i\,\pi\,\hat{W}(z)\ , \tag{D-5}$$

where

$$\hat{W}(z) = \frac{1}{i\pi} \int_{-\infty+i\varepsilon}^{\infty+i\varepsilon} \frac{e^{-t^2}}{t-z}\, dt \ , \qquad \text{(D-6)}$$

as long as

$$\varepsilon < \mathrm{Im}(z) \ .$$

But from (D-3) and (D-6) it is clear that

$$i\pi W(z) - i\pi \hat{W}(z) = \oint \frac{e^{-x^2}}{x-z}\, dx = 2\pi i e^{-z^2} \ . \qquad \text{(D-7)}$$

Combined with (D-2) and (D-5), (D-7) implies that

$$I(E, -\Gamma) = i\pi e^{-z^2} \mathrm{erfc}\,(-iz) - 2\pi i e^{-z^2} \ .$$

REFERENCE--APPENDIX D

D-1. M. Abromowitz and I.A. Stegun (Eds.), *Handbook of Mathematical Functions*, N.B.S. Applied Math. Ser. 55, 10th Printing (1972), p. 297.

APPENDIX E

INTEGRAL EVALUATION I

APPENDIX E
INTEGRAL EVALUATION I

In the limit

$$\Gamma \to \infty \text{ or } \Delta \to 0$$

the expression

$$I = \kappa\left(\frac{\Gamma}{2\Delta}\right)^3 \frac{\pi}{\Gamma}\int_{-\infty}^{\infty}\left[e^{z^2}\,\text{erfc}\,z \cdot e^{z_1^2}\,\text{erfc}\,z_1\left(e^{z_2^2}\,\text{erfc}\,z_2 - 2\pi i e^{-z_2}\right)\right]dE\ , \qquad \text{(E-1)}$$

where

$$z = \frac{\Gamma - iE}{2\Delta},\ z_1 = \frac{iE - \frac{\Gamma}{2}}{\Delta},\ z_2 = -\frac{iE + \frac{\Gamma}{2}}{\Delta}\ , \qquad \text{(E-2)}$$

can be evaluated explicitly.

The first step is to make the change of variable in the integral on the right-hand side of (E-1), after which the equation for I becomes

$$I = \kappa\left(\frac{\Gamma}{2\Delta}\right)^3 \Gamma\pi \int_{-\infty}^{\infty} e^{z'^2}\ \text{erfc}\,z' \cdot e^{z_1'^2}\,\text{erfc}\,z_1'\left(e^{z_2'^2}\,\text{erfc}\,z_2' - 2\pi i e^{-z_2'}\right)dE'\ , \qquad \text{(E-3)}$$

where

$$z' = \frac{\Gamma}{2\Delta}(1 + iE'),\ z_1' = \frac{\Gamma}{2\Delta}(2iE' - 1),\ z_2' = -\frac{\Gamma}{2\Delta}(2iE' + 1)\ \text{ and } E' = \frac{E}{\Gamma}\ .$$

The next step is to introduce the asymptotic limit

$$\lim_{z \to \infty} e^{z^2}\,\text{erfc}\,z = \frac{1}{z\sqrt{\pi}}\ , \qquad \text{(E-4)}$$

which (cf. Ref. E-1) is valid for

$$|\arg z| < \frac{3\pi}{4}\ .$$

Then the equation for I becomes

$$I = -\frac{\kappa}{\sqrt{\pi}} \int_{-\infty}^{\infty} \frac{dE'}{(1 + iE')\,(2iE' - 1)\,(2iE' + 1)} \,. \qquad \text{(E-5)}$$

Evaluating the integral on the right-hand side of (E-5) by residues is straightforward and gives the result

$$I = \frac{\kappa\sqrt{\pi}}{3} \,.$$

REFERENCE--APPENDIX E

E-1. M. Abromowitz and I.A. Stegun (Eds.), *Handbook of Mathematical Functions*, N.B.S. Applied Math. Ser. 55, 10th Printing (1972), p. 298.

APPENDIX F

INTEGRAL EVALUATION II

APPENDIX F
INTEGRAL EVALUATION II

$$I(\Gamma, \gamma, E_0, E') = \int_{-\infty}^{\infty} \frac{dE}{\left[(E-E')^2 + \left(\frac{\Gamma}{2}\right)^2\right]\left[(E-E')^2 + \left(\frac{\gamma}{2}\right)^2\right]} \quad . \tag{F-1}$$

Writing

$$a_1 = E_0,\ b_1 = \frac{\Gamma}{2},\ a_2 = E',\ b_2 = \frac{\gamma}{2} \quad , \tag{F-2}$$

after factoring the denominators in the integrand on the right-hand side, Eq. (F-1) becomes

$$I = \int_{-\infty}^{\infty} \frac{dz}{\left[z-(a_1+ib_1)\right]\left[z-(a_1-ib_1)\right]\left[z-(a_2+ib_2)\right]\left[z-(a_2-ib_2)\right]} \quad . \tag{F-3}$$

Evaluating the integral on the right-hand side of Eq. (F-3) by residues after closing the real axis contour in the upper half of the complex plane leads to

$$I = 2\pi i \left\{ \frac{1}{2ib_1[(a_1-a_2) + i(b_1-b_2)]\,[(a_1-a_2) + i(b_1+b_2)]} + \frac{1}{2ib_2[(a_2-a_1) + i(b_2-b_1)]\,[(a_2-a_1) + i(b_2+b_1)]} \right\}$$

$$= \pi \left\{ \frac{1}{b_1[(a_1-a_2)+i(b_1-b_2)]\,[(a_1-a_2)+i(b_1+b_2)]} + \frac{1}{b_2[(a_1-a_2)+i(b_1-b_2)]\,[(a_1-a_2)+i(b_1+b_2)]} \right\}$$

$$= \pi \left\{ \frac{b_1[(a_1-a_2) + i(b_1+b_2)] + b_2[(a_1-a_2) - i(b_1+b_2)]}{b_1 b_2[(a_1-a_2) + i(b_1-b_2)]\,[(a_1-a_2)^2 + (b_1+b_2)^2]} \right\}$$

$$= \pi \left\{ \frac{(b_1+b_2)\,(a_1-a_2) + i(b_1+b_2)\,(b_1-b_2)}{b_1 b_2[(a_1-a_2) + i(b_1-b_2)]\,[(a_1-a_2)^2 + (b_1+b_2)^2]} \right\} \quad ,$$

which reduces to

$$I = \frac{\pi(b_1+b_2)}{b_1 b_2[a_1-a_2]^2 + (b_1+b_2)^2]} \quad . \tag{F-4}$$

Substituting from Eq. (F-1) into Eq. (F-4) gives the value of the integral on the right-hand side of Eq. (F-1), i.e.,

$$I(\Gamma, \gamma, E_0, E') = \frac{\pi\frac{\Gamma+\gamma}{2}}{\frac{\Gamma\gamma}{4}\left[\left(E_0-E'\right)^2+\left(\frac{\Gamma+\gamma}{2}\right)^2\right]}$$

$$= \frac{2\pi(\Gamma+\gamma)}{\Gamma\gamma\left[(E_0-E')^2+\left(\frac{\Gamma+\gamma}{2}\right)^2\right]}$$

$$= \frac{2\pi\left(\frac{1}{\Gamma}+\frac{1}{\gamma}\right)}{(E-E')^2+\left(\frac{\Gamma+\gamma}{2}\right)^2} \quad . \qquad \text{(F-5)}$$